STUDY ON FREE VIBRATION BEHAVIOR OF FUNCTIONALLY GRADED MICRO BEAMS UNDER CENTRIFUGAL LOADING AND TRANSVERSE LOADING BASED ON MODIFIED COUPLE STRESS THEORY

Thesis Submitted in Partial Fulfillment of the

Requirements for the Degree of

Master of Engineering in Mechanical Engineering

By

Sujash Bhattacharya

[Examination Roll No: M4MEC19026]

[University Registration No: 140884 of 2017-2018]

Under the Guidance of

Dr. DEBABRATA DAS

DEPARTMENT OF MECHANICAL ENGINEERING

FACULTY OF ENGINEERING & TECHNOLOGY

JADAVPUR UNIVERSITY

KOLKATA – 700032

MAY 2019

FACULTY OF ENGINEERING AND TECHNOLOGY
JADAVPUR UNIVERSITY

CERTIFICATE OF APPROVAL*

This foregoing thesis is hereby approved as a credible study of an engineering subject carried out and presented in a manner satisfactory to warrant its acceptance as a prerequisite to the degree for which it has been submitted. It is understood that by this approval the undersigned do not endorse or approve any statement made, opinion expressed or conclusion drawn therein but approve the thesis only for the purpose for which it has been submitted.

COMMITTEE --

ON FINAL EXAMINATION FOR

EVALUATION OF THE THESIS --

***Only in case the thesis is approved**

FACULTY OF ENGINEERING AND TECHNOLOGY

JADAVPUR UNIVERSITY

CERTIFICATE OF RECOMMENDATION

I hereby recommend that the thesis presented under my supervision by ***SRI SUJASH BHATTACHARYA*** *entitled* "STUDY ON FREE VIBRATION BEHAVIOR OF FUNCTIONALLY GRADED MICRO BEAMS UNDER CENTRIFUGAL LOADING AND TRANSVERSE LOADING BASED ON MODIFIED COUPLE STRESS THEORY" *be accepted in partial fulfillment of the requirements for the degree of* ***Master of Engineering in Mechanical Engineering***.

Countersigned

Thesis Supervisor

Head of the Department

Department of Mechanical Engineering

Dean

Faculty of Engineering and Technology

DECLARATION OF ORIGINALITY AND COMPLIANCE OF ACADEMIC ETHICS

I hereby declare that the thesis contains literature survey and original research work by the undersigned candidate, as a part of his *MASTER OF ENGINEERING IN MECHANICAL ENGINEERING* studies. All information in this document have been obtained and presented in accordance with the academic rules and ethical conduct.

I also declare that, as required by these rules of conduct, I have fully cited and referenced all the material and results that are not original to this work.

Name: SUJASH BHATTACHARYA

Examination Roll Number: M4MEC19026

Class Roll Number: 001711202025

University Registration No: 140884 of 2017-18

Thesis Title: *STUDY ON FREE VIBRATION BEHAVIOR OF FUNCTIONALLY GRADED MICRO BEAMS UNDER CENTRIFUGAL LOADING AND TRANSVERSE LOADING BASED ON MODIFIED COUPLE STRESS THEORY*

Signature with Date:

ACKNOWLEDGEMENT

I would like to offer my sincere thanks to all who provided me this opportunity and granted me the capability to proceed successfully with my thesis. This thesis appears in its current form due to the assistance and guidance of several people.

I express my deep sense of gratitude to my supervisor, Dr. Debabrata Das, Associate Professor, Department of Mechanical Engineering, Jadavpur University, for his inspiration, support, academic and personal guidance throughout the course work. I'm grateful to him for being very supportive in letting me pursue my interests outside of academics, and encouraging me to learn and read widely. I'm grateful for this opportunity and look forward to continue my interactions with him in future.

I'm very fortunate to be a part of the Applied Mechanics Lab, Jadavpur University and my thanks also goes to all lab assistants for providing excellent working experience.

My thanks also goes to all my batch mates who have made the atmosphere in my classes lively. This work would not have been successful without the support and suggestions of respected professors of Mechanical Engineering Department, Jadavpur University. The excellent cooperation and support by research scholars, namely Mr. S. Pal and Mr. T. Jana are thankfully acknowledged.

Last, but most importantly, I'm grateful to my parents and family for their love, blessings and support throughout this endeavor. This thesis, a fruit of the combined efforts of my family members, is dedicated to them as a token of love and gratitude.

Date: May 2019 (Sujash Bhattacharya)

Contents

Page No

List of Symbols

b	Width
(b_{max}, b_{min})	Maximum and minimum width
c_j	Time-independent generalized coordinates
d_j	Time-dependent generalized coordinates
$\vec{f}_i$	Inertia force per unit volume
h	Thickness
(h_{max}, h_{min})	Maximum and minimum thickness
$\hat{i}, \hat{j}, \hat{k}$	Unit vectors in x, y, z direction
k_l	Volume fraction index along axial gradation
k_s	Shear correction factor
k_t	Volume fraction index along thickness gradation
l	Material length scale parameter
$\mathbf{m}$	Couple stress tensor
p	Transverse uniformly distributed load
$\vec{q}_Q$	Velocity vector of any point $Q(x, y', z')$ on the beam
$\vec{s}_Q$	Displacement vector of any point $Q(x, y', z')$ on the beam
t	Time
u, v, w	Displacement fields along x, y, z direction
u_0, v_0, w_0	Mid-plane displacement fields along x, y, z direction
$x - y - z$	Non-inertial global reference frame
$x' - y' - z'$	Non-inertial local reference frame
A	Cross sectional area

A_{max}	Maximum cross sectional area
A_i	Stiffness coefficients $[i=1,2,3]$
B_1	Stiffness coefficient
C_b	Taperness parameter for width
C_h	Taperness parameter for thickness
C_i	Inertia coefficients $[i=1,2,3]$
E_f	Effective Young's modulus
$[G]$	Gyroscopic matrix
G_f	Effective shear modulus
$\{H\}$	State vector
$\{H_c\}$	Time-independent part of state vector
I	Area moment of inertia
I_{max}	Maximum area moment of inertia
K_f	Effective bulk modulus
$[K^{SS}]$	Spin-softening matrix
$[K^t]$	Tangent stiffness matrix
$[K^T]$	Total stiffness matrix
L	Length of the Beam
$[M]$	Mass matrix
$\{P\}$	Load vector
P_f	General property of material
$\{P^r\}$	Restoring force vector

$P_0, P_{-1}, P_1, P_2, P_3$	Coefficients of temperature
$[R]$	Coordinate transformation matrix
R_0	Hub radius
$\vec{R}_Q$	Position vector of any point $Q(x, y', z')$ on the beam
T	Temperature
T_f	High operating temperature
T_0	Reference temperature
U_{ke}	Kinetic energy
U_{se}	Strain energy due to deformation
U_{wp}	Work potential of external load
U_{se}^{cl}	Classical strain snergy of the beam
U_{se}^{ncl}	Non-classical strain energy of the beam
V_c	Volume fraction of ceramic
V_m	Volume fraction of metal
$X - Y - Z$	Inertial reference frame
α_f	Effective thermal expansion coefficient
β	Pre-twist angle at any axial location x
$\bar{\beta}$	Total pre-twist angle
γ	Shear strain
ν_f	Effective Poisson's ratio
δ	Variational operator
η	Hub parameter (R_0/L)
$\boldsymbol{\varepsilon}$	Classical strain tensor
λ	Non-dimensional frequency

μ	Size-dependent parameter
λ', μ'	Lame's parameters
ξ	Slenderness parameter
κ	Aspect ratio of beam section
κ_f	Effective thermal conductivity
$\boldsymbol{\chi}$	Curvature tensor
ρ_f	Effective mass density
$\vec{\theta}$	Rotation vector
$\boldsymbol{\sigma}$	Classical stress tensor
$\phi_j^k(x)$	Set of orthogonal admissible functions $[k = u, v, w, rz, ry]$
ψ_y, ψ_z	Cross sectional rotations about y and z axis respectively
ψ'_y, ψ'_z	Cross sectional rotation about y' and z' axis respectively
ω	Frequency of vibration (rad/s)
Π	Total potential energy
ζ	Lagrangian
$\boldsymbol{\chi}$	Curvature tensor
Ω	Angular velocity
Ω^*	Non-dimensional speed

List of Figures

List of Tables

Chapter 1

INTRODUCTION

1.1. Introduction

With the advancement in technological field, research works on micro and nano structural components have gained interest over the past few years. The advent of micro fabrication in the 1980s, led to the manufacturing of micro- and nano-sized beams and plates for various uses. These thin structures and films are being extensively used in micro-/nano-electro-mechanical-systems (MEMS/NEMS) due their mechanical, optical, corrosion-resistant and hardness properties (Li et al., 2003; Lü et al., 2009; Yang et al., 2012). Vibration shock absorbers, atomic force microscopes, resonant testing equipments, electro-statically excited micro actuators, micro switches etc. are some of the MEMS that find the use of micro beams and micro plates. In optoelectronics, these structural elements are used for purposes like diverting photons. Micro beams are presently being utilized in micro pumps, micro turbines and in many other micro-fluidics applications in aerospace, mechanical, medical and biotechnological applications (Epstein and Senturia, 1997; Mehra et al., 2000; Kosasih and Jafari, 2014; London et al., 2001; Iverson and Garimella, 2008; Amirouche et al., 2009; Watson et al., 2009). So there is a huge importance of knowing the mechanical behavior of these micro- and nano-sized structures in detail to operate the state-of-the-art systems with accuracy and precision.

As researchers became interested on investigating the mechanics of micro beams and plates for its ample opportunity in engineering applications, conventional continuum mechanics is largely being used to predict its mechanical behavior. But the experimental studies showed that the static and dynamic characteristics of micro scale structures differ significantly from that predicted by the classical mechanics and it was seen that the behavior depends on the size factor (Lam et al., 2003; Liu et al., 2008; Li et al., 2018). Various new theories have been developed since then to accommodate the size-dependent behavior of micro structural elements. Modified coupled stress theory (MCST) (Yang et al., 2002; Park and Gao, 2006), strain gradient theory (SGT) (Fleck and Hutchinson, 1997; Kong et al, 2009), nonlocal elasticity theory (Eringen, 1983; Wang, 2005; Reddy, 2007), surface elasticity theory (Gurtin and Murdoch, 1978; Wang and Feng, 2007; Lü et al., 2009) are some of the path-breaking developments in this field. For the present work, MCST is used to capture the size-dependency of micro beams as it is widely used by the present day researchers for its simplicity due to involvement of a single material length scale parameter.

From the material considerations of the structural elements, especially in thermal environment, composite materials are being used for many years because they have better mechanical and thermal properties than its homogeneous counterparts. But the problem with composite structures, is the stress concentration generated in the interlaminar spaces. This results in delamination of composites in the high-temperature operating conditions. Functionally graded materials (FGMs), a class of advanced composites, is considered to be an alternative to the conventional composites. In addition to corrosion and wear resistivity, FGMs show better thermal and mechanical properties than the conventional metals or composites, and thus gained a very high importance in industrial applications. First introduced in Japan in 1984, in FGMs, unlike in conventional composites, the volume fractions of the constituents (metals and ceramics) and thus the material properties can be varied in smooth and continuous manner in any desired direction. The metal constituents contribute in enhancing the toughness of the structure, while the ceramic constituents impart better thermal properties to the structure, thus making it suitable to be used in high-temperature environment. For a beam-type component, the functional gradation along the thickness direction makes a thickness-FGM (TFGM) (Reddy and Chin, 1998; Reddy et al., 1999; Efraim and Eisenberger, 2007), and along the axial direction makes an axial-FGM (AFGM) (Shahba et al., 2011a). Recent advancements in manufacturing technologies have widened the path for considering bidirectional-FGMs (BFGMs) for beams including micro-beams (Şimşek, 2015; Hao and Wei, 2016; Nguyen and Lee, 2018; Mirjavadi et al., 2017; Trinh et al., 2018). In a BFGM beam, the material is graded in both thickness and axial directions. FGMs are considered to be one of the most promising materials for future in many engineering applications, e.g., the aerospace, mechanical, chemical, automobile and defense industries. Specific examples of FGM components include wear-resistant linings to handle large heavy abrasive ore particles, rocket heat shields, heat exchanger tubes, thermoelectric generators, heat-engine components, thermal shields for nuclear reactors and chemical plants, plasma facings for fusion reactors, electrically insulating metal/ceramic joints, bone and dental implants, cutting tools, fuel cells, solar cells etc. Though fabrication of FGM materials cannot yet be commercialized, but different techniques are being introduced in recent times, namely controlled segregation (sedimentation forming, slip casting, centrifugal casting, thixotropic casting etc.) and controlled blending (thermal spraying, vapour deposition, electrophoretic deposition, filter pressing, blended spray drying etc.) for manufacturing it in bulk at low cost.

The rapidly increasing applications of micro beams in modern applications have motivated the researchers to study its static, dynamic and stability behavior in minute details. Specifically, the study on free vibration behavior of non-rotating and rotating micro beams is important from design point of view in order to make them safe from resonance to occur under time-varying external forces. Considering tremendous applications in various micro turbo-machineries and micro pumps, rotating micro beams call for greater attention to study its free vibration behavior for both straight (without pre-twist) and pre-twisted configurations Also, keeping in view the existing and futuristic applications of FGMs, it is important to study the free vibration behavior of micro beams made of FGMs.

Here, in the present work, three studies have been carried out. The first one studies the free vibration behavior of a straight tapered rotating micro beam made of BFGM. The second one deals with the free vibration behavior of a pre-twisted tapered rotating micro beam made of BFGM. The last one deals with a homogeneous micro beam and presents how it behaves dynamically on application of a static force in the form of a uniformly distributed load. For the present thesis work, MCST is considered as the size-dependent theory, and Timoshenko beam theory (TBT) along with von Kármán type geometric nonlinearity are used for describing the strain-displacement relations. Voigt Law of volume fraction is considered to model the functional gradation, and Touloukian model of temperature-dependency of the mechanical properties are considered to incorporate the thermal environmental effect. The present models for various studies are validated with the available results in the literature for different reduced problems. The results are presented mostly in non-dimensional plane to study the effects of various important parameters on the free vibration behavior of micro beams.

1.2. Literature Review

Various researchers have investigated and reported the static and dynamic behavior of micro and nano beams over the past few years. A good amount of literature involving study of FGM beams, rotating classical and size-dependent beams using different methods of analysis are also available. In the following sub-sections, some of the notable works are presented in brief.

1.2.1. Mechanical Behavior of Micro and Nano Beams and Structures

In the last decade of the twentieth century, research works on static and dynamic behavior of micro and nano structural elements grew heavily. Several experimental studies were done on the size-dependent deformation of micron scale metals and polymers. Research investigation by Nix (1989) on thin films of metal, micro indentation study of Tungsten and Molybdenum single crystals by Stelmashenko et al. (1993), hardness study of single silver crystal by Ma and Clarke (1995), experiments to study strain gradient plasticity by Fleck et. al. (1994) and Lam and Chong (1999) for thin metals and polymers, all showed that the behavior cannot be explained by conventional continuum mechanics. Fleck and Hutchinson (1997) discussed the importance of strain gradient theory using the classical couple stress theory (Toupin, 1962; Mindlin and Tiersten, 1962; Koiter, 1964; Mindlin, 1964). Eringen (1983) developed nonlocal elasticity theory on the basis of conservation of momentum and moment of momentum and investigated micro scale continua. Anthoine (2000) showed the effect of couple stresses on pure bending of beams. Yang et al. (2002) developed a new couple stress based strain gradient theory. They simplified the classical couple stress theory by developing an additional equilibrium equation and used this modified theory, named as modified couple stress theory, to analyze pure bending of flat plate and torsion of cylindrical shaft. Beskou et al. (2003) investigated the bending and stability of beams using strain gradient theory and surface elasticity. Lam et al. (2003) modified the strain gradient theory to reduce the number of material length scale parameters from five to three to describe the size-dependent behavior and conducted experiments to validate the theory. Li et al. (2003) worked on micro/nano mechanical characterization of single crystal silicon and thin films of metals to determine their modulus of elasticity, hardness, scratch resistance and fracture toughness for designing MEMS/NEMS. Incorporating nonlocal elasticity theory, Peddieson et al. (2003) conducted study on Euler-Bernoulli beams.

These profound studies also resulted in more developments in analysis, application and fabrication of micro and nano beams and plates. Pei et al. (2004) used micro fabricated cantilevers for quantitative detection of blood glucose levels. McFarland and Colton (2005) fabricated polypropylene micro cantilevers to use them as sensors. Park and Gao (2006) developed a new model of Euler-Bernoulli beam using MCST by variational formulation of minimum potential energy principle. Kong et al. (2008) investigated the size-dependent natural frequency of Euler-Bernoulli beams using MCST and showed how the dynamic behavior is different from classical beams. Fabricating silicon micro cantilever beams of different sizes, experimental evaluations of Young's modulus, dimensional effects and failure modes were studied by Liu et al. (2008). Based on MCST, Ma et al. (2008) developed a Timoshenko beam model and predicted its size-dependent dynamic behavior. The study was based on Hamilton's principle and variational formulation, and it showed the necessity to employ Timoshenko beam model for analysis of micro beams. Park and Gao (2008) analytically solved simple shear problems using MCST. Kong et al. (2009) presented how the dynamic behavior of micro beams change with the change of thickness using strain gradient elasticity theory. Asghari et al. (2010) utilized method of multiple scales and perturbation techniques to determine the static and free vibration behavior of nonlinear Timoshenko micro beam. Experimental and analytical investigation of dimensional effects on mechanical behavior of a curved micro cantilever beam made of metallic alloy was done by Shooshtari et al. (2011). Tang and Alici (2011) experimentally evaluated material length scale factors of silicon micro cantilevers by micro indentation method. Based on strain gradient theory, Zhao et al. (2012) showed the effect of nonlinearity in dynamic behavior of nano beams. Ghayesh et al. (2013) constructed frequency response curve and showed the effect of different parameters on resonant dynamic response of micro beams using MCST, by studying its nonlinear vibration. The static deflection and pull-in voltage of electrostatically actuated silicon micro cantilever were evaluated by Kahrobaiyan et al. (2014) employing Timoshenko beam element and the results were compared to the experimental data and results based on finite element method (FEM). The effect of size dependent shear deformation on the behavior of microstructures-dependent beam based on MCST was investigated by Dehrouyeh-Semnani and Nikkhah-Bahrami (2015). Wang et al. (2015) accommodated von Kármán nonlinearity in nonlinear bending and thermal post buckling problem of micro scale beams. Attia and Mahmoud (2016) applied nonlocal elasticity and surface energy theories to model and analyze nano beams. Lei et al. (2016) experimentally showed the vibrational behavior of nickel micro cantilever beams. Liebold and Muller (2016) carried out a comparative study of strain gradient theory and micro polar theory both numerically and experimentally. Noori et al. (2016) used differential quadrature method (DQM) to analyze free vibration of Timoshenko and Euler-Bernoulli micro beams. Bambill et al. (2017) showed the implications of non-rigid realistic boundary conditions on the vibration characteristics of micro beams. Rajasekaran and Khaniki (2017) discussed the effect of different parameters like non-uniformity, non-local and strain gradient terms on natural frequency, buckling load and deformation of tapered micro beams. Thai et al. (2017) presented a comprehensive review of the size-dependent theories that are being used in the analyses of micro and nano structural elements. Li et al. (2018) investigated different modes of vibration of micro cantilever beams by experiment.

1.2.2. Mechanical Behavior of FGM Classical and Micro/Nano Beams

The concept of FGM was first introduced in 1984 in Japan during a space plane project. Yamanouchi et al. (1990) and Koizumi (1993) presented a detailed concept of FGMs, fabrication and their merits over conventional composites for mechanical structures in high-temperature environments and high speed spacecrafts. In 1991, FGM forum of Japan conducted a survey, listing many potential applications of FGM. It gained attention of the researchers very fast, and many important investigations have been done to easily manufacture the ceramic-metal FGM by continuously varying the volume fractions of the constituents (Fukui, 1991; Sata, 1993; Yamaoka et al., 1993; Rabin and Heaps, 1993). Different material gradation laws like power law, exponential law etc. and their effect on stress-strain constitutive relations were also explained by the researchers (Fuchiyama et al., 1993; Williamson et al., 1993; Fukui et al., 1993; Jin and Noda, 1993; Noda and Jin, 1993).

Goupee and Vel (2006) used element-free Galerkin approach and genetic algorithm to tailor volume fractions to optimize natural frequency of FGM beams. A study on static and free vibration behavior of functionally graded (FG) beam were conducted by Kapuria et al. (2008). In that study, a theoretical model using modified rule of mixtures for effective modulus of elasticity was validated by experiments on FG beams manufactured by powder metallurgy. Malekzadeh et al. (2009) used first order shear deformation theory (FSDT) to model a FG circular arch with temperature-dependent mechanical properties and implemented DQM to analyze its in-plane free vibration. Şimşek and Kocatürk (2009) presented a study on free and forced vibration of simply supported FG beams, subjected to concentrated moving harmonic load and discussed the effect of material distribution, velocity of the load and the excitation frequency on the dynamic responses of the beam. Mahi et al. (2010) analytically obtained the free vibration frequencies of FG beam for power, exponential and sigmoid law distribution of constituents. Ma and Lee (2011) discussed the nonlinear behavior of FG beams with in-plane thermal loading. Shahba et al. (2011a) investigated the free vibration behavior and stability of an AFGM beam by FEM. Zhang (2013) conducted nonlinear bending analysis of TFGM beams based on physical neutral surface and higher order shear deformation theory (HSDT). Esfahani et al. (2013) performed a non-linear thermal stability analysis of temperature-dependent FGM beams supported on non-linear hardening elastic foundations. Shen and Wang (2014) used both Voigt and Mori-Tanaka model of FG beams to determine nonlinear frequencies when the beam is resting on elastic foundation. Şimşek (2015) varied the material properties in both axial and thickness direction exponentially to model a BFGM beam and analyzed its dynamic behavior due to a moving load. Hao and Wei (2016) analyzed the influence of material gradation parameters on dynamic characteristics of BFGM beams. Pydah and Sabale (2017) analyzed the static behavior of BFGM curved beams based on Euler-Bernoulli theory (EBT). Reddy (2011) analyzed microstructure dependent mechanical behavior of TFGM beam using MCST, and von Kármán nonlinearity. MCST was also used by Asghari et al. (2011) to capture the small-scale size effect in static and free vibration behavior of Timoshenko beam. Li et al. (2017) investigated the buckling and free vibration of AFGM micro beam where non-local strain gradient theory was used to capture the size-effect. Mirjavadi et al. (2017) used MCST and DQM to analyze effect of non-uniform temperature gradient and porosity in a BFGM Timoshenko micro beam. Free vibration of TFGM micro beam was analyzed using MCST by Trinh et al. (2018) for arbitrary boundary conditions using state-space concept. Yang et al. (2018) used DQM to solve nonlinear vibration and bending problem associated with the BFGM nano beams applying nonlocal strain gradient theory.

1.2.3. Dynamic Behavior of Homogeneous Rotating Beams Based on Classical Theory

Anderson (1975) derived equations of motion of a bar rotating with constant velocity carrying a tip mass and also showed how the frequencies would increase monotonically with the increase in rotating velocity. Swaminathan and Rao (1977) showed how turbo-machinery blades could be modeled as pre-twisted tapered rotating cantilever beams and presented the effect of pre-twist and taperness on free vibration behavior. Wright et al. (1982) solved the frequencies and mode shapes for a rotating beam with varying mass distribution, varying flexural rigidity, tip mass and root offset. Free vibration of compact uniform rotating cantilever beams were investigated by Fox (1985) with taking account of centrifugal coupling between motions of principal planes. Yokoyama (1988) studied the in-plane and out-of-plane vibrations of Timoshenko beam with the help of FEM. Bazoune and Khulief (1992) formulated a finite beam element to analyze free vibration of tapered rotating beam. Naguleswaran (1994) described lateral vibration of rotating uniform Euler beam attached to a hub for various boundary conditions. Lin and Hsiao (2001) investigated the dynamic behavior of rotating Timoshenko beam with the help of virtual work principle, including the effect of Coriolis acceleration. Song et al. (2001) studied the effects of steady temperature gradient on the vibrational characteristics of a pre-twisted rotating thin walled anisotropic beam. Banerjee (2001) formulated a dynamic stiffness matrix to analyze the free vibration of a pre-twisted beam. Yoo et al. (2001) investigated the effect of various dimensionless parameters on the modal characteristics of a pre-twisted rotating cantilever beam. Lin and Lee (2002) analyzed forced vibration of pre-twisted Timoshenko beam with time-dependent elastic boundary conditions. Lin et al. (2003) derived the governing equation of motion for coupled bending-bending vibration of a pre-twisted rotating beam which is elastically restrained at the root and had a tip mass. Banerjee et al. (2006) studied the free vibration behavior of a rotating beam using dynamic stiffness method. Avramov et al. (2007) used Galerkin technique to derive equation of motion for flexural-flexural-torsional vibrations of rotating beams with asymmetric cross section. Ozgumus and Kaya (2007) used Hamilton's principle and differential transform method (DTM) for free vibration analysis of double-tapered Timoshenko beam and presented the coupling between flap-wise bending and torsional vibration. New interpolation functions were introduced by Gunda and Ganguli (2008) for finite element (FE) analysis of rotating beams. Elastic and post-elastic dynamic behavior of tapered rotating beam was presented by Das et al. (2009a). Lee et al. (2009) investigated the effect of precone angle on instability and vibration of rotating Timoshenko beam. Shavezipur and Hashemi (2009) applied refined dynamic finite element and Galerkin method to investigate the free vibration of centrifugally stiffened beams. Huang et al. (2010) investigated the natural frequency of coupled bending-axial-flapwise vibration of beams rotating at a high angular velocity. Nonlinear modal analysis was carried out by Arvin and Bakhtiari-Nejad (2011) using Hamilton's principle and Galerkin discretization method for rotating beams. Shahba et al. (2011b) introduced basic displacement functions to accurately predict the displacement fields of a rotating beam. The effects of hub radius, rotational speed and variable cross section were reported in the paper. Zhu (2012) investigated the free flap-wise vibration of rotating Timoshenko beam which was doubly-tapered. Bambill et al. (2013) applied DQM for solving modal characteristics of elastically clamped rotating Timoshenko beam. Banerjee and Kennedy (2014) illustrated the effect of Coriolis force on rotating beams using dynamic stiffness method. Spectral-Tchebychev technique was applied by Filiz et al. (2014) for solving three-dimensional dynamics of unconstrained pre-twisted beam. Kim and Chung (2016) proposed an accurate and efficient nonlinear model for rotating cantilever beams. Adair and Jaeger (2017) used modified adomian decomposition method (AMDM) and derived closed form solutions for mode shapes of pre-twisted rotating Euler-Bernoulli beams. Both geometric stiffening and softening effects of rotating cantilever beams were presented by Zhao et al. (2017) using energy principle.

1.2.4. Dynamic Behavior of FGM Rotating Beams Based on Classical Theory

Oh et al. (2003) modeled turbo-machinery blades as thin walled beams made of TFGM rotating in high-temperature field. They considered the material properties as temperature-dependent and analyzed the vibration numerically. Librescu et al. (2005) investigated the instability by flutter and divergence due to gyroscopic force of rotating thin walled beams in high-temperature field. The beam was considered as made of FGM and Mori-Tanaka scheme was applied to model the FGM. Fazelzadeh et al. (2006) investigated the dynamic behavior of rotating FG blades under high temperature supersonic gas flow using DQM and presented the effects of Mach number, rotating speed, geometric parameters and blade material properties on the natural frequencies of the blade. Piovan and Sampaio (2009) studied the geometric stiffening effect of high-speed rotation in case of a rotating TFGM beam. Shahba et al. (2011a) investigated the free vibration and stability of a tapered rotating AFGM beam and explained the effect of different parameters on frequencies and critical buckling load. Free vibration behavior of AFGM tapered beam was studied by Zarrinzadeh et al. (2012) for six boundary conditions by using FEM. Rajasekaran (2013) presented the variation of natural frequencies for different parameters for centrifugally loaded AFGM Timoshenko beam using DTM and DQM. Ramesh and Rao (2013) investigated the free vibration characteristics of a TFGM pre-twisted rotating beam and showed the effect of coupling between chord-wise and flap-wise modes using energy method. Shahba et al. (2013) obtained exact shape function using basic displacement functions for FE analysis of tapered rotating FG beams. Li et al. (2014) investigated the dynamic free vibration of rotating FGM beam. The results showed the effects of bending-stretching coupling and mode shift phenomena in chord-wise vibration. Ebrahimi and Mokhtari (2015) used semi-analytical DTM to analyze the transverse vibration for rotating porous FG Timoshenko beams. Dynamics of rotating AFGM tapered beams were studied based on a new dynamic model by using the B-spline method (BSM) by Li and Zhang (2015), considering the bending-stretching coupling. Maganti and Nalluri (2015) investigated the effect of material composition gradient, taper ratios, hub radius ratio and rotational speed on flap-wise bending natural frequencies of double-tapered rotating FG beams. Ebrahimi and Hashemi (2016) analyzed the free vibration characteristics of rotating double tapered FG Euler-Bernoulli beams made of porous materials using DTM. Oh and

Yoo (2016) presented a model of rotating pre-twisted tapered FG blades with the help of Rayleigh-Ritz assumed modes method and Kane's method. Das (2017) investigated in-plane and out-of-plane free bending vibration of FGM beam fixed to the inside of a rotating ream. Geometric nonlinearity and shear deformability was taken into account for critical buckling analysis in this work. Fang et al. (2018a) varied the material properties of FG beam in both thickness and axial directions and analyzed the dynamic stiffening effects for a rotating three-dimensional beam. Pal and Das (2017) studied the free vibration behavior of geometrically nonlinear rotating prismatic FG beams for different boundary conditions. Mazanoglu and Guler (2017) presented flexural vibration analysis for AFGM tapered beam rotating around a hub considering centrifugal stiffening. Pal and Das (2018) took a tangent stiffness based approach to describe the free vibration of geometrically nonlinear rotating double-tapered FG beams considering shear deformability and Coriolis force.

1.2.5. Dynamic Behavior of Homogeneous Rotating Micro/Nano Beams Based on Non-classical Theory

As various size-dependent theories are developed very recently, literature on theoretical investigation on rotating micro/nano beams are limited in number. Dehrouyeh-Semnani (2015) investigated the size effect on the flap-wise frequency of rotating micro-beams. Hamilton's principle and FSDT was used to model the problem and MCST was used to take care of the size-dependent behavior. Using MCST, Dehrouyeh-Semnani et al. (2016) developed finite elements for free vibration analysis of rotating beams employing EBT and TBT. Ilkhani and Hosseini-Hashemi (2016) investigated the free vibration and stability of rotating micro beam using MCST to model micro pump and turbine blades. MCST was implemented to study the lead-lag vibration of micro cantilever beams rotating around a hub and it was found that increase in angular velocity and hub radius, lessen the influence of the size-dependency on the flexural frequencies. Shafiei et al. (2017) studied the transverse vibration of rotating tapered micro beam for cantilever and propped cantilever boundary conditions. In that work, Euler-Bernoulli beam model and MCST were chosen for analysis and equation of motion was solved by DQM. Arvin (2017) compared Timoshenko and Euler-Bernoulli beam models in the analysis of free vibration of rotating micro beams.

Strain gradient theory was used to model the size-dependent behavior and DTM was used to solve coupled differential equations. The influence of material length scale, shear deformation, rotating speed and the slenderness ratio on the natural frequencies of flap-wise bending vibration of rotating micro Timoshenko beam were examined by Arvin (2018). Guo et al. (2018) investigated the vibro-buckling characteristics of rotating and axially moving nano beam using nonlocal strain gradient theory.

1.2.6. Dynamic Behavior of FGM Rotating Micro/Nano Beams Based on Non-classical Theory

Very few literatures can be found on the dynamic behavior of FG rotating micro/nano beams. Ghadiri and Shafiei (2016) investigated the free vibration behavior of TFGM rotating Timoshenko micro beam in a thermal environment. The material properties were taken as temperature-dependent and MCST was used to model the size-dependency of the structure. Results were presented explaining the effects of temperature changes, angular velocity, different boundary conditions, length scale parameter, FG index and thickness on the fundamental, second and third natural frequencies. Based on MCST and employing generalized differential quadrature element method (GDQEM), vibrational characteristics of tapered AFGM micro beam was also studied by Shafiei et al. (2016a). Shafiei et al. (2016b) modeled the rotating parts of micro motors as non-uniform TFG rotating micro beams and analyzed the size-dependent dynamic behavior. GDQEM and Hamilton's principle were used for governing equations, and MCST was used for considering the size-effect. Shenas et al. (2016) used modified strain gradient theory and FSDT to model pre-twisted FG rotating micro cantilever beam. The Chebyshev–Ritz method was used to derive the algebraic eigen-frequency equations and the effects of angular velocity, angle of twist along the axis, temperature rise, material gradient index and material length scale parameter on the free vibration were studied. Using DQM, Azimi et al. (2017) employed Eringen's nonlocal theory to investigate the vibration of AFGM rotating micro Timoshenko beam under in-plane nonlinear thermal loading. The centrifugal stiffening effects and chord-flap coupling in the vibration of rotary FG micro beam was studied by Fang et al. (2018b).

1.3. Mathematical Background

` In the present thesis work, energy principles of structural mechanics have been used as basis of mathematical formulation. Minimum total potential energy principle and Hamilton's principle are utilized to derive the governing equation for static and free vibration problems respectively. The solutions of the governing equations are obtained by approximating the displacement fields following Ritz method. For approximating the displacement fields, lowest order displacement functions are selected to satisfy the boundary conditions. Subsequently, higher order orthogonal admissible functions are generated using Gram-Schmidt orthogonalization algorithm. For analyzing the mechanics of rotating beams, the equations governing the relative motion are used. Various mathematical laws and principles followed in the thesis work are briefly described in the following section.

1.3.1. Minimum Total Potential Energy Principle

Static structural analysis of a continuous system like beam can be achieved by using minimum total potential energy principle. The governing equation of static equilibrium for computing deformations and in turn strains and stresses, are derived employing this principle. The principle of minimum total potential energy is defined as follows (Shames and Dym, 2009): A kinematically admissible displacement field, being related through some constitutive law to a stress field satisfying equilibrium requirements in a body acted on by statically compatible external loads, must extremize the total potential energy with respect to all other kinematically admissible displacement fields.

To be specific, total potential energy should be minimum for the equilibrium to be stable. So, the total potential energy is minimized to get the kinematically admissible displacement fields, i.e., the displacement fields which satisfy the geometric boundary conditions. After deriving the displacements, strain-displacement relationships are used to get the strain fields and constitutive relations are used to get the stress fields.

A mathematical representation of total potential energy can be given as,

$$\Pi = U_{se} + U_{wp} \tag{1.1}$$

where Π is the total potential energy, U_{se} is the strain energy generated in the structure due to deformation and U_{wp} is the work potential of the external load. Thus, the minimum total potential energy principle can be written as,

$$\delta(\Pi) = \delta\left(U_{se} + U_{wp}\right) = 0 \tag{1.2}$$

where δ is the variational operator.

1.3.2. Hamilton's Principle

Hamilton's principle is an important variational principle in structural dynamics. The Hamilton's principle can be expressed in the following form,

$$\int_{t_1}^{t_2} \delta(\zeta)\,dt = \int_{t_1}^{t_2} \delta\left(U_{ke} - U_{se} - U_{wp}\right)dt = 0 \tag{1.3}$$

where ζ called the Lagrangian, given by $U_{ke} - \Pi$. Here U_{ke} is the kinetic energy. Hamilton's principle states that of all the paths of admissible configurations that the body can take as it goes from configuration ‘1’ at time t_1 to configuration ‘2’ at time t_2, the path that satisfies Newton's law at each instant during the interval (and is thus the actual locus of configurations) is the path that extremizes the time integral of the Lagrangian $\zeta\left(= U_{ke} - U_{se} - U_{wp}\right)$ during the interval (Shames and Dym, 2009; Reddy, 2002).

1.3.3. Rayleigh-Ritz Method

Rayleigh Ritz method is one of the most useful approximate methods originating from variational considerations. In this method, the displacement field components of the total potential energy functional are replaced by approximate functions (Shames and Dym, 2009). If in a structural analysis problem, there are three displacement fields u_0, v_0 and w_0, then they are replaced by the approximate functions as follows:

$$\begin{aligned} u_0 &= \phi_0^u(x,y,z) + \sum_{i=1}^{n} a_j \phi_j^u(x,y,z) \\ v_0 &= \phi_0^v(x,y,z) + \sum_{i=1}^{n} b_j \phi_j^v(x,y,z) \\ w_0 &= \phi_0^w(x,y,z) + \sum_{i=1}^{n} c_j \phi_j^w(x,y,z) \end{aligned} \tag{1.4}$$

The functions with subscript '0' satisfy the kinematic boundary conditions of the problem. The remaining 3*n* functions are zero at the boundaries. Coefficients a_i, b_i, c_i are unknown coefficients. The scheme of Ritz method is to determine the values of these coefficients to minimize the total potential energy. When the values of the coefficients are thus determined, they are called Ritz coefficients. With the complete knowledge of the functions ϕ_j^u, ϕ_j^v and ϕ_j^w and if *n* tends to infinity, exact solutions for the problem can be achieved. But if *n* is finite or small, good approximations can be achieved by choosing ϕ_j^u, ϕ_j^v and ϕ_j^w wisely.

By replacing these functions in the total potential energy, a functional involving 3*n* unknowns are constructed. Now as per minimum total potential energy principle, the values of the unknown coefficients are to be calculated so as to make the potential energy minimum given as follows

$$\frac{\partial \Pi}{\partial a_j} = 0, \frac{\partial \Pi}{\partial b_j} = 0, \frac{\partial \Pi}{\partial c_j} = 0 \qquad j = 1, 2, ..., n \tag{1.5}$$

Then if a function $\phi_0(x, y, z)$ satisfies the boundary conditions of the problem so will $K\phi_0(x, y, z)$ where *K* is an arbitrary constant. Then following possible arrangement can be done for approximate displacement field components u_0, v_0 and w_0 to be used in the Ritz method:

$$\begin{aligned}
u_0 &= \left(\sum_{j=1}^{n} a_j\right)\phi_0^u(x, y, z) + \sum_{j=1}^{n} a_j \phi_j^u(x, y, z) \\
v_0 &= \left(\sum_{j=1}^{n} b_j\right)\phi_0^v(x, y, z) + \sum_{j=1}^{n} b_j \phi_j^v(x, y, z) \\
w_0 &= \left(\sum_{j=1}^{n} c_j\right)\phi_0^w(x, y, z) + \sum_{j=1}^{n} c_j \phi_j^w(x, y, z)
\end{aligned} \tag{1.6}$$

Now these equations can be rearranged as,

$$u_0 = \sum_{j=1}^{n} a_j \left(\phi_0^u + \phi_j^u\right) = \sum_{j=1}^{n} a_j \phi_j^u$$
$$v_0 = \sum_{j=1}^{n} b_j \left(\phi_0^v + \phi_j^v\right) = \sum_{j=1}^{n} b_j \phi_j^v \tag{1.7}$$
$$w_0 = \sum_{j=1}^{n} c_j \left(\phi_0^w + \phi_j^w\right) = \sum_{j=1}^{n} c_j \phi_j^w$$

1.3.4. Equations of Relative Motion in Rotating Coordinate Frame

Use of rotating reference axes greatly facilitates the solution of many problems in rotating structures where motion is generated within a system or observed from a system which itself is rotating. An example of such a motion is the movement of a fluid particle along the curved vane of a centrifugal pump, where the path relative to the vanes of the impeller becomes an important design consideration. The description of motion using rotating axes can be considered for plane motion of two particles A and B in the fixed $X-Y$ plane, as shown in Fig. 1.1. For the sake of generality, it is considered that the particles A and B are moving independently of one another. Now the motion of A is observed from a moving reference frame $x-y$ which has its origin attached to B and which rotates with an angular velocity $\Omega = \dot{\varphi}$. The angular velocity vector is given as $\vec{\Omega} = \Omega\hat{k}$, where the vector is normal to the plane of motion and where its positive sense is in the positive z-direction (out from the paper), as established by the right hand rule. Hence, the absolute position vector of A is given by

$$\vec{r}_A = \vec{r}_B + \vec{r} = \vec{r}_B + \left(x\hat{i} + y\hat{j}\right) \tag{1.8}$$

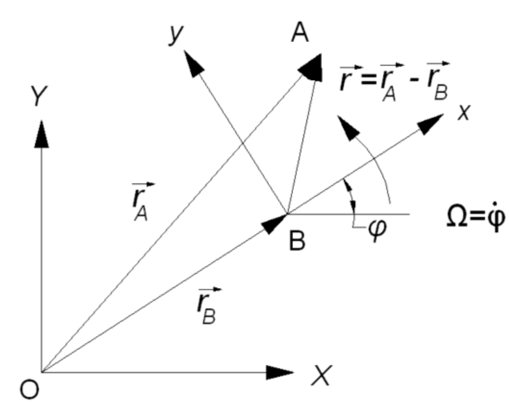

Fig. 1.1: Schematic diagram for motion of two particles *A* and *B*.

Relative Velocity: Taking the time derivative of the absolute position-vector equation for A, i.e., differentiation of Eq. (1.8) gives

$$\begin{aligned}\dot{\vec{r}}_A &= \dot{\vec{r}}_B + \frac{d}{dt}\left(x\hat{i} + y\hat{j}\right)\\ &= \dot{\vec{r}}_B + \left(x\dot{\hat{i}} + y\dot{\hat{j}}\right) + \left(\dot{x}\hat{i} + \dot{y}\hat{j}\right) \qquad (1.9)\end{aligned}$$

But $x\dot{\hat{i}} + y\dot{\hat{j}} = \vec{\Omega}\times x\hat{i} + \vec{\Omega}\times y\hat{j} = \vec{\Omega}\times\left(x\hat{i} + y\hat{j}\right) = \vec{\Omega}\times\vec{r}$ Also, since the observer in x-y measures velocity components $\dot{x}$ and $\dot{y}$, it is seen that $\dot{x}\hat{i} + \dot{y}\hat{j} = \vec{V}_{rel}$, which is the velocity of A relative to the x-y frame of reference. Thus, the relative-velocity equation becomes (Meriam and Kraige, 2013)

$$\vec{V}_A = \vec{V}_B + \vec{\Omega}\times\vec{r} + \vec{V}_{rel} \qquad (1.10)$$

Relative Acceleration**:** The relative-acceleration equation may be obtained by differentiating the relative-velocity relation, given by Eq. (1.10). Thus,

$$\vec{a}_A = \vec{a}_B + \dot{\vec{\Omega}}\times\vec{r} + \vec{\Omega}\times\dot{\vec{r}} + \dot{\vec{V}}_{rel} \qquad (1.11)$$

In the derivation of Eq. (1.9), we saw that

$$\dot{\vec{r}} = \frac{d}{dt}\left(x\hat{i} + y\hat{j}\right) = \left(x\dot{\hat{i}} + y\dot{\hat{j}}\right) + \left(\dot{x}\hat{i} + \dot{y}\hat{j}\right) = \vec{\Omega}\times\vec{r} + \vec{V}_{rel} \qquad (1.12)$$

Therefore, the third term on the right side of the acceleration equation becomes,

$$\vec{\Omega}\times\dot{\vec{r}} = \vec{\Omega}\times\left(\vec{\Omega}\times\vec{r} + \vec{V}_{rel}\right) = \vec{\Omega}\times\left(\vec{\Omega}\times\vec{r}\right) + \vec{\Omega}\times\vec{V}_{rel} \qquad (1.13)$$

With the aid of Eq. (1.9), the last term on the right side of the equation for $\vec{a}_A$ becomes

$$\begin{aligned}\dot{V}_{rel} &= \frac{d}{dt}\left(\dot{x}\hat{i} + \dot{y}\hat{j}\right) = \left(\dot{x}\dot{\hat{i}} + \dot{y}\dot{\hat{j}}\right) + \left(\ddot{x}\hat{i} + \ddot{y}\hat{j}\right)\\ &= \vec{\Omega}\times\left(\dot{x}\hat{i} + \dot{y}\hat{j}\right) + \left(\ddot{x}\hat{i} + \ddot{y}\hat{j}\right)\\ &= \vec{\Omega}\times\vec{V}_{rel} + \vec{a}_{rel} \qquad (1.14)\end{aligned}$$

Substituting this into the expression for $\vec{a}_A$ and collecting terms, the following is obtained:

$$\vec{a}_A = \vec{a}_B + \vec{\Omega}\times\left(\vec{\Omega}\times\vec{r}\right) + \dot{\vec{\Omega}}\times\vec{r} + 2\vec{\Omega}\times\vec{V}_{rel} + \vec{a}_{rel} \qquad (1.15)$$

1.4. FGM Modeling

An FGM material is an advanced composite, in which the proportions of constituents (usually metal and ceramic) vary smoothly and gives the structure better thermal resistance, corrosion resistance and toughness. In the present thesis work, the beam is modeled with bi-directional FGM (BFGM) where the material properties vary smoothly and continuously through thickness as well as in axial direction. This is achieved by varying the volume fractions of the two constituents. For a TFGM beam, the volume fraction of ceramic material (V_c) is usually varied in z direction (thickness) according to power law: $V_c = \left(\frac{z}{h}+\frac{1}{2}\right)^{k_t}$ where, h is the thickness of the structure and $k_t (0 \le k_t \le \infty)$ is the volume fraction exponent, which dictates the material variation profile through thickness. Changing the value of k_t generates an infinite number of composition distributions. In order to accurately model the material properties of FGMs, the properties must be temperature- and position-dependent. The position-dependency of properties can be achieved by several models. Two important and rigorously used models namely Voigt model and Mori-Tanaka model are described here (Shen, 2009).

Voigt Model: This model follows a simple rule of mixture. This does not consider the detailed microstructure. The effective material properties P_f of the FGM layer, like Young's modulus E_f, thermal expansion coefficient α_f, density ρ_f etc. can then be expressed as,

$$P_f = \sum_{j=1} P_j V_{f_j} \tag{1.16}$$

where P_j and V_{f_j} are the material properties and volume fractions of the constituent material *j*, and the sum of the volume fractions of all the constituent materials makes unity, i.e.,

$$\sum_{j=1} V_{f_j} = 1 \tag{1.17}$$

Mori-Tanaka Model: In this model, the effective material properties are evaluated based on the volume fraction distribution and the approximate shape of the dispersed phase. This scheme (Mori and Tanaka, 1973) is applicable for estimating the effective moduli to regions of the graded microstructure, which have a well-defined continuous matrix and a discontinuous particulate phase. According to this scheme, the effective local bulk modulus K_f, the shear modulus G_f, thermal expansion coefficient α_f and thermal conductivity κ_f obtained for a random distribution of isotropic particles in an isotropic matrix are given by,

$$
\begin{aligned}
&\frac{K_f - K_1}{K_2 - K_1} = \frac{V_2}{1+(1-V_2)\left(3(K_2-K_1)/(3K_1+4G_1)\right)} \\
&\frac{G_f - G_1}{G_2 - G_1} = \frac{V_2}{1+(1-V_2)\left((G_2-G_1)/(G_1+f_1)\right)} \\
&\frac{\alpha_f - \alpha_1}{\alpha_2 - \alpha_1} = \frac{(1/K_f)-(1/K_1)}{(1/K_2)-(1/K_1)} \\
&\frac{\kappa_f - \kappa_1}{\kappa_2 - \kappa_1} = \frac{V_2}{1+(1-V_2)\left((\kappa_2-\kappa_1)/3\kappa_1\right)}
\end{aligned}
\tag{1.18}
$$

K_1, G_1 and V_1 denote, respectively, the bulk modulus, the shear modulus, and the volume fraction of the matrix phase, whereas K_2, G_2, and V_2 denote the corresponding material properties and volume fraction of the particulate phase. It should be noted that

$$V_1 + V_2 = 1 \text{ and } f_1 = \frac{G_1(9K_1+8G_1)}{6(K_1+2G_1)}. \tag{1.19}$$

The temperature dependency of the FGM properties can be incorporated by the Touloukian model.

Touloukian Model: As FG structures are commonly used in high-temperature environment where changes in mechanical properties of the constituent materials are to be expected (Reddy and Chin, 1998), it is important to consider this temperature-dependency for accurately predicting of the mechanical behavior. Thus, the effective material properties are assumed to be temperature-dependent and can be expressed as a function of temperature (Touloukian, 1967) as follows,

$$P_j = P_0\left(P_{-1}T^{-1} + 1 + P_1T + P_2T^2 + P_3T^3\right) \tag{1.20}$$

where P_0, P_{-1}, P_1, P_2, and P_3 are the coefficients of temperature T (in K) and are unique to the constituent materials. In the present thesis work, Voigt model along with Touloukian temperature-dependency is considered. Also, for rotating beams, BFGM is used whereas for non-rotating beams, TFGM is used.

1.5. Modified Couple Stress Theory

As mentioned in the introduction, several theories have been developed in the recent past to accurately model the size-dependent behavior of micro and nano beams. In this regard, MCST is the mostly used theory by the researchers to study the mechanical behavior of micro beams. Yang et al. (2002) developed modified couple stress theory based on the original version of the couple stress theory (Toupin, 1962; Mindlin and Tiersen, 1962; Koiter, 1964; Mindlin, 1964) by introducing an additional equilibrium equation. This theory considers moments as fixed vector as opposed to free vectors, considered by classical continuum mechanics. According to this theory, the total strain energy (U_{se}) is determined as follows:

$$U_{se} = \frac{1}{2}\int_V (\boldsymbol{\sigma} : \boldsymbol{\varepsilon})\, dV + \frac{1}{2}\int_V (\mathbf{m} : \boldsymbol{\chi})\, dV \tag{1.21}$$

where the first part of the right hand side represents the strain energy due to classical stress ($\boldsymbol{\sigma}$) and strain ($\boldsymbol{\varepsilon}$) tensors, and the second part represents the strain energy due to couple stress ($\mathbf{m}$) and symmetric curvature tensors ($\boldsymbol{\chi}$). The symmetric curvature tensor $\boldsymbol{\chi}$ is given as,

$$\boldsymbol{\chi} = \frac{1}{2}\left[\nabla\vec{\theta} + \left(\nabla\vec{\theta}\right)^T\right] \tag{1.22}$$

where $\vec{\theta}$ is the rotation vector which is related to the displacement vector $\vec{u}$ as,

$$\vec{\theta} = \frac{1}{2}(\nabla \times \vec{u}) \tag{1.23}$$

Accordingly to MCST, a single material length scale parameter l is used to incorporate the size-effect. For isotropic and linear elastic materials, the three-dimensional relations between the classical stress and strain tensors, and between the couple stress and curvature tensors are given as follows:

$$\sigma_{ij} = 2\mu'\varepsilon_{ij} + \lambda'\delta_{ij}\varepsilon_{kk} \tag{1.24}$$

$$m_{ij} = 2\mu' l^2 \chi_{ij} \tag{1.25}$$

Here δ_{ij} is kronecker delta, and $\lambda' = \dfrac{E\nu}{(1+\nu)(1-2\nu)}$ and $\mu' = G = \dfrac{E}{2(1+\nu)}$ are Lame's constants (Yang et al., 2002; Reddy, 2011) where *E*, *G* and *v* being Young's modulus, shear modulus and Poisson's ratio respectively. Reddy (2011) showed that, for a problem involving micro beam, one-dimensional stress-strain relationship should be used for the classical stress-strain relations as opposed to the three-dimensional version given by Eq. (1.24).

1.6. Description of the Thesis Problems

In the present thesis, three problems involving the dynamic behavior of micro beams are addressed. In the first two problems, free vibration behaviors are investigated for BFGM tapered rotating micro beams for straight and pre-twisted geometry. The rotating beams are taken as cantilevers attached with a hub rotating with constant angular speed. This results in a time-invariant centrifugal loading for the micro beam. The third problem deals with the free vibration of homogeneous straight prismatic micro beam under a static uniformly distributed transverse loading.

All the problems are formulated in two steps. In the first step, the deformed configuration is evaluated using minimum total potential energy principle where the governing equations are solved using Ritz method. In the second step, Hamilton's principle is applied to formulate the governing equations for dynamic response. A tangent stiffness based method including geometric nonlinearity is employed to investigate the free vibration behavior in the neighborhood of the deformed configuration. In this step, an eigenvalue problem is formulated. The transformation to eigenvalue problem is direct for the third problem. But it requires to follow a state-space approach for the first two problems. The eigenvalue problem is solved using Ritz method. In all the three problems, the size-effect is incorporated using MCST. The FG beams are modeled using Voigt Law and Touloukian model is considered to incorporate the thermo-elastic changes in the material properties. In the results, the variation of free vibration frequencies for different parameters are shown and discussed.

As presented in the literature survey, there are very few literatures available, which deal with the straight and pre-twisted homogeneous and FGM rotating beams. It is also seen that studies on BFGM rotating beams for both straight and pre-twisted geometries are not available. This motivates to take up the first two problems for the present thesis work. Also the problem involving the free vibration behavior of statically loaded micro beams is not available in the literature. This motivates the selection of the third problem of the thesis. In this thesis work, a detailed and thorough study of the above-mentioned problems are presented.

1.6.1. Free Vibration Analysis of BFGM Straight Tapered Rotating Micro Beams

The first problem investigates the free vibration behavior of BFGM straight tapered rotating micro-beams at elevated thermal condition. The size-dependent behavior is addressed employing MCST. In this case, the through-thickness functional gradation is assumed to be symmetric about the mid-plane of the beam, where the beam is metal-rich at the core and ceramic-rich towards outer layers. This restricts the beam to bend under time-invariant centrifugal loading. Axial gradation is considered with metal at the hub end and ceramic towards the free end. von Kármán type geometric non-linearity is considered. The shear deformation effect is addressed within the framework of Timoshenko beam theory. The governing equations for determining the beam configuration under time-invariant centrifugal loading is non-linear in nature and is solved using iterative substitution method with successive relaxation. The mathematical formulation of free vibration problem considers the effects of Coriolis forces and spin-softening. The governing equation is transformed into a state-space problem resulting into an eigenvalue problem. The effect of constant centrifugal loading is taken into account in the dynamic problem by using the tangent stiffness (Das, 2016) in the neighborhood of the centrifugally deformed beam configuration. The mathematical formulation for this problem is reduced from that of the BFGM pre-twisted tapered rotating micro beam, by putting the pre-twist angle zero. It is to be mentioned that the bending vibratory motions taking place in-the-plane and out-of the-plane of rotation are respectively called chord-wise and flap-wise motions. The model is validated with some reduced problems that are available in the literature. For the results, the speed-frequency behaviors for each of the first two chord-wise and flap-wise modes are presented in non-dimensional plane to show the effects of various parameters like size-dependent thickness, axial and thickness gradation indices, taperness parameters, hub parameter, length-thickness ratio, operating temperature and FGM composition. Also the effect of size on shear deformation and that of geometric non-linearity are discussed separately.

1.6.2. Free Vibration Analysis of BFGM Pre-twisted Tapered Rotating Micro Beams

In the second problem, an improved mathematical model of BFGM pre-twisted tapered rotating micro beam is presented to investigate its free vibration behavior. Modeling of BFGM is considered as same as that of the previous problem. MCST is employed to incorporate the size effect. Based on Timoshenko beam theory, the displacement based mathematical formulation is developed in a global non-inertial frame with appropriate transformations for the global inertial frame and the local non-inertial frame. As explained for the previous problem, two interrelated steps are employed: first to determine the deformed configuration due to constant centrifugal loading using minimum total potential energy principle and second to get the free vibration behavior using Hamilton's principle. Tangent stiffness method is considered to incorporate the centrifugal stiffening effect for the vibrating beam and the governing equation is transformed into a state-space problem resulting into an eigenvalue problem. The beam model is validated with the available reduced problems. The coupling between chord-wise and flap-wise vibration is examined and mode-veering phenomena is reported. The effects of spin-softening, Coriolis acceleration and pre-twist angle are shown and discussed. The non-dimensional speed-frequency behaviors for the first four bending modes are presented for variations of different parameters such as size-dependent parameter, aspect ratio, material gradation indices, operating temperature, FGM constituent, slenderness parameter, taperness parameters and hub parameter.

1.6.3. Free Vibration Analysis of Homogeneous Straight Prismatic Micro Beam under Uniformly Distributed Transverse Load

The third problem investigates the free vibration behavior of micro beams which are subjected to uniformly distributed transverse loading. The beam is assumed to be homogeneous and of straight and prismatic geometry. The aim of the study is to determine the free vibration frequency at large deflected configuration for different classical boundary conditions. TBT along with von Kármán nonlinearity are employed to formulate the beam model and micro-size factor is incorporated based on MCST. In the first step, the beam configuration under static loading is obtained through a non-linear static problem employing minimum potential energy principle. In the subsequent step, the free vibration behavior of the statically deflected micro beam is investigated employing Hamilton's principle and using the tangent stiffness of the deflected configuration. The solutions of the governing equations are obtained following Ritz method by approximating the displacement fields. The beam model is validated with some reduced problems that are available in the literature. The results of first two vibration modes in nromalized frequency-amplitude plane are presented for beams with ends clamped, simply supported and clamped-simply supported.

1.7. Layout of the Thesis

The three problems mentioned in the previous section, are presented in detail in the subsequent chapters. Chapter 2 discusses the generalized mathematical formulation for investigating the free vibration behavior of BFGM pre-twisted tapered rotating micro beam. This mathematical formulation is valid for both the first and the second problems mentioned in section 1.6. It is worthwhile to mention here that if the pre-twist angle is put zero, the formulation of the first problem i.e., of straight beam is obtained. In Chapter 3, results for BFGM straight tapered rotating micro beams are presented and discussed, whereas, Chapter 4 presents and discusses the results for BFGM pre-twisted tapered rotating micro beams. Chapter 5 presents the entire problem of free vibration behavior of statically loaded homogeneous straight prismatic micro beam, starting from its mathematical formulation up to the presentation and discussion of results. Finally, Chapter 6 summarizes the theme of the present thesis, presents the significant findings and contributions of the thesis, and finally paves the way for future scope of the present thesis work.

1.8. Chapter Summary

This chapter presents the introductory discussion for the present thesis along with broader outlines on the applications and latest trends on micro and nano structures and FGMs. An extensive literature survey has been presented covering all the direct and allied fields related to the problems of the thesis. It presents brief discussions about the related mathematical laws and principles, and also the fundamentals of the modified couple stress theory and FGM modeling. It provides a quick but comprehensive overview of the problems that are dealt in this thesis work. At the end, the chapter-wise organization of the thesis is mentioned.

"This page is intentionally left blank"

Chapter 2

MATHEMATICAL FORMULATION FOR BFGM TAPERED ROTATING MICRO BEAM

2.1. Introduction

Mathematical formulation of the free vibration problem of BFGM tapered rotating micro-beam is presented in this chapter. As mentioned in the previous chapter, this formulation is presented for the BFGM pre-twisted tapered rotating micro beam problem. It is to be mentioned that if the value of the pre-twist angle is made zero, then it becomes the formulation for a BFGM straight tapered rotating micro beam. The pre-twisted beam is considered to be attached to a hub rotating at constant angular speed. A displacement based formulation is adapted and energy based methods are employed to derive the governing equations. The entire formulation is based within the frame-work of TBT to address the effects of shear deformation and rotary inertia. von Kármán type linear strain-displacement relationships for the classical strain tensor are considered to develop the generalized formulation. Further MCST is used to address the size-effect. It is to be noted that one-dimensional stress-strain relationships are used for the present micro beam-type problem (Reddy, 2011).

The problem is formulated in two different but interrelated steps. The first step deals with the deformation of the micro beam due to time-independent centrifugal loading and the governing equations are derived using minimum total potential energy principle. Ritz method is followed to discretize the governing differential equations and the system of non-linear governing equations is solved using iterative substitution technique with successive relaxation. In the second step, using Hamilton's principle, the governing equations for free vibration in the neighborhood of the deformed state are determined employing tangent stiffness of the centrifugally deformed configuration. It is worthwhile to mention that the effect of centrifugal stiffening is taken into consideration for the free vibration phenomenon through stretching-bending coupling with the aid of tangent stiffness matrix. In this case also, Ritz method is used to discretize the governing equations, which are then transformed to the state-space to formulate an eigenvalue problem. The solution of the eigenvalue problem provides the free vibration frequencies and the corresponding mode shapes.

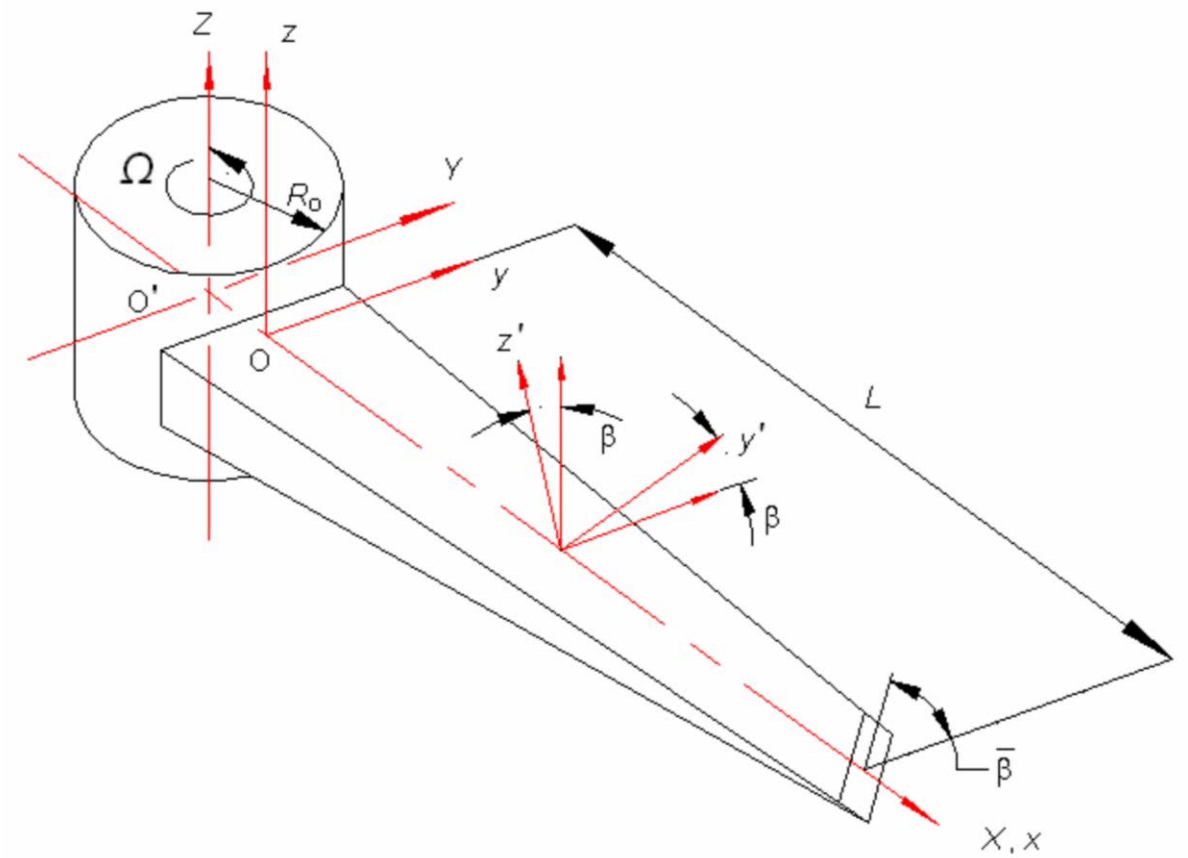

Fig. 2.1: Dimensions and axes of a pre-twisted rotating beam.

2.2. Theoretical Formulation

The generalized formulation is presented to investigate the free vibration behavior of a BFGM pre-twisted double-tapered rotating micro beam. The pre-twisted beam of length L is fixed to a hub of radius R_O, which is considered to be rotating with constant angular speed Ω as shown Fig. 2.1. $X-Y-Z$ is an inertial reference frame originated at the hub centre O' where Z-axis is perpendicular to the plane of rotation. $x-y-z$ is a global non-inertial frame, originated at the hub end of the beam O and parallel to the inertial $X-Y-Z$ frame.

$x-y'-z'$ is a local non-inertial frame, where y' and z' are the two principal axes along the local width and thickness directions respectively. Both $x-y-z$ and $x-y'-z'$ rotates with constant angular speed Ω. The cross section of the tapered beam is rectangular and the width and thickness at any location on axis x are given by $b(x)=b_{max}\left(1-C_b\frac{x}{L}\right)$ and $h(x)=h_{max}\left(1-C_h\frac{x}{L}\right)$. Here C_b and C_h $\left(0\le C_b, C_h<1\right)$ are the taperness parameters for the width and thickness respectively defined as $C_b=1-\left(b_{min}/b_{max}\right)$ and $C_h=1-\left(h_{min}/h_{max}\right)$; $\left(b_{max}, h_{max}\right)$ are the maximum values of width and thickness of the beam respectively at hub end and $\left(b_{min}, h_{min}\right)$ are its minimum values at free end. Putting $C_b=C_h=0$, a prismatic beam is obtained.

The total pre-twist angle over the entire beam length is $\bar{\beta}$. Assuming uniform axial twist, the pre-twist angle at any axial location x is $\beta=\bar{\beta}x/L$. A straight beam can be obtained by setting $\bar{\beta}$ =0. Due to uniform axial twist, we have

$$\frac{d\beta}{dx}=\bar{\beta}/L=\text{constant} \tag{2.1}$$

The transformation equations between the local (principal) and global non-inertial coordinates and vice versa at any axial location x are given as follows:

$$\begin{Bmatrix} y \\ z \end{Bmatrix}=\left[R\right]\begin{Bmatrix} y' \\ z' \end{Bmatrix}, \text{where } \left[R\right]=\begin{bmatrix} \cos\beta & \text{-}\sin\beta \\ \sin\beta & \cos\beta \end{bmatrix} \tag{2.2a}$$

$$\begin{Bmatrix} y' \\ z' \end{Bmatrix}=\left[R\right]^{-1}\begin{Bmatrix} y \\ z \end{Bmatrix}, \text{where } \left[R\right]^{-1}=\begin{bmatrix} \cos\beta & \sin\beta \\ \text{-}\sin\beta & \cos\beta \end{bmatrix} \tag{2.2b}$$

Using (2.1) and (2.2), the gradients of the local coordinates with respect to the global ones can be derived as:

$$\frac{\partial y'}{\partial x}=\bar{\beta}z'/L,\ \frac{\partial y'}{\partial y}=\cos\beta,\ \frac{\partial y'}{\partial z}=\sin\beta \tag{2.3a}$$

$$\frac{\partial z'}{\partial x}=-\bar{\beta}y'/L,\ \frac{\partial z'}{\partial y}=-\sin\beta,\ \frac{\partial z'}{\partial z}=\cos\beta \tag{2.3b}$$

Table 2.1: Temperature coefficients of different FGM constituents

Constituent	Property	P_0	P_{-1}	P_1	P_2	P_3
Stainless Steel (SUS304)	E (Pa)	201.04×10^9	0	3.079×10^{-4}	-6.534×10^{-7}	0
	υ	0.3262	0	-2.002×10^{-4}	3.797×10^{-7}	0
	ρ (kg/m^3)	8166	0	0	0	0
Titanium Alloy (Ti-6Al-4V)	E (Pa)	122.56×10^9	0	-4.586×10^{-4}	0	0
	υ	0.2884	0	1.121×10^{-4}	0	0
	ρ (kg/m^3)	4429	0	0	0	0
Silicon Nitride (Si_3N_4)	E (Pa)	348.43×10^9	0	-3.070×10^{-4}	2.160×10^{-7}	-8.946×10^{-11}
	υ	0.2400	0	0	0	0
	ρ (kg/m^3)	2730	0	0	0	0
Alumina (Al_2O_3)	E (Pa)	349.55×10^9	0	-3.853×10^{-4}	4.027×10^{-7}	-1.673×10^{-10}
	υ	0.2600	0	0	0	0
	ρ (kg/m^3)	3750	0	0	0	0
Zirconia (ZrO_2)	E (Pa)	244.27×10^9	0	-1.371×10^{-3}	1.214×10^{-6}	-3.681×10^{-10}
	υ	0.2882	0	1.133×10^{-4}	0	0
	ρ (kg/m^3)	3000	0	0	0	0

2.2.1. FGM Modeling

The beam material is considered as functionally graded in both the z' (local thickness) and x (axial) directions. The metal and ceramic constituents follow a power law variations of volume fractions to constitute the FGM. So, following Voigt model (Shen,

2009) and using Eq. (1.16), the generalized material property (P_f) at any location of the beam can be given as

$$P_f\left(x,z'\right)=P_cV_c+P_mV_m \tag{2.4}$$

Here the volume fraction of ceramic (V_c) according to a power law is given as follows:

$$V_c=\left|\frac{z'}{h/2}\right|^{k_t}\times\left(\frac{x}{L}\right)^{k_l} \tag{2.5}$$

where k_t and k_l are power law indexes $\left(0\le k_l\,,k_t\le\infty\right)$ in thickness and axial directions respectively. The variation of volume fraction of ceramic in thickness direction is taken so that the material properties are symmetric about the *x* axis. As per Eq. (1.17), the volume fraction of metal is, $V_m=1-V_c$.

So, P_f becomes

$$P_f\left(x,z'\right)=P_m+\left(P_c-P_m\right)\times\left|\frac{z'}{h/2}\right|^{k_t}\times\left(\frac{x}{L}\right)^{k_l} \tag{2.6}$$

This equation implies that, in the thickness direction, the beam is metallic at the mid plane $\left(z=0\right)$ and gradually becomes ceramic-rich at the upper and lower layers $\left(z=\pm h_{\max}/2\right)$. And in the axial direction, the beam is metallic at the hub end and becomes ceramic-rich at the free end. In (2.6), putting $k_l=k_t=0$ yields a homogeneous ceramic beam and putting $k_l=k_t=\infty$ yields a homogeneous metallic beam.

The mechanical properties like Young's modulus $\left(E_f\right)$, Poisson's ratio $\left(\nu_f\right)$ and density $\left(\rho_f\right)$ of the BFGM are taken as a function of temperature following Touloukian model (Shen, 2009) given as

$$P_j=P_0\left(P_{-1}T^{-1}+1+P_1T+P_2T^2+P_3T^3\right) \tag{1.20}$$

where P_0, P_{-1}, P_1, P_2 and P_3 are the coefficients of temperature T (in K) , which are given in Table 1 for various metal and ceramic constituents that are used as beam material in this thesis work (Reddy and Chin, 1998). The shear modulus $\left(G_f\right)$ is determined using the relation $G_f = E_f / \left\{2\left(1+\upsilon_f\right)\right\}$.

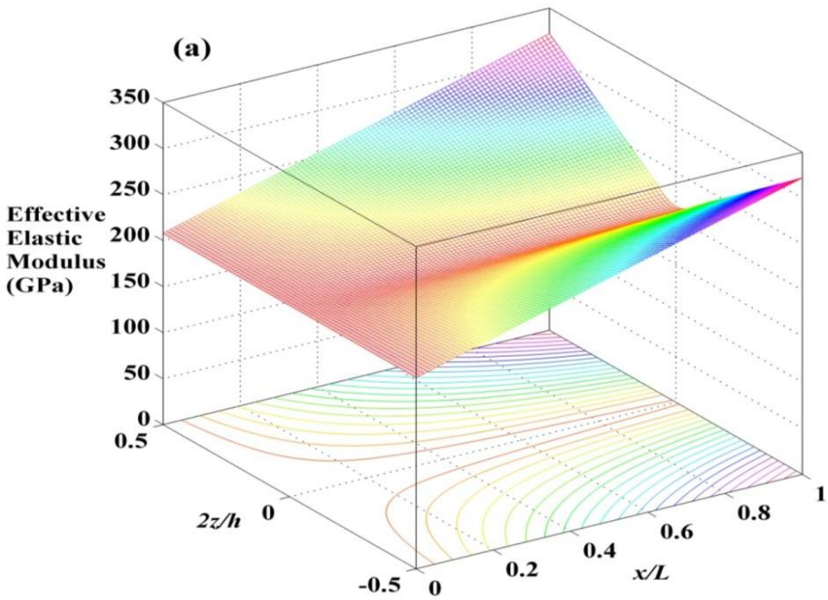

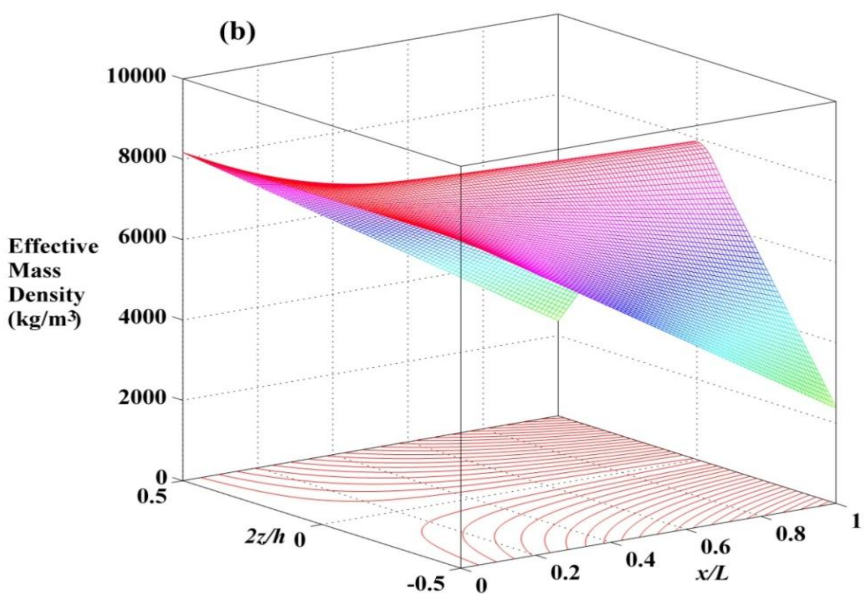

Fig. 2.2: Surface plots showing variation of effective material properties of Stainless Steel/Silicon Nitride beam over axial and thickness directions for k_l =1.0, k_t =1.0 and T_f =300 K: **(a)** Elastic modulus and **(b)** Mass density.

Surface plots are presented in Figs. 2.2(a) and (b) to show the variation of effective Young's modulus and density respectively along the thickness and axial directions for Stainless Steel/Silicon Nitride composition. The plots are generated at ambient temperature ($T = T_0$ =300 K) considering k_l =1.0, k_t =1.0. It is important to mention here that, the increase in operating temperature only results in degradation of material properties. As the beam properties are symmetric about the x axis and the boundary condition is clamped-free, temperature increment allows free expansion of the beam, without resulting any thermal stress.

2.2.2. Displacement, Strain and Curvature fields

In the present thesis work, displacement based mathematical formulation is employed. The formulation is based on non-inertial global coordinate system ($x-y-z$) where any point $Q(x,y',z')$ is referenced in non-inertial local coordinate system ($x-y'-z'$). Following TBT, the displacement fields along the x, y and z directions respectively are given by

$$
\begin{aligned}
u(x,y,z,t) &= u_0 - y'\psi_z'(x,t) + z'\psi_y'(x,t) \\
&= u_0(x,t) - y'\left\{-\psi_y(x,t)\sin\beta + \psi_z(x,t)\cos\beta\right\} + z'\left\{\psi_y(x,t)\cos\beta + \psi_z(x,t)\sin\beta\right\} \\
v(x,y,z,t) &= v_0(x,t) \\
w(x,y,z,t) &= w_0(x,t)
\end{aligned}
\tag{2.7}
$$

where u_0, v_0 and w_0 are the mid-plane displacements along the x, y and z directions respectively; ψ_y', ψ_z' are the cross sectional rotations about the y' and z' directions respectively; ψ_y, ψ_z are the cross sectional rotations about the y and z directions respectively. It is worthwhile to mention that these rotation variables about the local and global axes are related to each other using Eqs. (2.2a) and (2.2b). Hence, the displacement $\left(\vec{s}_Q\right)$ and position $\left(\vec{R}_Q\right)$ vectors of $Q(x,y',z')$ in global frame are given by

$$
\vec{s}_Q = \left\{u_0 - y'\left(-\psi_y\sin\beta + \psi_z\cos\beta\right) + z'\left(\psi_y\cos\beta + \psi_z\sin\beta\right)\right\}\hat{i} + \left(v_0\right)\hat{j} + \left(w_0\right)\hat{k} \tag{2.8a}
$$

$$\vec{R}_Q = (x+u)\hat{i} + (y+v)\hat{j} + (z+w)\hat{k}$$

$$= \left\{ x + u_0 - y'\left(-\psi_y \sin\beta + \psi_z \cos\beta\right) + z'\left(\psi_y \cos\beta + \psi_z \sin\beta\right)\right\}\hat{i} \tag{2.8b}$$

$$+\left(y'\cos\beta - z'\sin\beta + v_0\right)\hat{j} + \left(y'\sin\beta + z'\cos\beta + w_0\right)\hat{k}$$

Considering geometric non-linearity, the classical strain fields in global frame (non-inertial) of reference are derived to the following form:

$$\begin{aligned}\varepsilon_x &= \frac{\partial u}{\partial x} + \frac{1}{2}\left(\frac{\partial u}{\partial x}\right)^2 + \frac{1}{2}\left(\frac{\partial v}{\partial x}\right)^2 + \frac{1}{2}\left(\frac{\partial w}{\partial x}\right)^2 \\ &= \left\{\frac{\partial u_0}{\partial x} - y'\left(-\frac{\partial \psi_y}{\partial x}\sin\beta + \frac{\partial \psi_z}{\partial x}\cos\beta\right) + z'\left(\frac{\partial \psi_y}{\partial x}\cos\beta + \frac{\partial \psi_z}{\partial x}\sin\beta\right)\right\} \\ &+ \left\{\frac{\partial u_0}{\partial x} - y'\left(-\frac{\partial \psi_y}{\partial x}\sin\beta + \frac{\partial \psi_z}{\partial x}\cos\beta\right) + z'\left(\frac{\partial \psi_y}{\partial x}\cos\beta + \frac{\partial \psi_z}{\partial x}\sin\beta\right)\right\}^2 \\ &+ \frac{1}{2}\left(\frac{\partial v_0}{\partial x}\right)^2 + \frac{1}{2}\left(\frac{\partial w_0}{\partial x}\right)^2\end{aligned} \tag{2.9a}$$

$$\begin{aligned}\gamma_{xy} &= \frac{\partial u}{\partial y} + \frac{\partial v}{\partial x} + \frac{\partial u}{\partial x}\frac{\partial u}{\partial y} + \frac{\partial v}{\partial x}\frac{\partial v}{\partial y} \\ &= \frac{\partial v_0}{\partial x} - \psi_z\end{aligned} \tag{2.9b}$$

$$\begin{aligned}\gamma_{xz} &= \frac{\partial u}{\partial z} + \frac{\partial w}{\partial x} + \frac{\partial u}{\partial x}\frac{\partial u}{\partial z} + \frac{\partial w}{\partial x}\frac{\partial w}{\partial z} \\ &= \frac{\partial w_0}{\partial x} + \psi_y\end{aligned} \tag{2.9c}$$

It is to be noted that the displacement fields given by (2.7) along with the relations (2.1), (2.3a) and (2.3b) are used to obtain the simplified form of the strain fields given by (2.9a)-(2.9c). It is to be noted that the expressions $\frac{1}{2}\left(\frac{\partial v}{\partial x}\right)^2$ and $\frac{1}{2}\left(\frac{\partial w}{\partial x}\right)^2$ are von Kármán type strain-displacement relations used (2.9a)

Defining the rotation vector ($\vec{\theta}$) as $\vec{\theta} = \frac{1}{2}\left(\nabla \times \vec{s}_Q\right)$ and using the relations (2.3a) and (2.3b), its components in global frame are derived as follows:

$$\begin{aligned}
\theta_x &= \frac{1}{2}\left(\frac{\partial w}{\partial y}-\frac{\partial v}{\partial z}\right)=0 \\
\theta_y &= \frac{1}{2}\left(\frac{\partial u}{\partial z}-\frac{\partial w}{\partial x}\right)=\frac{1}{2}\left(-\frac{\partial w_0}{\partial x}+\psi_y\right) \\
\theta_z &= \frac{1}{2}\left(\frac{\partial v}{\partial x}-\frac{\partial u}{\partial y}\right)=\frac{1}{2}\left(\frac{\partial v_0}{\partial x}+\psi_z\right)
\end{aligned} \tag{2.10}$$

Using (2.10), the components of the curvature tensor, given by $\boldsymbol{\chi}=\frac{1}{2}\left[\nabla\vec{\theta}+\left(\nabla\vec{\theta}\right)^T\right]$, are derived to the following form:

$$\begin{aligned}
&\chi_{xx}=\chi_{yy}=\chi_{zz}=\chi_{yz}=\chi_{zy}=0 \\
&\chi_{xy}=\chi_{yx}=\frac{1}{4}\left(-\frac{\partial^2 w_0}{\partial x^2}+\frac{\partial \psi_y}{\partial x}\right) \\
&\chi_{xz}=\chi_{zx}=\frac{1}{4}\left(\frac{\partial^2 v_0}{\partial x^2}+\frac{\partial \psi_z}{\partial x}\right)
\end{aligned} \tag{2.11}$$

Considering linear elastic material behavior and using the one-dimensional stress-strain relation (Reddy, 2011), the non-zero components of the classical stress tensor $\left(\sigma_{xx},\sigma_{xy},\sigma_{xz}\right)$ are given by

$$\sigma_{xx}=E_f\varepsilon_x,\ \sigma_{xy}=k_sG_f\gamma_{xy},\ \sigma_{xz}=k_sG_f\gamma_{xz} \tag{2.12}$$

where k_s is the shear correction factor used to account for the non-uniformity of shear stress across the width and thickness of the section. In the present work, k_s =5/6 (Shafiei et al., 2016b) is considered. Employing MCST, the non-zero components of couple stress tensor $\left(m_{xy},m_{xz}\right)$ are given by,

$$m_{xy}=2G_fl^2\chi_{xy},\ m_{xz}=2G_fl^2\chi_{xz} \tag{2.13}$$

where l is the material length scale parameter that incorporates the size-effect. As the values of l for the FGM constituents considered are not available in the literature, it is taken to be constant for the present work.

For the clamped-free configuration of the rotating beam having through-thickness symmetric material gradation, the temperature rise of the beam to T_f will not induce any bending of the beam and also it is assumed that the beam will undergo free thermal expansion without generation of any axial stress. The effect of high-temperature would be due to the thermo-elastic change in the material properties.

2.2.3. Derivation of Strain Energy

According to MCST (Yang et al., 2002), the classical stress $(\boldsymbol{\sigma})$ and strain $(\boldsymbol{\varepsilon})$ tensors contribute to the classical strain energy whereas the symmetric couple stress $(\mathbf{m})$ and curvature $(\boldsymbol{\chi})$ tensors contribute to the non-classical strain energy. Knowing the components the classical stress and strain tensors, and the symmetric couple stress and curvature tensors, the classical and non-classical strain energies are derived to following form:

$$
\begin{aligned}
U_{se}^{cl} &= \frac{1}{2}\int_V (\boldsymbol{\sigma}:\boldsymbol{\varepsilon})\,dV \\
&= \int_0^L A_1\left[\frac{1}{2}\left(\frac{\partial u_0}{\partial x}\right)^2 + \frac{1}{2}\frac{\partial u_0}{\partial x}\left(\frac{\partial v_0}{\partial x}\right)^2 + \frac{1}{2}\frac{\partial u_0}{\partial x}\left(\frac{\partial w_0}{\partial x}\right)^2 + \frac{1}{4}\left(\frac{\partial v_0}{\partial x}\frac{\partial w_0}{\partial x}\right)^2\right. \\
&\quad \left. + \frac{1}{4}\left(\frac{\partial u_0}{\partial x}\frac{\partial v_0}{\partial x}\right)^2 + \frac{1}{4}\left(\frac{\partial u_0}{\partial x}\frac{\partial w_0}{\partial x}\right)^2\right]dx \\
&\quad + \int_0^L A_2\left[\frac{1}{4}\left(\frac{\partial \psi_z}{\partial x}\right)^2(1+\cos 2\beta) + \frac{1}{4}\left(\frac{\partial \psi_y}{\partial x}\right)^2(1-\cos 2\beta) - \frac{1}{2}\frac{\partial \psi_z}{\partial x}\frac{\partial \psi_y}{\partial x}(\sin 2\beta)\right]dx \\
&\quad + \int_0^L A_3\left[\frac{1}{4}\left(\frac{\partial \psi_z}{\partial x}\right)^2(1-\cos 2\beta) + \frac{1}{4}\left(\frac{\partial \psi_y}{\partial x}\right)^2(1+\cos 2\beta) + \frac{1}{2}\frac{\partial \psi_z}{\partial x}\frac{\partial \psi_y}{\partial x}(\sin 2\beta)\right]dx \\
&\quad + k_s\int_0^L B_1\left[\frac{1}{2}\left(\frac{\partial v_0}{\partial x}\right)^2 + \frac{1}{2}\left(\frac{\partial w_0}{\partial x}\right)^2 + \frac{1}{2}(\psi_z)^2 + \frac{1}{2}(\psi_y)^2 - \frac{\partial v_0}{\partial x}\psi_z + \frac{\partial w_0}{\partial x}\psi_y\right]dx
\end{aligned}
\tag{2.14a}
$$

$$
\begin{aligned}
U_{se}^{ncl} &= \frac{1}{2}\int_V (\mathbf{m}:\boldsymbol{\chi})\,dV \\
&= \frac{l^2}{8}\int_0^L B_1\left[\left(\frac{\partial^2 v_0}{\partial x^2}\right)^2 + \left(\frac{\partial^2 w_0}{\partial x^2}\right)^2 + \left(\frac{\partial \psi_z}{\partial x}\right)^2 + \left(\frac{\partial \psi_y}{\partial x}\right)^2 + 2\frac{\partial^2 v_0}{\partial x^2}\frac{\partial \psi_z}{\partial x} - 2\frac{\partial^2 w_0}{\partial x^2}\frac{\partial \psi_y}{\partial x}\right]dx
\end{aligned}
\tag{2.14b}
$$

where V denotes volume. The stiffness coefficients used in (2.14a) and (2.14b) are defined as follows:

$$A_1(x) = b(x)\int_{-h(x)/2}^{+h(x)/2} E_f dz',\ A_2(x) = \frac{\{b(x)\}^3}{12}\int_{-h(x)/2}^{+h(x)/2} E_f dz',$$
$$A_3(x) = b(x)\int_{-h(x)/2}^{+h(x)/2} (z')^2 E_f dz', B_1(x) = b(x)\int_{-h(x)/2}^{+h(x)/2} G_f dz' \tag{2.15}$$

As the principal directions (y' and z') are axes of symmetry and material gradation is symmetric along the z' direction, the following simplifications are considered to derive (2.14a) and (2.14b):

$$\int_{-b(x)/2}^{b(x)/2}\int_{-h(x)/2}^{+h(x)/2} E_f y'dy'dz' = 0,\ \int_{-b(x)/2}^{b(x)/2}\int_{-h(x)/2}^{+h(x)/2} E_f z'dy'dz' = 0,\ \int_{-b(x)/2}^{b(x)/2}\int_{-h(x)/2}^{+h(x)/2} E_f y'z'dy'dz' = 0 .$$

2.2.4. Derivation of Work Potential

The beam is subjected to time-independent centrifugal force due to rotation under constant angular speed. The angular speed and hub radius in vector form are given as $\vec{\Omega} = \Omega\hat{k}$ and $\vec{R}_O = R_O\hat{i}$ respectively and accordingly, the constant (time-independent) absolute acceleration of any point $Q(x, y', z')$ is given as $\vec{\Omega}\times\left\{\vec{\Omega}\times\left(\vec{R}_O + \vec{R}_Q\right)\right\}$ (the first two terms of (1.15)). Hence the intensity of the constant inertia force (per unit volume) is derived as follows:

$$\begin{aligned}\vec{f}_i &= -\rho_f\left[\vec{\Omega}\times\left\{\vec{\Omega}\times\left(\vec{R}_O + \vec{R}_Q\right)\right\}\right]\\ &= \rho_f\Omega^2\left[\left\{R_O + x + u_0 - y'\left(-\psi_y\sin\beta + \psi_z\cos\beta\right) + z'\left(\psi_y\cos\beta + \psi_z\sin\beta\right)\right\}\hat{i}\right.\\ &\quad\left. + \left(y'\cos\beta - z'\sin\beta + v_0\right)\hat{j}\right]\end{aligned} \tag{2.16}$$

So the work potential of the centrifugal force can be derived as:

$$U_{wp} = -\int_V\left\{\int_s \vec{f}_i\cdot d\vec{s}\right\}dV$$

$$= -\Omega^2\left[\int_0^L C_1\left\{u_0\left(R_0 + x\right)\right\}dx\right]$$

$$-\Omega^2\left[\frac{1}{2}\int_0^L C_1\left\{u_0^2 + v_0^2\right\}dx + \frac{1}{4}\int_0^L C_2\left\{\psi_z^2\left(1+\cos 2\beta\right) + \psi_y^2\left(1-\cos 2\beta\right)dx\right.\right.$$

$$-2\psi_z\psi_y \sin 2\beta\Big\} dx + \frac{1}{4}\int_0^L C_3 \left\{\psi_z^2\left(1-\cos 2\beta\right)+\psi_y^2\left(1+\cos 2\beta\right)+2\psi_z\psi_y \sin 2\beta\right\} dx \Bigg] \quad (2.17)$$

where the inertia coefficients can be defined as:

$$C_1\left(x\right)=b\left(x\right)\int_{-h(x)/2}^{+h(x)/2}\rho_f\,dz',\; C_2\left(x\right)=\frac{\left\{b\left(x\right)\right\}^3}{12}\int_{-h(x)/2}^{+h(x)/2}\rho_f\,dz',$$
$$C_3\left(x\right)=b\left(x\right)\int_{-h(x)/2}^{+h(x)/2}\left(z'\right)^2\rho_f\,dz' \quad (2.18)$$

Due to symmetric nature of the principal axes and material gradation, the following simplifications are considered to derive (2.17):

$$\int_{-b(x)/2}^{b(x)/2}\int_{-h(x)/2}^{+h(x)/2}\rho_f\,y'dy'dz'=0,\; \int_{-b(x)/2}^{b(x)/2}\int_{-h(x)/2}^{+h(x)/2}\rho_f\,z'dy'dz'=0,\; \int_{-b(x)/2}^{b(x)/2}\int_{-h(x)/2}^{+h(x)/2}\rho_f\,y'z'dy'dz'=0.$$

2.2.5. Derivation of Kinetic Energy

The velocity vector of any point $Q\left(x,y',z'\right)$ in global non-inertial frame rotating with uniform velocity $\vec{\Omega}$ is given as, $\dot{\vec{R}}_Q=\frac{\partial\vec{s}_Q}{\partial t}$. Thus its absolute velocity vector ($\vec{q}_Q$) is obtained as (using relation (1.10)):

$$\vec{q}_Q=\left\{\vec{\Omega}\times\left(\vec{R}_O+\vec{R}_Q\right)\right\}+\dot{\vec{R}}_Q$$
$$=\left[\dot{u}_0-y'\left(-\dot{\psi}_y\sin\beta+\dot{\psi}_z\cos\beta\right)+z'\left(\dot{\psi}_y\cos\beta+\dot{\psi}_z\sin\beta\right)-\Omega(y'\cos\beta-z'\sin\beta+v_0)\right]\hat{i}$$
$$+\left[\dot{v}_0+\Omega\left\{R_0+x+u_0-y'\left(-\psi_y\sin\beta+\psi_z\cos\beta\right)+z'\left(\psi_y\cos\beta+\psi_z\sin\beta\right)\right\}\right]\hat{j}+\left[\dot{w}_0\right]\hat{k} \quad (2.19)$$

A dot $(\cdot)$ over any parameter symbolizes its rate of change with time. The complete expression of kinetic energy (U'_{ke}) of the rotating beam is derived as follows:

$$U'_{ke}=\frac{1}{2}\int_V\rho_f\left(\vec{q}_Q\cdot\vec{q}_Q\right)dV$$
$$=\Bigg[\frac{1}{2}\int_0^L C_1\left(\dot{u}_0^2+\dot{v}_0^2+\dot{w}_0^2\right)dx+\frac{1}{4}\int_0^L C_2\Big\{\dot{\psi}_z^2\left(1+\cos 2\beta\right)+\dot{\psi}_y^2\left(1-\cos 2\beta\right)$$
$$-2\dot{\psi}_z\dot{\psi}_y\left(\sin 2\beta\right)\Big\}dx+\frac{1}{4}\int_0^L C_3\left\{\dot{\psi}_z^2\left(1-\cos 2\beta\right)+\dot{\psi}_y^2\left(1+\cos 2\beta\right)+2\dot{\psi}_z\dot{\psi}_y\left(\sin 2\beta\right)\right\}dx\Bigg]$$

$$
\begin{aligned}
&+\underline{\Omega}\left[\int_0^L C_1\left(u_0\dot{v}_0 - v_0\dot{u}_0\right)dx\right] \\
&+\underline{\underline{\Omega}}\left[\int_0^L C_1\left\{(R_0+x)\dot{v}_0\right\}dx + \frac{1}{2}\int_0^L C_2\left\{\dot{\psi}_z\left(1+\cos 2\beta\right) - \dot{\psi}_y\left(\sin 2\beta\right)\right\}dx \right.\\
&\qquad \left. + \frac{1}{2}\int_0^L C_3\left\{\dot{\psi}_z\left(1-\cos 2\beta\right) + \dot{\psi}_y\left(\sin 2\beta\right)\right\}dx\right] \\
&+\Omega^2\left[\frac{1}{2}\int_0^L C_1(R_0+x)^2dx + \frac{1}{4}\int_0^L C_2\left(1+\cos 2\beta\right)dx + \frac{1}{4}\int_0^L C_3\left(1-\cos 2\beta\right)dx\right] \\
&+\underline{\Omega^2}\left[\int_0^L C_1(R_0+x)u_0dx\right] \\
&+\underline{\underline{\Omega^2}}\left[\frac{1}{2}\int_0^L C_1\left(u_0^2+v_0^2\right)dx \right.\\
&\qquad + \frac{1}{4}\int_0^L C_2\left\{\psi_z^2\left(1+\cos 2\beta\right) + \psi_y^2\left(1-\cos 2\beta\right) - 2\psi_z\psi_y\left(\sin 2\beta\right)\right\}dx \\
&\qquad \left. + \frac{1}{4}\int_0^L C_3\left\{\psi_z^2\left(1-\cos 2\beta\right) + \psi_y^2\left(1+\cos 2\beta\right) + 2\psi_z\psi_y\left(\sin 2\beta\right)\right\}dx\right]
\end{aligned}
\tag{2.20}
$$

Each term of U'_{ke} given by (2.20) should be explained here. The terms not associated with the angular speed Ω are generated due to the relative linear and angular acceleration of the beam with reference to the non-inertial global frame. In this case, some of the terms indicate coupling of chord-wise and flap-wise bending motion. The terms associated with the first occurrence of Ω (single underlined) are due to the effects of Coriolis acceleration and provides coupling between stretching and chord-wise deformations. The terms associated with the second occurrence of Ω (double underlined) are due to the angular acceleration of the beam and are omitted. The terms associated with the first occurrence of Ω^2 are due to the kinetic energy of the beam considered as a rigid body. The terms associated with the second occurrence of Ω^2 (single underlined) are due the energy stored as a result of work done by the centrifugal force. The terms associated with the third occurrence of Ω^2 (double underlined) are due to the spin-softening effect which has already been considered in the previous step involving constant centrifugal loading. In connection with (2.17), it can be mentioned that the spin-softening effect originates due to the consideration of displaced configuration of the beam for determining the velocity vector $\left(\vec{\Omega}\times\vec{R}_Q\right)$ while transforming the velocity vector from non-inertial $\left(x,y,z\right)$ to inertial frame $\left(X,Y,Z\right)$.

2.2.6. Governing Equations under Centrifugal Loading

The first step of the problem is to formulate the governing equations to get the deformed configuration of the rotating micro beam. The governing equations for the time-independent deformation due to centrifugal loading are derived employing minimum potential energy principle given by,

$$\delta\left(U_{se}+U_{wp}\right)=0 \tag{1.2}$$

where U_{se} is the total strain energy due to centrifugal loading given as $U_{se}=U_{se}^{cl}+U_{se}^{ncl}$, U_{wp} is the work potential due to centrifugal loading and δ is the variational operator. Here U_{se}^{cl} and U_{se}^{ncl} are the classical and non-classical strain energies respectively.

Following Ritz method (as discussed in sub-section 1.3.3.), the displacement and rotation fields are approximated as,

$$\begin{aligned}
&u_0(x)=\sum_{j=1}^{n}c_j\phi_j^u(x),\ v_0(x)=\sum_{j=1}^{n}c_{n+j}\phi_j^v(x),\ w_0(x)=\sum_{j=1}^{n}c_{2n+j}\phi_j^w(x),\\
&\psi_z(x)=\sum_{j=1}^{n}c_{3n+j}\phi_j^{rz}(x),\ \psi_y(x)=\sum_{j=1}^{n}c_{4n+j}\phi_j^{ry}(x)
\end{aligned} \tag{2.21}$$

In (2.21), $\phi_j^u\left(x\right)$, $\phi_j^v\left(x\right)$, $\phi_j^w\left(x\right)$, $\phi_j^{rz}\left(x\right)$and $\phi_j^{ry}\left(x\right)$ are the sets of admissible orthogonal functions with n number of functions in each set; c_j is the set of time-independent generalized coordinates. The lowest order admissible functions are selected for the clamped-free boundary condition. These lowest order functions and the corresponding boundary conditions are given in Table 2.1. Gram-Schmidt orthogonalization scheme is used to derive the higher order kinematically admissible orthogonal functions.

Table 2.2: Boundary conditions and the corresponding lowest order admissible functions

Boundary conditions	Function
$u_0\big\rvert_{x=0} = 0, u_0\big\rvert_{x=L} \neq 0$	$\phi_1^u = (x/L)$
$v_0\big\rvert_{x=0} = 0, v_0\big\rvert_{x=L} \neq 0; \frac{dv_0}{dx}\Big\rvert_{x=0} = 0, \frac{dv_0}{dx}\Big\rvert_{x=L} \neq 0;$ $\frac{d^2v_0}{dx^2}\Big\rvert_{x=0} \neq 0, \frac{d^2v_0}{dx^2}\Big\rvert_{x=L} = 0; \frac{d^3v_0}{dx^3}\Big\rvert_{x=0} \neq 0, \frac{d^3v_0}{dx^3}\Big\rvert_{x=L} = 0$	$\phi_1^v = (x/L)^2\left\{6-4(x/L)+(x/L)^2\right\}$
$w_0\big\rvert_{x=0} = 0, w_0\big\rvert_{x=L} \neq 0; \frac{dw_0}{dx}\Big\rvert_{x=0} = 0, \frac{dw_0}{dx}\Big\rvert_{x=L} \neq 0;$ $\frac{d^2w_0}{dx^2}\Big\rvert_{x=0} \neq 0, \frac{d^2w_0}{dx^2}\Big\rvert_{x=L} = 0; \frac{d^3w_0}{dx^3}\Big\rvert_{x=0} \neq 0, \frac{d^3w_0}{dx^3}\Big\rvert_{x=L} = 0$	$\phi_1^w = (x/L)^2\left\{6-4(x/L)+(x/L)^2\right\}$
$\psi_z\big\rvert_{x=0} = 0, \psi_z\big\rvert_{x=L} \neq 0$	$\phi_1^{rz} = \sin\left\{(\pi x)/(2L)\right\}$
$\psi_y\big\rvert_{x=0} = 0, \psi_y\big\rvert_{x=L} \neq 0$	$\phi_1^{ry} = \sin\left\{(\pi x)/(2L)\right\}$

To derive the governing equations, first the expressions of strain energies and work potential are substituted in Eq. (1.2), and then the assumed displacement and rotation fields given by (2.21) are substituted. In this manner, the system of governing equations are derived which in matrix form is given as follows:

$$\left(\left[K^T\right]+\left[K^{SS}\right]\right)\{C\} = \{P\} \tag{2.22}$$

In Eq. (2.22), $\left[K^T\right]$ and $\left[K^{SS}\right]$ are total stiffness matrix and spin-softening matrix respectively, and $\{P\}$ is the load vector. The elements of $\left[K^T\right]$, $\left[K^{SS}\right]$ and $\{P\}$ are provided in APPENDIX 2A. Eq. (2.22) is solved using iterative substitution method (Das et al., 2009b) to obtain the set of generalized coordinates $\{C\}$. These values can be substituted in (2.21) to obtain the deformed beam configuration under constant centrifugal loading.

Some discussions about the spin-softening matrix is presented here. The terms associated with the second occurrence of Ω^2 in (2.17) generates the spin-softening matrix. It can be seen from (2.17) that these terms are associated with Ω^2 with a negative sign. So, these terms arise from spinning or rotation of the beam and tend to reduce its stiffness or, in other words soften the beam. It can be seen from (2.16) that the inertia force is determined considering the displaced configuration of the centrifugally loaded beam and this fact results in the spin-softening matrix.

2.2.7. Governing Equations for Free Vibration

The second part of the problem is to formulate the governing equations for free vibration of the centrifugally deformed beam. In this step, the system of governing equations are derived employing Hamilton's principle given by (putting U_{wp} =0 in Eq. (1.3)),

$$\delta\left(\int_{t1}^{t2}\left(U_{ke}-U_{se}\right)dt\right)=0 \tag{2.23}$$

where U_{ke} symbolizes kinetic energy of the beam executing free vibration in the neighborhood of the centrifugally deformed configuration and t denotes time.

Revisiting the expression of kinetic energy given by (2.20) reveals that, the terms which are not associated with the angular speed Ω are due to the relative linear and angular acceleration of the beam with reference to the non-inertial global frame and generates the mass matrix when used in Eq. (2.23). The terms occurring with the first occurrence of Ω (single underlined) are due to Coriolis acceleration and provides coupling between stretching and chord-wise deformations. These terms produce the gyroscopic matrix in conjunction with Eq. (2.23). The terms associated with the second occurrence of Ω (double underlined) are omitted as it would lead to the presence of angular acceleration when used in Eq. (2.23), which is taken as zero for the present work. The terms occurring with the first occurrence of Ω^2 are due to the kinetic energy of the beam if considered as a rigid body and would not contribute in the equations of motion. The terms associated with the second and third occurrence of Ω^2 (single and double underlined respectively) are not considered in this step as they have already been considered in the work potential formulation and subsequently in Eq. (2.22), and represent the effect of constant centrifugal force on the beam in the form of work done by the constant centrifugal force and spin-softening matrix. So in the formulation of governing equation for free vibration, the appropriate terms of kinetic energy are considered. Considering the appropriate terms as mentioned before, the variational form of U_{ke} as given in Eq. (2.23) is obtained as follows:

$$\begin{aligned}\delta\left(\int_{t1}^{t2} U_{ke}dt\right) = \int_{t1}^{t2}\Bigg(& -\int_0^L C_1\left\{\ddot{u}_0\delta\left(u_0\right)+\ddot{v}_0\delta\left(v_0\right)+\ddot{w}_0\delta\left(w_0\right)\right\}dx \\ & -\frac{1}{2}\int_0^L C_2\Big[\ddot{\psi}_z\delta\left(\psi_z\right)\left(1+\cos 2\beta\right)+\ddot{\psi}_y\delta\left(\psi_y\right)\left(1-\cos 2\beta\right) \\ & -\left\{\ddot{\psi}_y\delta\left(\psi_z\right)+\ddot{\psi}_z\delta\left(\psi_y\right)\right\}\sin 2\beta\Big]dx \\ & -\frac{1}{2}\int_0^L C_3\Big[\ddot{\psi}_z\delta\left(\psi_z\right)\left(1-\cos 2\beta\right)+\ddot{\psi}_y\delta\left(\psi_y\right)\left(1+\cos 2\beta\right) \\ & +\left\{\ddot{\psi}_y\delta\left(\psi_z\right)+\ddot{\psi}_z\delta\left(\psi_y\right)\right\}\sin 2\beta\Big]dx \\ & +2\Omega\int_0^L C_1\left\{\dot{v}_0\delta\left(u_0\right)-\dot{u}_0\delta\left(v_0\right)\right\}dx\Bigg)dt\end{aligned} \tag{2.24}$$

As the beam executes free vibration about its centrifugally deformed configuration, the strain energy term in Eq. (2.23) corresponds to the tangent stiffness of the centrifugally stiffened and spin-softened micro beam. The tangent stiffness $\left[K^t\right]$ for any angular speed is derived using the following relationship (Das, 2018):

$$\left[k_{ij}^t\right]=\frac{\partial}{\partial c_j}\left\{p_i^r\right\} \tag{2.25}$$

where $\left\{P^r\right\}$ is the restoring force vector. At any angular speed during the centrifugal loading, $\left\{P^r\right\}$ is given by $\left\{P^r\right\}=\left(\left[K^T\right]+\left[K^{SS}\right]\right)\left\{C\right\}$. The elements of $\left[K^t\right]$ are provided in APPENDIX 2B.

A similar set of orthogonal admissible functions as used in (2.21), can be assumed for approximating the displacement and rotation fields following Ritz method. It is given as

$$\begin{aligned}& u_0(x,t)=\sum_{j=1}^{n} d_j\left(t\right)\phi_j^u(x),\ v_0(x,t)=\sum_{j=1}^{n} d_{n+j}\left(t\right)\phi_j^v(x),\ w_0(x,t)=\sum_{j=1}^{n} d_{2n+j}\left(t\right)\phi_j^w(x), \\ & \psi_z(x,t)=\sum_{j=1}^{n} d_{3n+j}\left(t\right)\phi_j^{rz}(x),\ \psi_y(x,t)=\sum_{j=1}^{n} d_{4n+j}\left(t\right)\phi_j^{ry}(x)\end{aligned} \tag{2.26}$$

where d_j is the set of generalized coordinates dependent on time. To derive the governing equations, these approximate fields are substituted in the variational form of kinetic energy expression given by (2.24) and also in the tangent stiffness matrix. Then using the Hamilton's principle, the equations of motion are obtained as:

$$[M]\{\ddot{D}\}+[G]\{\dot{D}\}+[K^t]\{D\}=0 \tag{2.27}$$

In Eq. (2.27), $[M]$ is the mass matrix and $[G]$ is the gyroscopic matrix. The elements of $[M]$ and $[G]$ are given in APPENDIX 2C.

To transform Eq. (2.27) into an eigenvalue problem, a state vector is defined as $\{H\}=\{D^{\mathrm{T}},\dot{D}^{\mathrm{T}}\}^{\mathrm{T}}$. Using this, Eq. (2.27) is transformed to the following form:

$$[J]\{H\}=\{\dot{H}\} \tag{2.28}$$

where $[J]$ is given by

$$[J]=\left[\begin{array}{c|c} 0 & [I] \\ \hline -[M]^{-1}[K^t] & -[M]^{-1}[G] \end{array}\right] \tag{2.29}$$

In (2.29), $[I]$ is an identity matrix of dimension $5n$. The general solution of the state vector $\{H\}$ is assumed as $\{H\}=\{H_c\}\exp(\alpha t)$ where $\{H_c\}$ is the time-independent part of the state vector and α is the parameter to be determined. Substituting the general solution in Eq. (2.28), an eigenvalue problem of the following form is obtained:

$$[J]\{H_c\}-\alpha\{H_c\}=0 \tag{2.30}$$

Eq. (2.30) is solved with the help of a standard eigensolver. For the present problem, the eigenvalues are obtained in complex conjugate pairs given as $\alpha=\pm\mathbf{i}\omega$, signifying a stable oscillatory motion of the beam executing free vibration where ω is the frequency of vibration. Correspondingly, the top half of the eigenvector $\{H_c\}$ determines the relevant mode shape when substituted in (2.26). Evaluation of eigenvalues and eigenvectors provides the required free vibration frequencies and the corresponding mode shapes of the vibrating beam.

2.3. Chapter Summary

This chapter provides a detailed theoretical formulation for analyzing free vibration behavior of BFGM pre-twisted double-tapered rotating micro beams. The BFGM modeling following Voigt model is presented with illustrations of property variation by surface plots. Displacement, strain and curvature fields are evaluated using TBT and MCST. A step-by-step formulations of strain energies, work potential and kinetic energy are provided. Finally, following Ritz method and employing minimum potential energy principle and Hamilton's principle, the governing equations for both deformation due to constant centrifugal loading and free vibration are formulated. This formulation is applicable for both straight and pre-twisted beams. In the following two chapters, the results for BFGM straight and pre-twisted micro beams with double-tapered configuration are presented and discussed.

APPENDIX 2A

<u>Non-zero elements of total stiffness matrix</u>

$$\left[k_{ij}^T\right]_{\substack{i=1,n\\ j=1,n}} = \int_0^L A_1 \frac{d\phi_i^u}{dx}\frac{d\phi_j^u}{dx}dx$$

$$\left[k_{ij}^T\right]_{\substack{i=1,n\\ j=n+1,2n}} = \frac{1}{2}\int_0^L A_1\left(\frac{\partial v_0}{\partial x}\right)\frac{d\phi_i^u}{dx}\frac{d\phi_{j-n}^v}{dx}dx$$

$$\left[k_{ij}^T\right]_{\substack{i=1,n\\ j=2n+1,3n}} = \frac{1}{2}\int_0^L A_1\left(\frac{\partial w_0}{\partial x}\right)\frac{d\phi_i^u}{dx}\frac{d\phi_{j-2n}^w}{dx}dx$$

$$\left[k_{ij}^T\right]_{\substack{i=n+1,2n\\ j=n+1,2n}} = \int_0^L A_1\left[\frac{\partial u_0}{\partial x}+\frac{1}{2}\left(\frac{\partial v_0}{\partial x}\right)^2+\frac{1}{2}\left(\frac{\partial w_0}{\partial x}\right)^2\right]\frac{d\phi_{i-n}^v}{dx}\frac{d\phi_{j-n}^v}{dx}dx$$
$$+k_s\int_0^L B_1\frac{d\phi_{i-n}^v}{dx}\frac{d\phi_{j-n}^v}{dx}dx+\frac{l^2}{4}\int_0^L B_1\frac{d^2\phi_{i-n}^v}{dx^2}\frac{d^2\phi_{j-n}^v}{dx^2}dx$$

$$\left[k_{ij}^T\right]_{\substack{i=n+1,2n\\ j=3n+1,4n}} = -k_s\int_0^L B_1\frac{d\phi_{i-n}^v}{dx}\phi_{j-3n}^{rz}dx+\frac{l^2}{4}\int_0^L B_1\frac{d^2\phi_{i-n}^v}{dx^2}\frac{d\phi_{j-3n}^{rz}}{dx}dx$$

$$\left[k_{ij}^T\right]_{\substack{i=2n+1,3n\\ j=2n+1,3n}} = \int_0^L A_1\left[\frac{\partial u_0}{\partial x}+\frac{1}{2}\left(\frac{\partial v_0}{\partial x}\right)^2+\frac{1}{2}\left(\frac{\partial w_0}{\partial x}\right)^2\right]\frac{d\phi_{i-2n}^w}{dx}\frac{d\phi_{j-2n}^w}{dx}dx$$
$$+k_s\int_0^L B_1\frac{d\phi_{i-2n}^w}{dx}\frac{d\phi_{j-2n}^w}{dx}dx+\frac{l^2}{4}\int_0^L B_1\frac{d^2\phi_{i-2n}^w}{dx^2}\frac{d^2\phi_{j-2n}^w}{dx^2}dx$$

$$\left[k_{ij}^T\right]_{\substack{i=2n+1,3n\\ j=4n+1,5n}} = k_s\int_0^L B_1\frac{d\phi_{i-2n}^w}{dx}\phi_{j-4n}^{ry}dx-\frac{l^2}{4}\int_0^L B_1\frac{d^2\phi_{i-2n}^w}{dx^2}\frac{d\phi_{j-4n}^{ry}}{dx}dx$$

$$\left[k_{ij}^T\right]_{\substack{i=3n+1,4n\\ j=n+1,2n}} = -k_s\int_0^L B_1\phi_{i-3n}^{rz}\frac{d\phi_{j-n}^v}{dx}dx+\frac{l^2}{4}\int_0^L B_1\frac{d\phi_{i-3n}^{rz}}{dx}\frac{d^2\phi_{j-n}^v}{dx^2}dx$$

$$\left[k_{ij}^T\right]_{\substack{i=3n+1,4n\\ j=3n+1,4n}} = \frac{1}{2}\int_0^L\left\{\left(A_2+A_3\right)+\left(A_2-A_3\right)\cos 2\beta\right\}\frac{d\phi_{i-3n}^{rz}}{dx}\frac{d\phi_{j-3n}^{rz}}{dx}dx+k_s\int_0^L B_1\phi_{i-3n}^{rz}\phi_{j-3n}^{rz}dx$$
$$+\frac{l^2}{4}\int_0^L B_1\frac{d\phi_{i-3n}^{rz}}{dx}\frac{d\phi_{j-3n}^{rz}}{dx}dx$$

$$\left[k_{ij}^T\right]_{\substack{i=3n+1,4n\\ j=4n+1,5n}} = -\frac{1}{2}\int_0^L\left(A_2-A_3\right)\frac{d\phi_{i-3n}^{rz}}{dx}\frac{d\phi_{j-4n}^{ry}}{dx}\left(\sin 2\beta\right)dx$$

$$\left[k_{ij}^{T}\right]_{\substack{i=4n+1,5n\\ j=2n+1,3n}} = k_s\int_0^L B_1\phi_{i-4n}^{ry}\frac{d\phi_{j-2n}^{w}}{dx}dx - \frac{l^2}{4}\int_0^L B_1\frac{d\phi_{i-4n}^{ry}}{dx}\frac{d^2\phi_{j-2n}^{w}}{dx^2}dx$$

$$\left[k_{ij}^{T}\right]_{\substack{i=4n+1,5n\\ j=3n+1,4n}} = -\frac{1}{2}\int_0^L\left(A_2-A_3\right)\frac{d\phi_{i-4n}^{ry}}{dx}\frac{d\phi_{j-3n}^{rz}}{dx}\left(\sin 2\beta\right)dx$$

$$\left[k_{ij}^{T}\right]_{\substack{i=4n+1,5n\\ j=4n+1,5n}} = \frac{1}{2}\int_0^L\left\{\left(A_2+A_3\right)-\left(A_2-A_3\right)\cos 2\beta\right\}\frac{d\phi_{i-4n}^{ry}}{dx}\frac{d\phi_{j-4n}^{ry}}{dx}dx + k_s\int_0^L B_1\phi_{i-4n}^{ry}\phi_{j-4n}^{ry}dx$$
$$+\frac{l^2}{4}\int_0^L B_1\frac{d\phi_{i-4n}^{ry}}{dx}\frac{d\phi_{j-4n}^{ry}}{dx}dx$$

<u>Non-zero elements of spin-softening matrix</u>

$$\left[k_{ij}^{SS}\right]_{\substack{i=1,n\\ j=1,n}} = -\Omega^2\int_0^L C_1\phi_i^u\phi_j^u dx$$

$$\left[k_{ij}^{SS}\right]_{\substack{i=n+1,2n\\ j=n+1,2n}} = -\Omega^2\int_0^L C_1\phi_{i-n}^v\phi_{j-n}^v dx$$

$$\left[k_{ij}^{SS}\right]_{\substack{i=3n+1,4n\\ j=3n+1,4n}} = -\frac{\Omega^2}{2}\left[\int_0^L\left\{\left(C_2+C_3\right)+\left(C_2-C_3\right)\cos 2\beta\right\}\phi_{i-3n}^{rz}\phi_{j-3n}^{rz}dx\right]$$

$$\left[k_{ij}^{SS}\right]_{\substack{i=3n+1,4n\\ j=4n+1,5n}} = -\frac{\Omega^2}{2}\left[\int_0^L\left(C_3-C_2\right)\phi_{i-3n}^{rz}\phi_{j-4n}^{ry}\left(\sin 2\beta\right)dx\right]$$

$$\left[k_{ij}^{SS}\right]_{\substack{i=4n+1,5n\\ j=3n+1,4n}} = -\frac{\Omega^2}{2}\left[\int_0^L\left(C_3-C_2\right)\phi_{i-4n}^{ry}\phi_{j-3n}^{rz}\left(\sin 2\beta\right)dx\right]$$

$$\left[k_{ij}^{SS}\right]_{\substack{i=4n+1,5n\\ j=4n+1,5n}} = -\frac{\Omega^2}{2}\left[\int_0^L\left\{\left(C_2+C_3\right)-\left(C_2-C_3\right)\cos 2\beta\right\}\phi_{i-4n}^{ry}\phi_{j-4n}^{ry}dx\right]$$

<u>Elements of load vector</u>

$$\left\{p_i\right\}_{i=1,n} = \Omega^2\int_0^L C_1\left(R+x\right)\phi_i^u dx,\ \left\{p_i\right\}_{i=n+1,2n} = \left\{p_i\right\}_{i=2n+1,3n} = \left\{p_i\right\}_{i=3n+1,4n} = \left\{p_i\right\}_{i=4n+1,5n} = 0$$

APPENDIX 2B

Non-zero elements of tangent stiffness matrix

$$\left[k_{ij}^{t}\right]_{\substack{i=1,n\\ j=1,n}}=\int_0^L A_1\frac{d\phi_i^u}{dx}\frac{d\phi_j^u}{dx}dx-\Omega^2\int_0^L C_1\phi_i^u\phi_j^u dx$$

$$\left[k_{ij}^{t}\right]_{\substack{i=1,n\\ j=n+1,2n}}=\int_0^L A_1\left(\frac{\partial v_0}{\partial x}\right)\frac{d\phi_i^u}{dx}\frac{d\phi_{j-n}^v}{dx}dx$$

$$\left[k_{ij}^{t}\right]_{\substack{i=1,n\\ j=2n+1,3n}}=\int_0^L A_1\left(\frac{\partial w_0}{\partial x}\right)\frac{d\phi_i^u}{dx}\frac{d\phi_{j-2n}^w}{dx}dx$$

$$\left[k_{ij}^{t}\right]_{\substack{i=n+1,2n\\ j=1,n}}=\int_0^L A_1\left(\frac{\partial v_0}{\partial x}\right)\frac{d\phi_{i-n}^v}{dx}\frac{d\phi_j^u}{dx}dx$$

$$\left[k_{ij}^{t}\right]_{\substack{i=n+1,2n\\ j=n+1,2n}}=\int_0^L A_1\left[\frac{\partial u_0}{\partial x}+\frac{3}{2}\left(\frac{\partial v_0}{\partial x}\right)^2+\frac{1}{2}\left(\frac{\partial w_0}{\partial x}\right)^2\right]\frac{d\phi_{i-n}^v}{dx}\frac{d\phi_{j-n}^v}{dx}dx$$
$$+k_s\int_0^L B_1\frac{d\phi_{i-n}^v}{dx}\frac{d\phi_{j-n}^v}{dx}dx+\frac{l^2}{4}\int_0^L B_1\frac{d^2\phi_{i-n}^v}{dx^2}\frac{d^2\phi_{j-n}^v}{dx^2}dx-\Omega^2\int_0^L C_1\phi_{i-n}^v\phi_{j-n}^v dx$$

$$\left[k_{ij}^{t}\right]_{\substack{i=n+1,2n\\ j=n+1,3n}}=\int_0^L A_1\left(\frac{\partial v_0}{\partial x}\frac{\partial w_0}{\partial x}\right)\frac{d\phi_{i-n}^v}{dx}\frac{d\phi_{j-2n}^w}{dx}dx$$

$$\left[k_{ij}^{t}\right]_{\substack{i=n+1,2n\\ j=3n+1,4n}}=-k_s\int_0^L B_1\frac{d\phi_{i-n}^v}{dx}\phi_{j-n3}^{rz}dx+\frac{l^2}{4}\int_0^L B_1\frac{d^2\phi_{i-n}^v}{dx^2}\frac{d\phi_{j-3n}^{rz}}{dx}dx$$

$$\left[k_{ij}^{t}\right]_{\substack{i=2n+1,3n\\ j=1,n}}=\int_0^L A_1\left(\frac{\partial w_0}{\partial x}\right)\frac{d\phi_{i-2n}^w}{dx}\frac{d\phi_j^u}{dx}dx$$

$$\left[k_{ij}^{t}\right]_{\substack{i=2n+1,3n\\ j=n+1,2n}}=\int_0^L A_1\left(\frac{\partial v_0}{\partial x}\frac{\partial w_0}{\partial x}\right)\frac{d\phi_{i-2n}^w}{dx}\frac{d\phi_{j-n}^v}{dx}dx$$

$$\left[k_{ij}^{t}\right]_{\substack{i=2n+1,3n\\ j=2n+1,3n}}=\int_0^L A_1\left[\frac{\partial u_0}{\partial x}+\frac{1}{2}\left(\frac{\partial v_0}{\partial x}\right)^2+\frac{3}{2}\left(\frac{\partial w_0}{\partial x}\right)^2\right]\frac{d\phi_{i-2n}^w}{dx}\frac{d\phi_{j-2n}^w}{dx}dx$$
$$+k_s\int_0^L B_1\frac{d\phi_{i-2n}^w}{dx}\frac{d\phi_{j-2n}^w}{dx}dx+\frac{l^2}{4}\int_0^L B_1\frac{d^2\phi_{i-2n}^w}{dx^2}\frac{d^2\phi_{j-2n}^w}{dx^2}dx$$

$$\left[k_{ij}^{t}\right]_{\substack{i=2n+1,3n\\ j=4n+1,5n}}=k_s\int_0^L B_1\frac{d\phi_{i-2n}^w}{dx}\phi_{j-4n}^{ry}dx-\frac{l^2}{4}\int_0^L B_1\frac{d^2\phi_{i-2n}^w}{dx^2}\frac{d\phi_{j-4n}^{ry}}{dx}dx$$

$$\left[k_{ij}^{t}\right]_{\substack{i=3n+1,4n\\ j=n+1,2n}}=-k_s\int_0^L B_1\phi_{i-3n}^{rz}\frac{d\phi_{j-n}^v}{dx}dx+\frac{l^2}{4}\int_0^L B_1\frac{d\phi_{i-3n}^{rz}}{dx}\frac{d^2\phi_{j-n}^v}{dx^2}dx$$

$$\left[k_{ij}^{t}\right]_{\substack{i=3n+1,4n\\ j=3n+1,4n}}=\frac{1}{2}\int_0^L\left\{\left(A_2+A_3\right)+\left(A_2-A_3\right)\cos 2\beta\right\}\frac{d\phi_{i-3n}^{rz}}{dx}\frac{d\phi_{j-3n}^{rz}}{dx}dx+k_s\int_0^L B_1\phi_{i-3n}^{rz}\phi_{j-3n}^{rz}dx$$
$$+\frac{l^2}{4}\int_0^L B_1\frac{d\phi_{i-3n}^{rz}}{dx}\frac{d\phi_{j-3n}^{rz}}{dx}dx-\frac{\Omega^2}{2}\left[\int_0^L\left\{\left(C_2+C_3\right)+\left(C_2-C_3\right)\cos 2\beta\right\}\phi_{i-3n}^{rz}\phi_{j-3n}^{rz}dx\right]$$

$$\left[k_{ij}^{t}\right]_{\substack{i=3n+1,4n\\ j=4n+1,5n}}=-\frac{1}{2}\int_0^L\left(A_2-A_3\right)\frac{d\phi_{i-3n}^{rz}}{dx}\frac{d\phi_{j-4n}^{ry}}{dx}\left(\sin 2\beta\right)dx$$
$$-\frac{\Omega^2}{2}\left[\int_0^L\left(C_3-C_2\right)\phi_{i-3n}^{rz}\phi_{j-4n}^{ry}\left(\sin 2\beta\right)dx\right]$$

$$\left[k_{ij}^{t}\right]_{\substack{i=4n+1,5n\\ j=2n+1,3n}}=k_s\int_0^L B_1\phi_{i-4n}^{ry}\frac{d\phi_{j-2n}^{w}}{dx}dx-\frac{l^2}{4}\int_0^L B_1\frac{d\phi_{i-4n}^{ry}}{dx}\frac{d^2\phi_{j-2n}^{w}}{dx^2}dx$$

$$\left[k_{ij}^{t}\right]_{\substack{i=4n+1,5n\\ j=3n+1,4n}}=-\frac{1}{2}\int_0^L\left(A_2-A_3\right)\frac{d\phi_{i-4n}^{ry}}{dx}\frac{d\phi_{j-3n}^{rz}}{dx}\left(\sin 2\beta\right)dx$$
$$-\frac{\Omega^2}{2}\left[\int_0^L\left(C_3-C_2\right)\phi_{i-4n}^{ry}\phi_{j-3n}^{rz}\left(\sin 2\beta\right)dx\right]$$

$$\left[k_{ij}^{t}\right]_{\substack{i=4n+1,5n\\ j=4n+1,5n}}=\frac{1}{2}\int_0^L\left\{\left(A_2+A_3\right)-\left(A_2-A_3\right)\cos 2\beta\right\}\frac{d\phi_{i-4n}^{ry}}{dx}\frac{d\phi_{j-4n}^{ry}}{dx}dx+k_s\int_0^L B_1\phi_{i-4n}^{ry}\phi_{j-4n}^{ry}dx$$
$$+\frac{l^2}{4}\int_0^L B_1\frac{d\phi_{i-4n}^{ry}}{dx}\frac{d\phi_{j-4n}^{ry}}{dx}dx-\frac{\Omega^2}{2}\left[\int_0^L\left\{\left(C_2+C_3\right)-\left(C_2-C_3\right)\cos 2\beta\right\}\phi_{i-4n}^{ry}\phi_{j-4n}^{ry}dx\right]$$

APPENDIX 2C

Non-zero elements of mass matrix

$$\left[m_{ij}\right]_{\substack{i=1,n\\ j=1,n}} = \int_0^L C_1 \phi_i^u \phi_j^u dx$$

$$\left[m_{ij}\right]_{\substack{i=n+1,2n\\ j=n+1,2n}} = \int_0^L C_1 \phi_{i-n}^v \phi_{j-n}^v dx$$

$$\left[m_{ij}\right]_{\substack{i=2n+1,3n\\ j=2n+1,3n}} = \int_0^L C_1 \phi_{i-2n}^w \phi_{j-2n}^w dx$$

$$\left[m_{ij}\right]_{\substack{i=3n+1,4n\\ j=3n+1,4n}} = \frac{1}{2}\int_0^L \left\{\left(C_2 + C_3\right) + \left(C_2 - C_3\right)\cos 2\beta\right\} \phi_{i-3n}^{rz} \phi_{j-3n}^{rz} dx$$

$$\left[m_{ij}\right]_{\substack{i=3n+1,4n\\ j=4n+1,5n}} = -\frac{1}{2}\int_0^L \left\{\left(C_2 - C_3\right)\sin 2\beta\right\} \phi_{i-3n}^{rz} \phi_{j-4n}^{ry} dx$$

$$\left[m_{ij}\right]_{\substack{i=4n+1,5n\\ j=3n+1,4n}} = -\frac{1}{2}\int_0^L \left\{\left(C_2 - C_3\right)\sin 2\beta\right\} \phi_{i-4n}^{ry} \phi_{j-3n}^{rz} dx$$

$$\left[m_{ij}\right]_{\substack{i=4n+1,5n\\ j=4n+1,5n}} = \frac{1}{2}\int_0^L \left\{\left(C_2 + C_3\right) - \left(C_2 - C_3\right)\cos 2\beta\right\} \phi_{i-4n}^{ry} \phi_{j-4n}^{ry} dx$$

Non-zero elements of gyroscopic matrix

$$\left[g_{ij}\right]_{\substack{i=1,n\\ j=n+1,2n}} = -2\Omega\int_0^L C_1 \phi_i^u \phi_{j-n}^v dx$$

$$\left[g_{ij}\right]_{\substack{i=n+1,2n\\ j=1,n}} = 2\Omega\int_0^L C_1 \phi_{i-n}^v \phi_j^u dx$$

Chapter 3

RESULTS AND DISCUSSION FOR BFGM STRAIGHT TAPERED ROTATING MICRO BEAM

3.1. Introduction

In the preceding chapter, the detailed mathematical formulation for free vibration study of BFGM pre-twisted double-tapered rotating micro beam is presented. It is also mentioned that if the value of pre-twist angle is put zero, i.e., $\bar{\beta}$ =0, a straight beam model is obtained. So, the mathematical formulation for free vibration of a BFGM straight rotating micro beam is omitted here and directly the results are presented in this chapter. For the straight rotating micro beam problem, as mentioned in sub-section 1.6.1., the same theoretical procedure is employed as that of a pre-twisted rotating micro beam. The size-effect is addressed using MCST. First, the deformed configuration of the beam due to time independent centrifugal force is evaluated by using minimum total potential energy principle. TBT in conjunction with von Kármán nonlinearity is employed to model the strain-displacement behavior. In the subsequent step, a tangent stiffness based formulation is executed and Hamilton's principle is used to formulate the governing equation for free vibration in the neighborhood of the centrifugally deformed configuration. Both the steps are solved by approximating the displacement fields according to Ritz method. The free vibration problem is transformed into an eigenvalue problem by transforming the governing equations to the state-space. It is worthwhile to mention here that there is no need of a local coordinate system $x-y'-z'$, which was used in the formulation of a pre-twisted beam. Because, in the present case involving straight beam (i.e., without pre-twist), the principal directions along the width and thickness directions of the beam are constant with respect to the beam axis (x). This means that the global ($x-y-z$) and local ($x-y'-z'$) non-inertial frames are identical. The geometry of the BFGM straight double-tapered rotating micro beam attached to a hub of radius R_O is shown in Fig. 3.1. Here $X-Y-Z$ is the inertial frame originating at O', the hub centre. As mentioned, $x-y-z$ is the global non-inertial frame originating at the hub end of the beam at O and rotates with the beam with constant angular speed Ω.

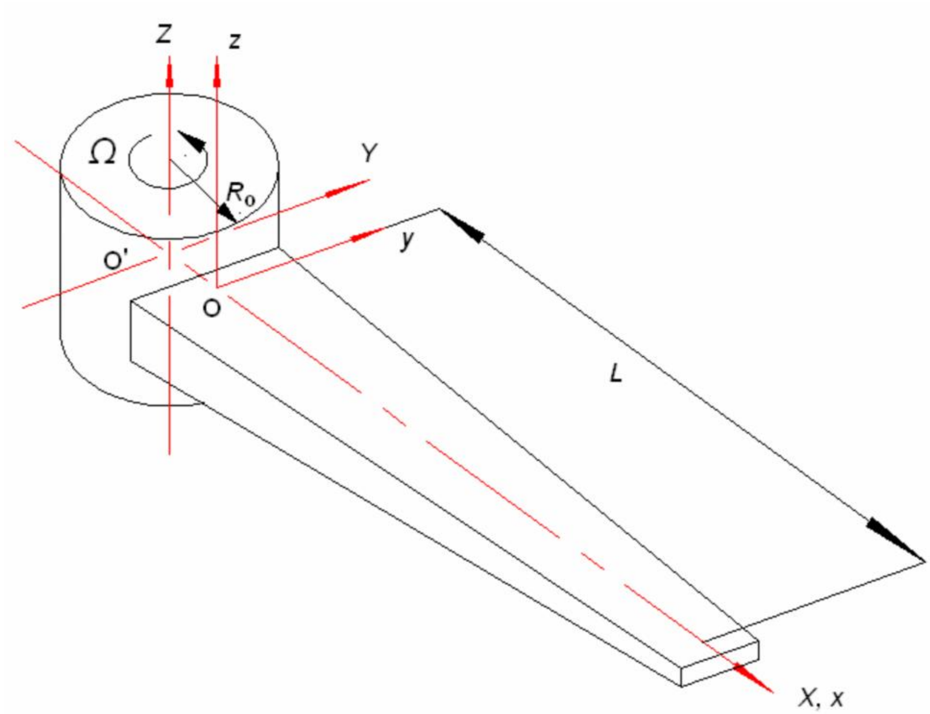

Fig. 3.1: Dimensions and axes of a straight rotating beam.

The results of this study are presented in three subsections. First some reduced problems are solved and the results are compared with those found in the relevant literatures, to validate the present model. Then the size-effect on shear deformation has been studied by considering different length-thickness ratios. Finally, speed versus frequency behaviors of the beam are presented for variations of different parameters. The non-dimensional angular speed $\left(\Omega^*\right)$, non-dimensional frequency of vibration $\left(\lambda\right)$, normalized hub parameter $\left(\eta\right)$, size-dependent thickness and length-thickness ratio are defined as follows:

Non-dimensional angular speed= $\Omega^* = \Omega L^2\left[\left(\rho_m A\right)/\left(E_m I\right)\right]^{1/2}$

Non-dimensional frequency of vibration= $\lambda = \omega L^2\left[\left(\rho_m A\right)/\left(E_m I\right)\right]^{1/2}$

Normalized hub parameter= $\eta = R_O / L$

Size-dependent thickness= h_{max} / l

Length-thickness ratio= L / h_{max}

Here $A(= b_{max} h_{max})$ is the cross sectional area and $I\left(= b_{max}\left(h_{max}\right)^3 / 12\right)$ is the area moment of inertia at the hub end; E_m and ρ_m are Young's modulus and mass density of the metallic constituent evaluated at ambient temperature T_0 =300 K. Unless otherwise stated and except the validation study, the results are generated considering Stainless Steel (SUS304)/Silicon Nitride (Si_3N_4) composition and using the following values: l =17.6 μm, h_{max} / l =1, L / h_{max} =25, η =0.25, $C_b = C_h$ =0.5, k_l =1, k_t =1, T_f =800 K. For each parameter variation, the speed-frequency behaviors are shown for the first and second modes, each for chord-wise and flap-wise vibrations. Chord-wise vibration is the in-plane bending vibration that occurs in the plane of rotation $(x - y)$, and the out-of-plane vibration which occurs perpendicular to the rotational plane $(x - z)$ is called flap-wise vibration.

3.2. Validation Study

Several studies are done to validate the current model by comparing the results of some reduced problems with the available results in the literature. The variation of free vibration frequency with thickness gradation index (k_t) for a TFGM uniform non-rotating micro beam is compared with the results of Reddy (2011) and it is presented in Fig. 3.2. The thickness gradation is asymmetric and to model that, $\left|\frac{z}{h/2}\right|^{k_t}$ is replaced by $\left(\frac{z}{h} + \frac{1}{2}\right)^{k_t}$ and k_l is put equal to zero in Eq. (2.6). For this study, the material properties and shear correction factor are taken as, E_m =1.44 GPa, E_c =14.4 GPa, ν_f =0.38=constant, ρ_m =1220 kg/m^3, ρ_c =12200 kg/m^3, $k_s = 5(1+\nu_f)/(6+5\nu_f)$. The comparison shows good agreement with the given result.

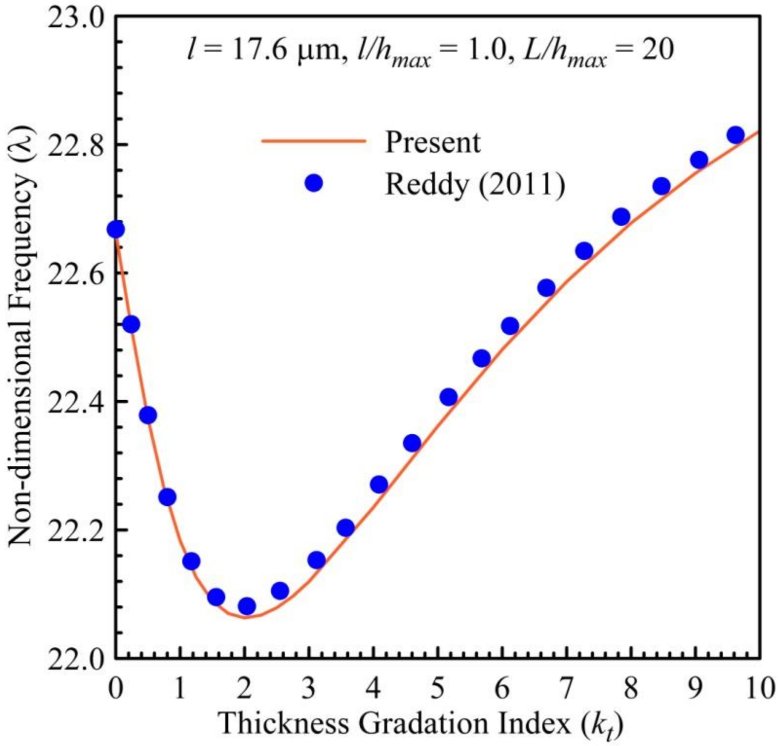

Fig. 3.2: Comparison plot for variation of non-dimensional frequency with thickness gradation index for a TFGM uniform non-rotating micro-beam.

The first flap-wise and chord-wise free vibration frequencies of Aluminum/Zirconia AFGM tapered rotating classical beam are compared with Mazanoglu and Guler (2017) and is presented in Table 3.1. The beam is modeled as a classical one by putting $l = 0$, and the following material properties are considered: E_m =70 GPa, E_c =200 GPa, ν_f =0.38, ρ_m =2702 kg/m^3, ρ_c =5700 kg/m^3 . The comparison shows excellent matching.

A comparison with Shafiei et al. (2016a) regarding the non-dimensional speed-frequency behavior of Stainless Steel/Alumina AFGM tapered rotating micro beam is shown in Fig. 3.3. The material properties used are: E_m =201.04 GPa, E_c =349.55 GPa, ν_m =0.3262, ν_c =0.24, ρ_m =8166 kg/m^3, ρ_c =3800 kg/m^3. The comparison exhibits very good agreement.

The variation of non-dimensional frequency for the first two flap-wise modes with normalized material length scale parameter $\left(l/h_{\max}\right)$ is compared with the results of Semnani (2016) and Arvin (2018) in Figs. 3.4(a) and (b) for a homogeneous uniform rotating micro beam. The comparison is conducted at $\Omega^* = 4$ with the following property values: E =1.4 GPa, ν =0.30, ρ =1000 kg/m^3, $l = 17.6\times10^{-6}$ m. This comparison also shows excellent matching.

Table 3.1: Comparison of non-dimensional frequency of an Aluminum/Zirconia AFGM tapered rotating classical beam at $\lambda = 2$ for $\eta = 0$ and $k_l = 2$.

Direction	Mode	Work Reference	$C_b = C_h$		
			0	0.3	0.6
Flap-wise	First	Present	4.8052	5.3922	6.3670
		Mazanoglu and Guler (2017)	4.8142	5.3933	6.3690
	Second	Present	23.6610	22.0611	20.4727
		Mazanoglu and Guler (2017)	23.6961	22.0865	20.4737
Chord-wise	First	Present	4.3742	5.0111	6.0489
		Mazanoglu and Guler (2017)	4.3790	5.0088	6.0468
	Second	Present	23.5786	21.9698	20.3712
		Mazanoglu and Guler (2017)	23.6116	21.9957	20.3757

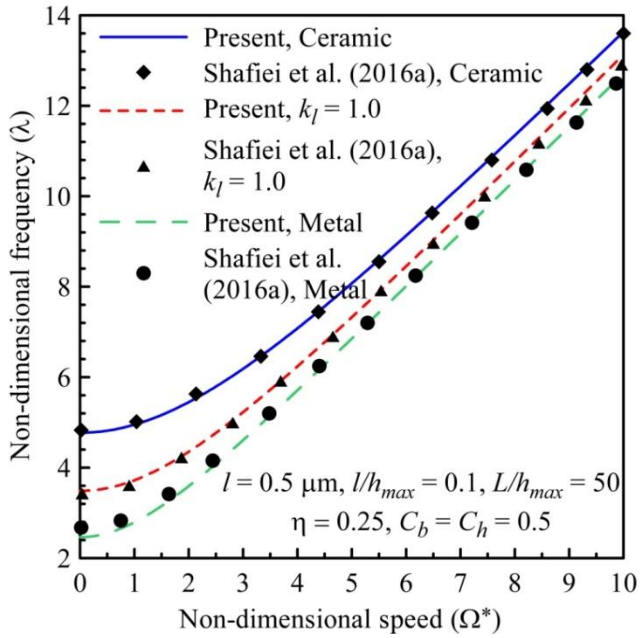

Fig. 3.3: Comparison plot of non-dimensional speed-frequency behavior for first flap-wise mode of a Stainless Steel/Alumina AFGM tapered rotating micro beam.

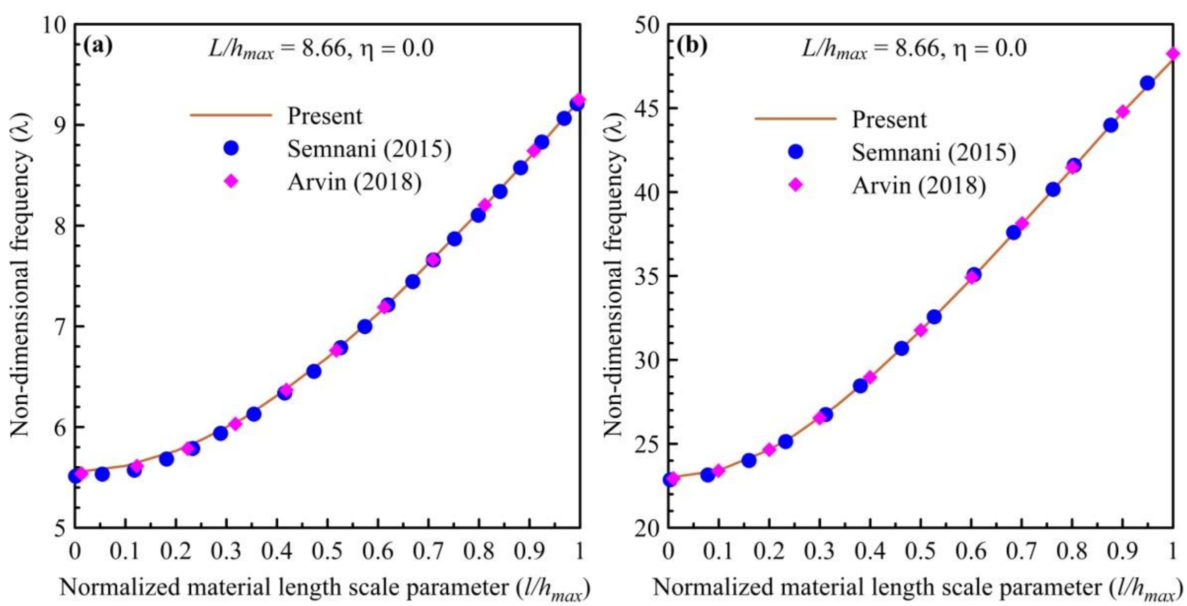

Fig. 3.4: Variation of non-dimensional frequency of flap-wise modes with normalized material length scale parameter for a homogeneous uniform rotating micro beam at Ω*=4: (a) First mode, (b) Second mode.

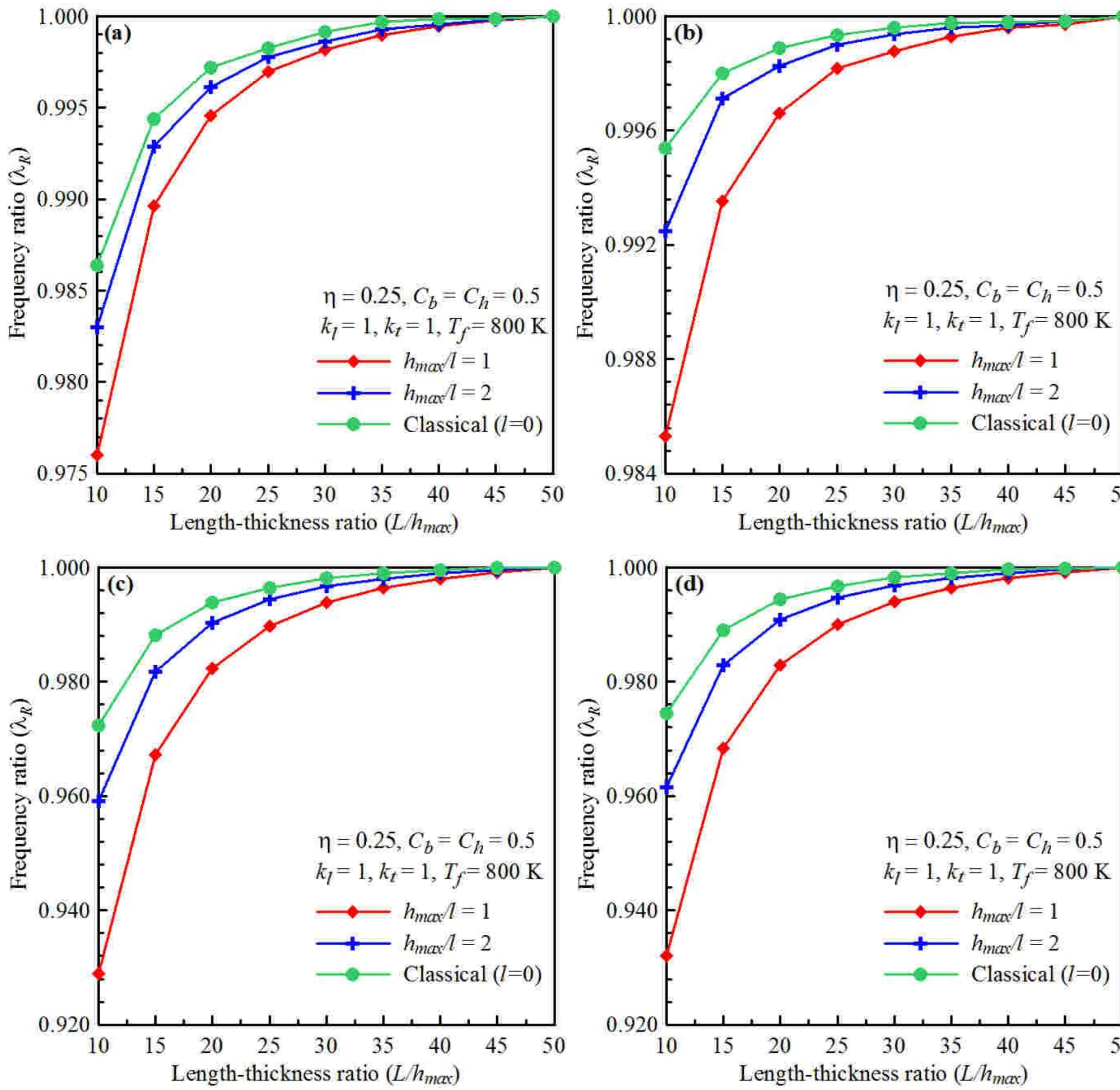

Fig. 3.5: Variation of frequency ratio with length-thickness ratio for different size-dependent thicknesses for a Stainless Steel/Silicon Nitride beam at Ω*=5: (a) First chord-wise mode, (b) First flap-wise mode, (c) Second chord-wise mode, (d) Second flap-wise mode.

3.3. Size-effect for Different Length Thickness Ratios

In the study of free vibration behavior of micro beams, it is of utmost importance to discuss the size-dependent shear deformation and its effect on the vibration frequencies. For this purpose, in the present thesis work, variation of frequency ratio (λ_R) is studied with changing length-thickness ratio (L/h_{max}) for different values of size-dependent thickness

(h_{max}/l). Here the term 'frequency ratio' is defined as the ratio of free vibration frequency of the beam to the frequency of the beam for $L/h_{max}=50$ (denoted by λ_{50}), for a particular value of h_{max}/l. So, frequency ratio is defined as $\lambda_R=\lambda/\lambda_{50}$. It is to be noted that λ_{50} has different values for different h_{max}/l ratios and for different modes of vibration. In Figs. 3.5(a)-(d), the variations of λ_R with L/h_{max} are shown for the first and second modes, each for chord-wise and flap-wise vibrations respectively. For Fig. 3.5, the non-dimensional speed is considered as $\Omega^*=5$ and the range of L/h_{max} is taken from 10 to 50 with h_{max}/l taken as 1, 2 and that corresponding to the classical $(l=0)$ theory. Stainless Steel/ Silicon Nitride is taken as the FGM constituents of the beam for all the plots.

It can be seen from the Figs. 3.5(a)-(d), that the frequency of the beam increases as L/h_{max} increases. This is because the effect of shear deformation decreases with increase in L/h_{max}. It can also be seen that the change in frequency with the increase of L/h_{max}, is maximum for $h_{max}/l=1$ and minimum for classical beam. The effects are more prominent for the second mode than the first mode for both chord-wise and flap-wise vibration.

3.4. Speed-Frequency Behavior for Different Parametric Variations

The parameters which are considered to see its effects on non-dimensional speed-frequency behavior are as follows: Size-dependent thickness (h_{max}/l), axial gradation index (k_l), thickness gradation index (k_t), taperness parameters (C_b, C_h), hub parameter (η), length thickness ratio $(L/h_{\max})$, operating temperature (T_f) and FGM composition. Each of the Figs. 3.6-3.13, presenting variations of the above-mentioned parameters, contains four figures namely, (a), (b), (c) and (d) which correspond to the first chord-wise, first flap-wise, second chord-wise and second flap-wise modes respectively.

There are some characteristics common for all the non-dimensional speed-frequency plots shown in Figs. 3.6-3.13. It represents monotonically increasing frequency with increase in non-dimensional angular speed and this is attributed to the effect of centrifugal stiffening. Further, the rate of increase of frequency with speed is more for the flap-wise modes compared to the chord-wise modes. This is due to the reason that the chord-wise modes are affected by the spin softening. As can be seen from the APPENDIX 2A that the spin softening matrix has no element corresponding to the out-of-plane displacement w_0.

Fig. 3.6 presents the speed-frequency behavior for different size-dependent thicknesses. As the cross-sectional dimensions approach the material length scale parameter (l), i.e., as h_{max}/l decreases, the free vibration frequency increases significantly. As the size-dependent thickness increases, the frequency decreases. It can be seen from the plots that when the thickness approaches ten times of l, the speed-frequency plots for micro beam almost match with the plots for classical beams. This depicts how the microstructure-effect modeled by MCST makes the beam stiffer. It can also be noted from the figure that the stiffening effect is more for the second mode than the first mode. In Figs. 3.6(a) and (c) which are represented for the chord-wise modes, the effect of spin-softening is also shown for $h_{max}/l = 2$. It clearly shows how the chord-wise modes are affected by spin-softening. The results illustrate the concept presented in the previous paragraph. It is also clear from the figures that the spin-softening has more influence for the first mode compared to the second mode.

In Figs. 3.7 and 3.8, the effects of varying axial gradation index (k_l) and thickness gradation index (k_t) are presented. Both these figures show that as k_l and k_t increases, the free vibration frequency decreases, irrespective of the mode of vibration considered. As increasing any of the gradation indices means increasing the volume fraction of metallic constituents in the beam. As metals has lower stiffness and higher density than ceramics, the free vibration frequency of the beam decreases. The effect of gradation indices is seen to be more pronounced for the second mode.

Fig. 3.9 presents the speed-frequency behavior with the variation in taperness parameters i.e., C_b and C_h. Here, as the values of taperness parameters increase, the non-dimensional free vibration frequency also increases for the beam and this effect is higher for higher values of C_b and C_h. This is a reverse phenomenon if compared with homogeneous double-tapered rotating beams. This is attributed to the fact that with decrease in the cross sectional dimensions from the hub end to the free end, the beam stiffness and weight increases and decreases respectively. And the resultant effect leads to increase in frequency with increase in taperness parameters.

Fig. 3.10 shows the effect of hub parameter (η) on the free vibration of the BFGM straight double-tapered rotating micro beam. It can be seen that the frequency increases with increase in the value of η and this effect becomes dominant when the rotational speed increases, resulting into a diverged nature of the plots. This effect is resulted from increasing centrifugal force as increasing the hub parameter means that the beam is mounted on the hub at a higher radius from the axis of rotation.

Effect of the length-thickness ratio (L/h_{max}) on the free vibration behavior is illustrated in Fig. 3.11. As the length-thickness ratio is increased from 10 to 50, the frequency increases and this effect is very prominent for the second mode for both chord-wise and flap-wise vibrations. This is due to the decreased effect of shear deformation effect with increasing length-thickness ratio. For lower L/h_{max} values, the relatively sharper change in the cross sectional dimensions is also an important factor to make the beam less stiffer and that results in decrease of frequency.

The effect of high-temperature operating environment on non-dimensional speed-frequency behavior is shown in Fig. 3.12. It shows that the frequency decreases with increasing operating temperature and this behavior is more prominent for the second modes of vibration. The thermo-elastic degradation of the material parameters resulting in decreased beam stiffness with increasing temperature is responsible for above-stated behavior.

Different constituent materials have different extent of effect on the speed-frequency behavior of the BFGM rotating micro beam and this is depicted in Fig. 3.13. As can be seen from the figure, the FGM constituents as sorted in exhibiting ascending nature of frequency are: Titanium Alloy/Zirconia, Stainless Steel/Zirconia, Stainless Steel/Alumina, Stainless Steel/Silicon Nitride. This pattern is consistent both for the first and second mode, but with different extent. For the first modes, the speed-frequency behavior for each of the compositions differs significantly from each other. But for the second mode, Stainless

Steel/Alumina and Stainless Steel/Silicon Nitride shows significant difference in behavior whereas the other two compositions exhibit very little difference in its speed-frequency behavior. The effect of changing material composition is due to the relative changes of the effective material properties in the operating temperature.

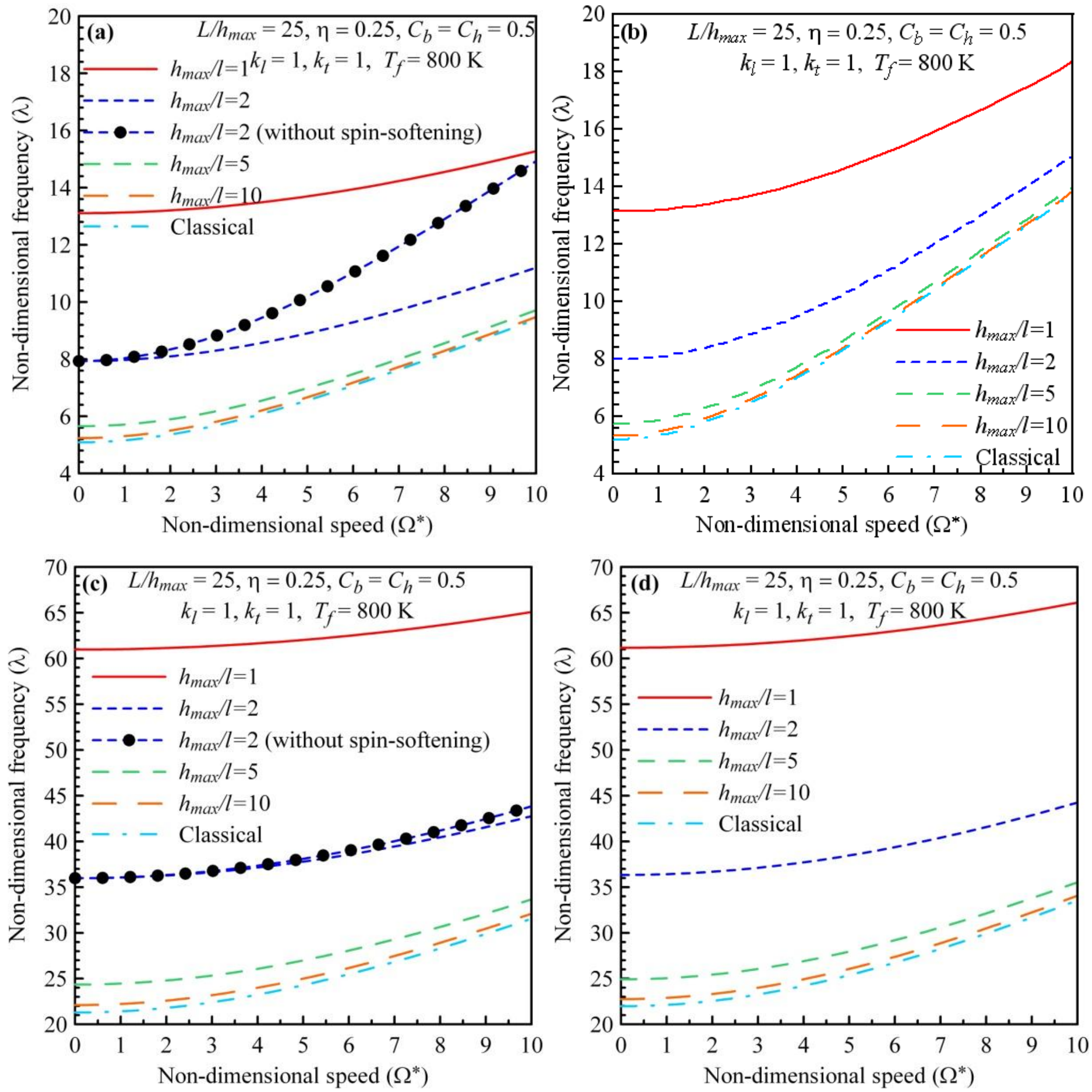

Fig. 3.6: Non-dimensional speed-frequency behavior for different size-dependent thicknesses of a Stainless Steel/Silicon Nitride beam: **(a)** First chord-wise mode, **(b)** First flap-wise mode, **(c)** Second chord-wise mode, **(d)** Second flap-wise mode.

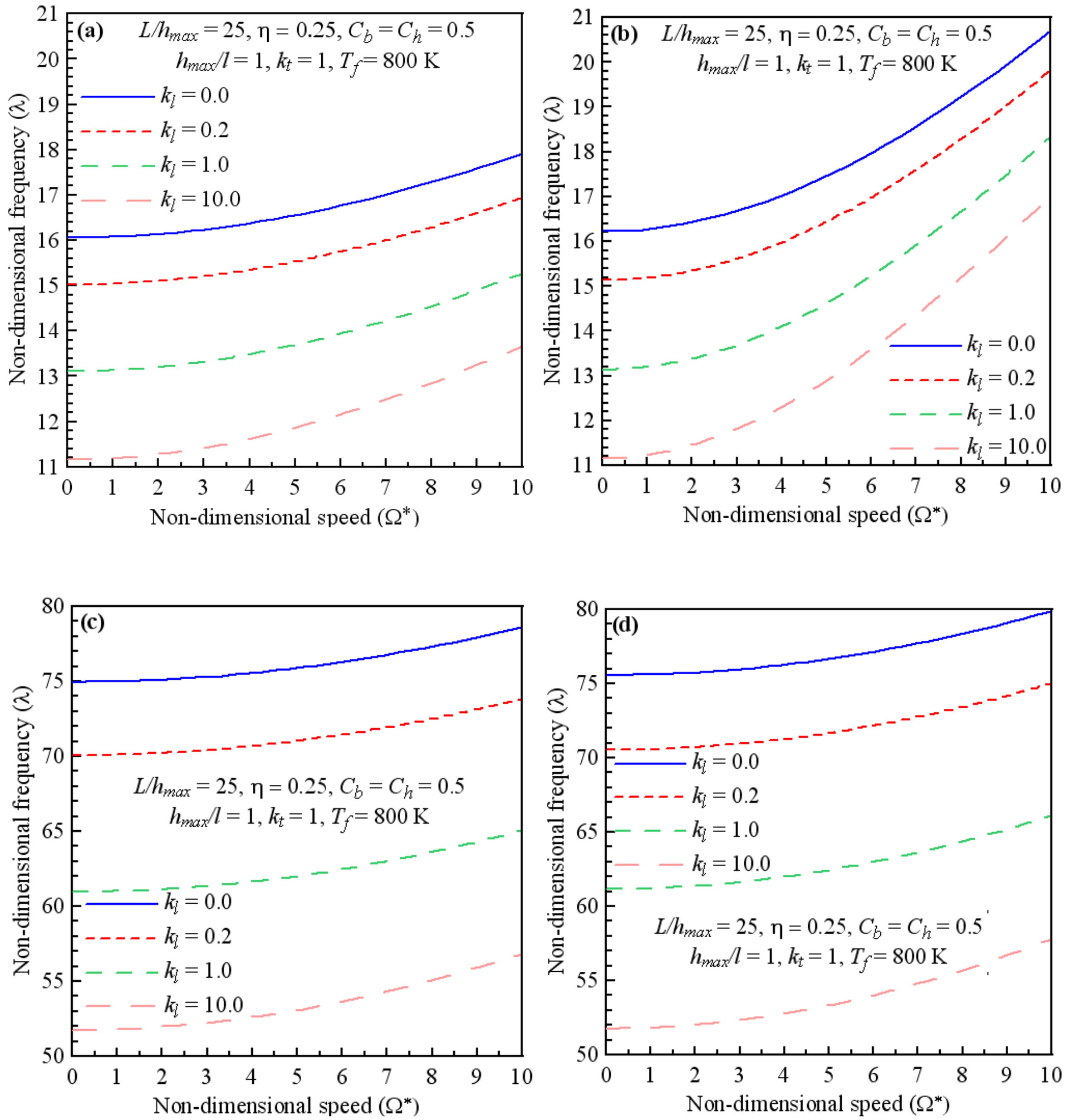

Fig. 3.7: Non-dimensional speed-frequency behavior for different axial gradation indices of a Stainless Steel/Silicon Nitride beam: **(a)** First chord-wise mode, **(b)** First flap-wise mode, **(c)** Second chord-wise mode, **(d)** Second flap-wise mode.

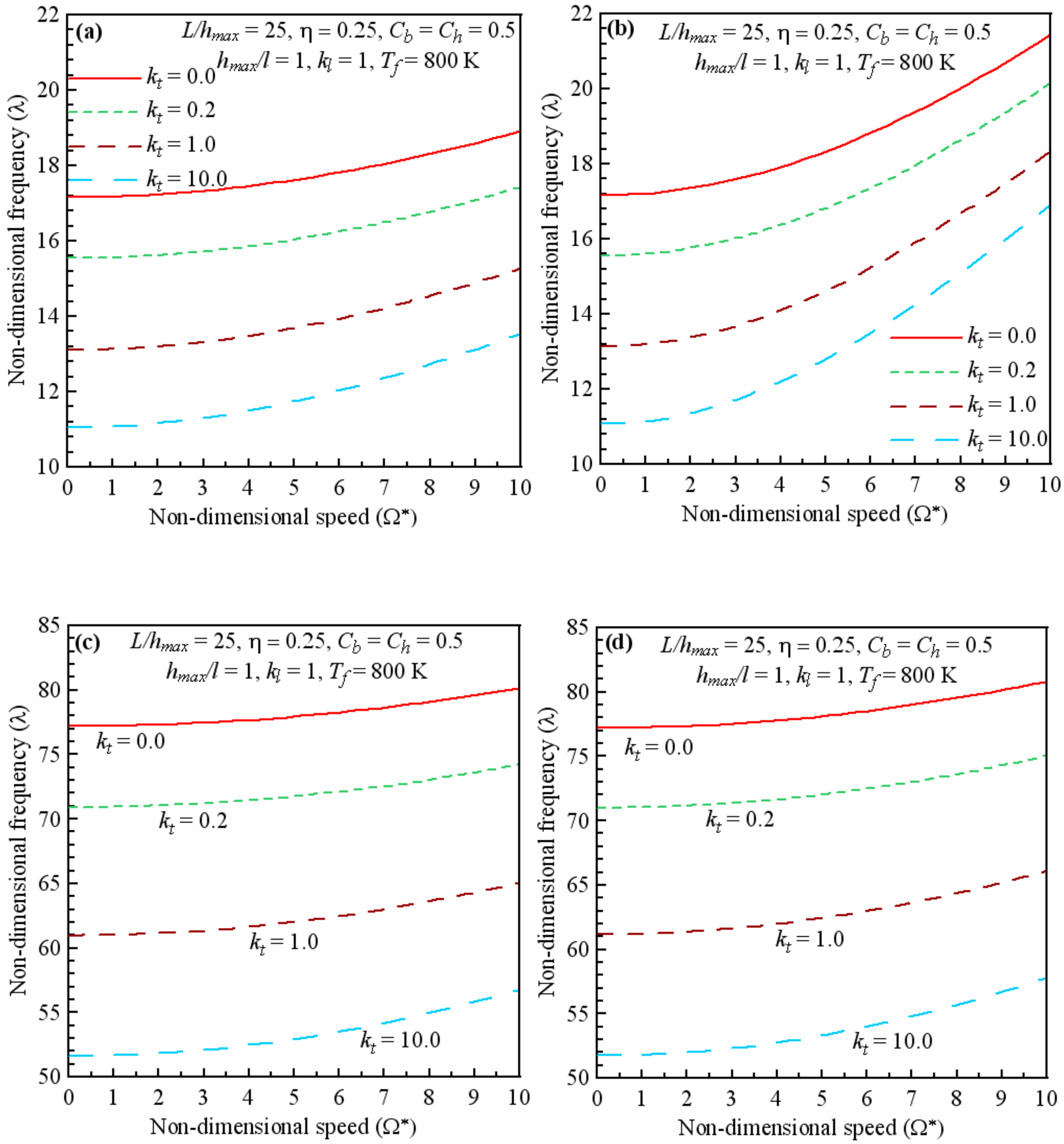

Fig. 3.8: Non-dimensional speed-frequency behavior for different thickness gradation indices of a Stainless Steel/Silicon Nitride beam: **(a)** First chord-wise mode, **(b)** First flap-wise mode, **(c)** Second chord-wise mode, **(d)** Second flap-wise mode.

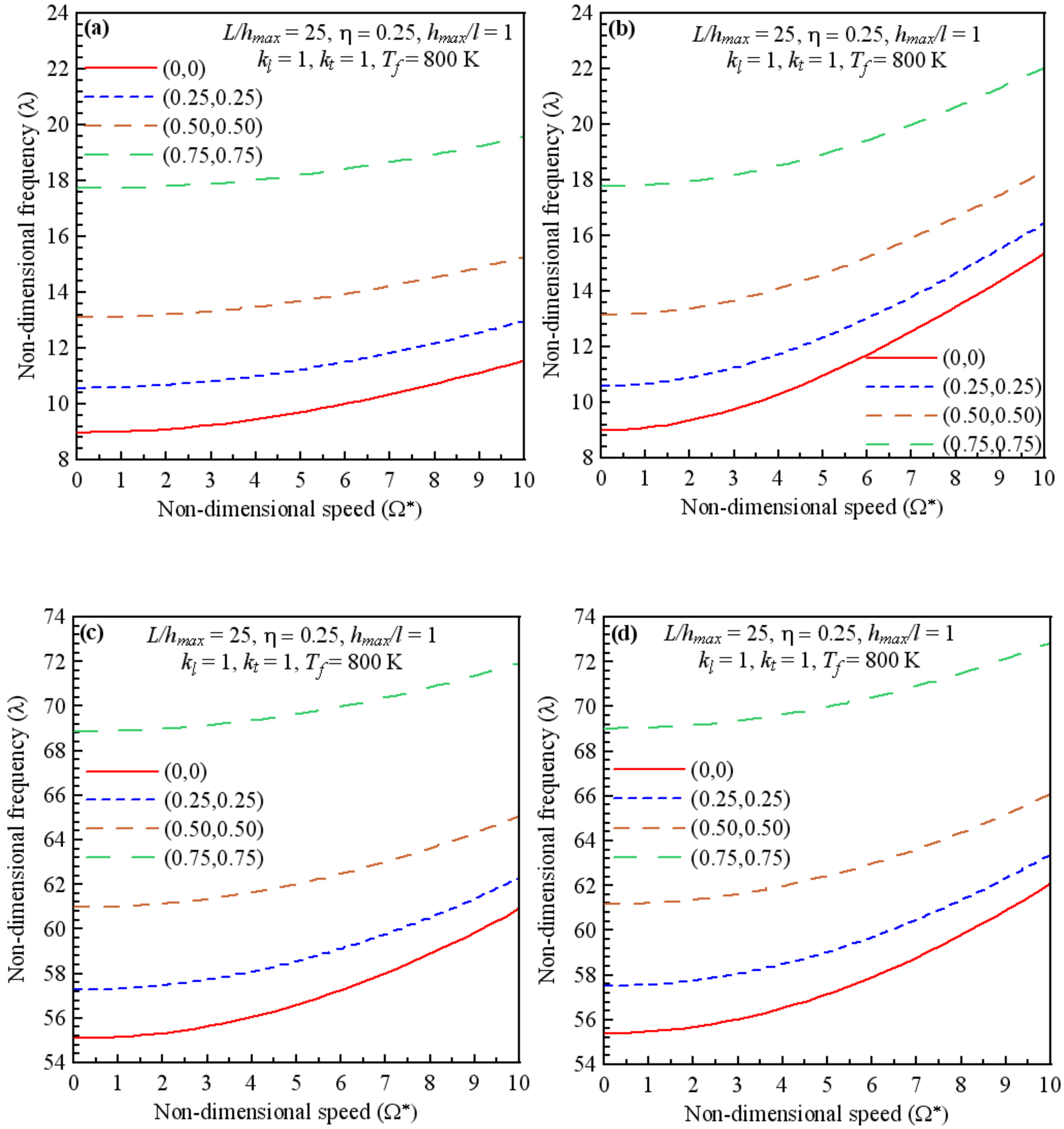

Fig. 3.9: Non-dimensional speed-frequency behavior for different taperness parameters (C_b, C_h) of a Stainless Steel/Silicon Nitride beam: **(a)** First chord-wise mode, **(b)** First flap-wise mode, **(c)** Second chord-wise mode, **(d)** Second flap-wise mode.

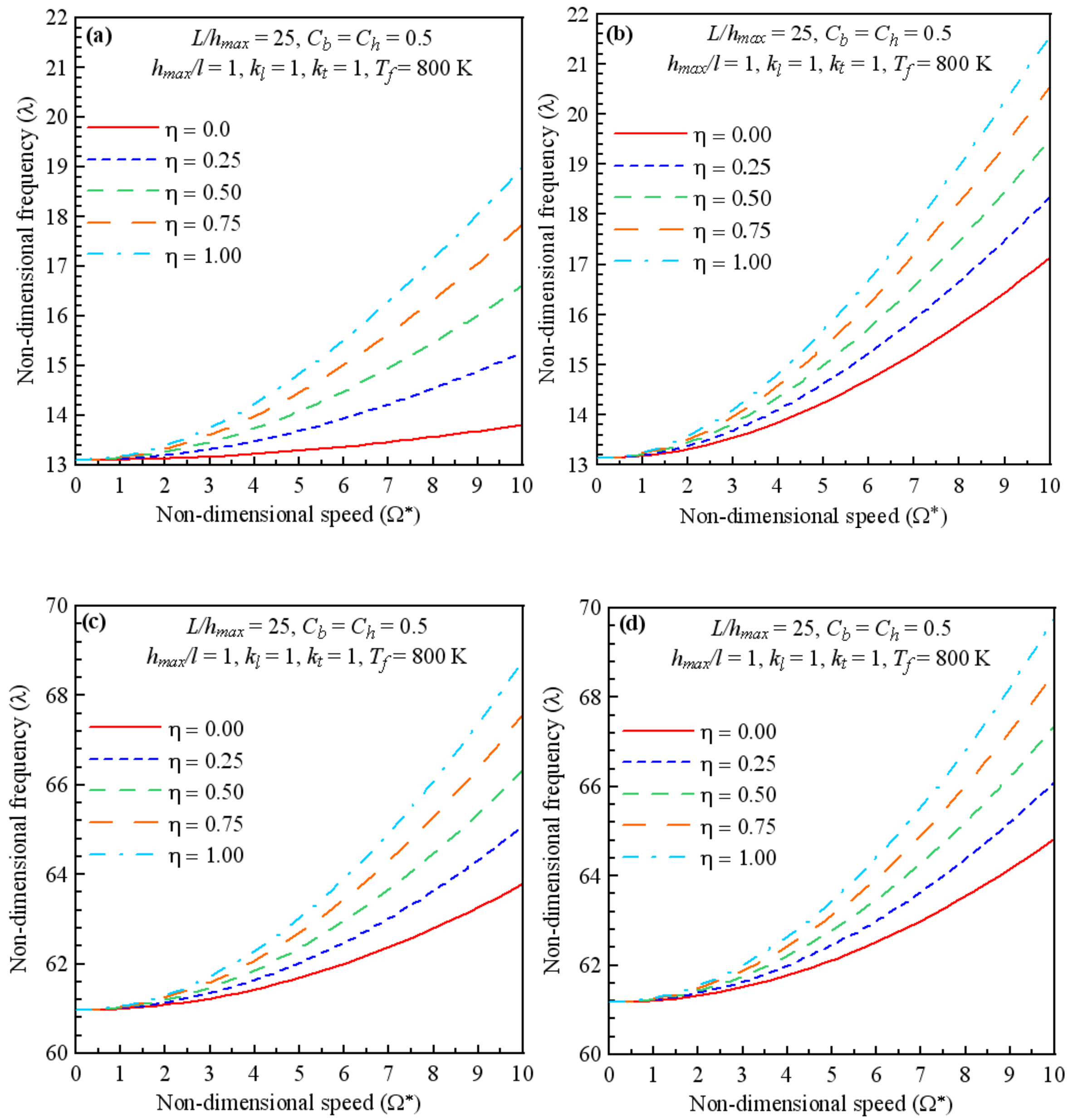

Fig. 3.10: Non-dimensional speed-frequency behavior for different hub radius parameters of a Stainless Steel/Silicon Nitride beam: **(a)** First chord-wise mode, **(b)** First flap-wise mode, **(c)** Second chord-wise mode, **(d)** Second flap-wise mode.

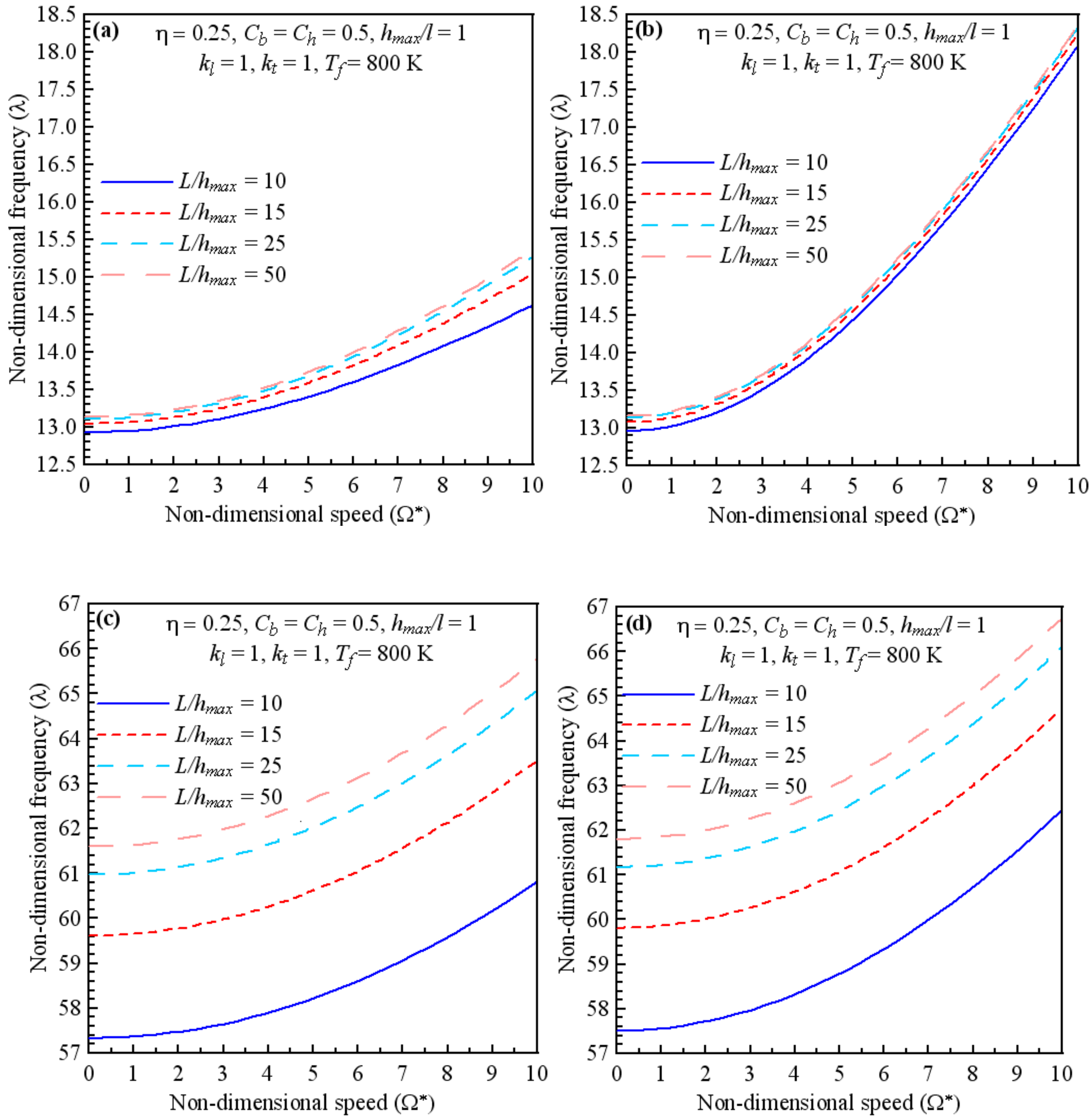

Fig. 3.11: Non-dimensional speed-frequency behavior for different length-to-thickness ratios of a Stainless Steel/Silicon Nitride beam: **(a)** First chord-wise mode, **(b)** First flap-wise mode, **(c)** Second chord-wise mode, **(d)** Second flap-wise mode.

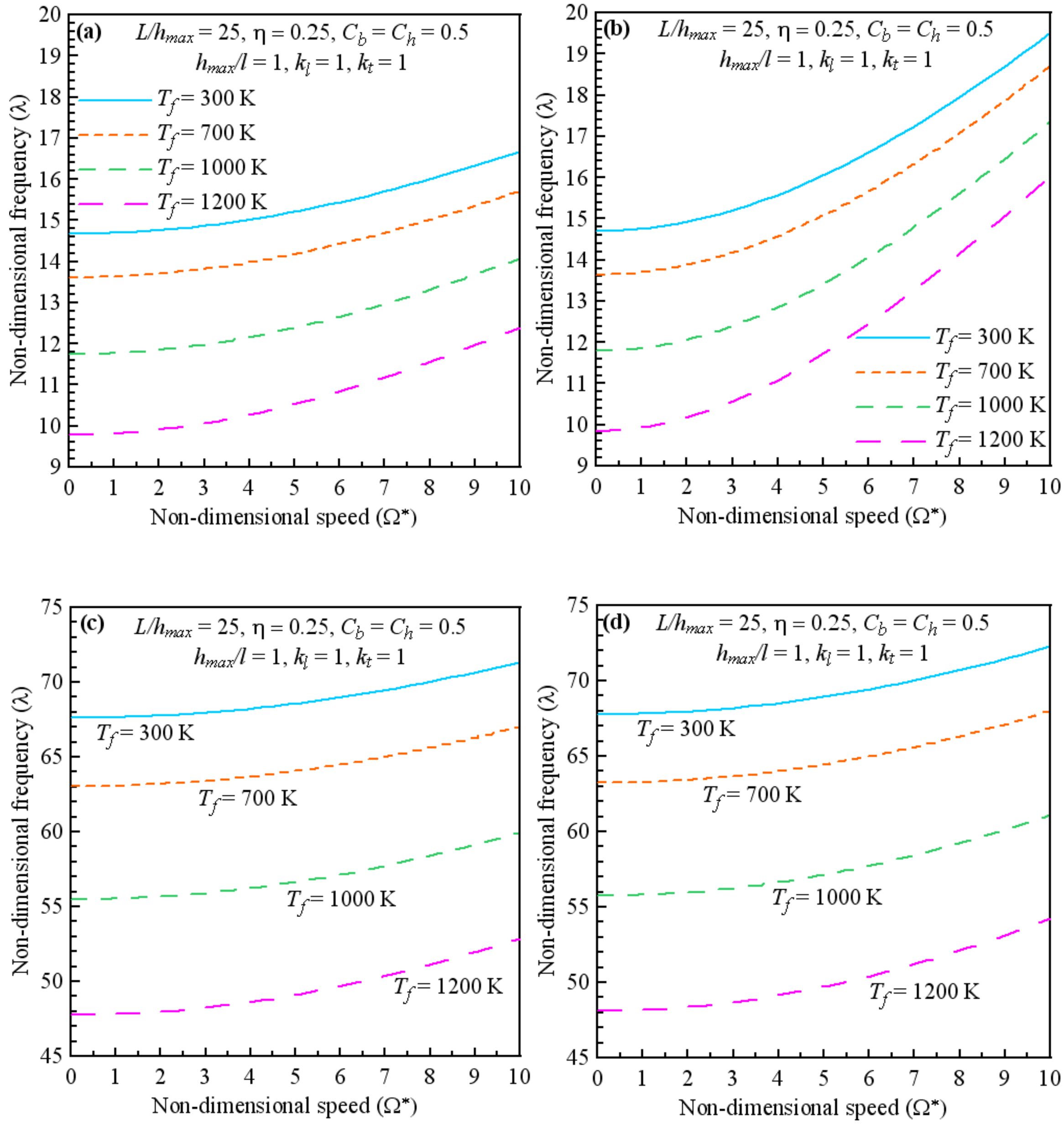

Fig. 3.12: Non-dimensional speed-frequency behavior for different temperatures of a Stainless Steel/Silicon Nitride beam: **(a)** First chord-wise mode, **(b)** First flap-wise mode, **(c)** Second chord-wise mode, **(d)** Second flap-wise mode.

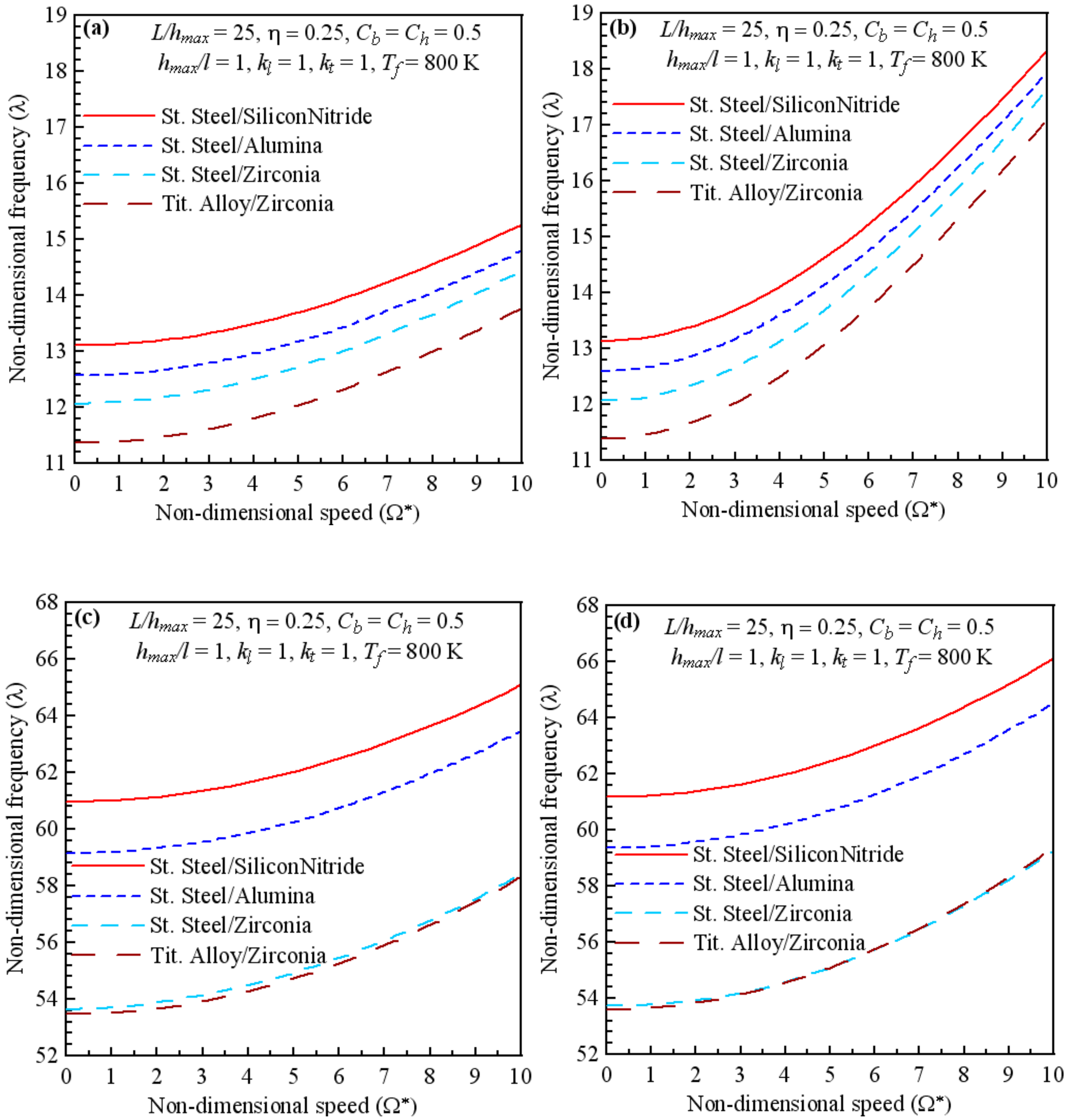

Fig. 3.13: Non-dimensional speed-frequency behavior for different FG compositions: **(a)** First chord-wise mode, **(b)** First flap-wise mode, **(c)** Second chord-wise mode, **(d)** Second flap-wise mode.

3.5. Chapter Summary

The results of the study of free vibration behavior of BFGM straight double-tapered rotating micro beam are presented in this chapter. The present model is successfully validated by comparing several results of the reduced problems available in the literature. The effect of size-dependent shear deformation is presented and discussed. The results are presented in non-dimensional speed-frequency plane for variations of size-dependent thickness, axial gradation index, thickness gradation index, taperness parameters, hub parameter, length-thickness ratio, operating temperature and FGM composition. The important findings are summarized as follows:

(i) As the cross sectional dimensions approach the material length scale parameter, the frequency of vibration increases due to increase in stiffness.

(ii) Spin-softening only affects the chord-wise modes and does not influence the flap-wise modes.

(iii) Increasing material gradation index (for both axial and thickness directions) reduces the frequency of vibration.

(iv) Increasing the taperness parameters reduce the frequency of vibration.

(v) Increasing the hub parameter increases the frequency of vibration.

(vi) Increasing length-thickness ratio increases the frequency of vibration.

(vii) High-temperature environment causes thermo-elastic degradation causing a reduction in frequency.

(viii) The effect of FGM composition is found to be prominent on the free vibration behavior.

"This page is intentionally left blank"

Chapter 4

RESULTS AND DISCUSSION FOR BFGM PRE-TWISTED TAPERED ROTATING MICRO BEAM

4.1. Introduction

In Chapter 2, the detailed mathematical formulation for free vibration study of BFGM pre-twisted double-tapered rotating micro beam is presented. First, the deformed configuration of the pre-twisted beam due to time-independent centrifugal force is determined using minimum total potential energy principle. TBT in conjunction with von Kármán nonlinearity is used to model the strain-displacement behavior. In the subsequent step, a tangent stiffness based formulation is executed and Hamilton's principle is used to formulate the governing equations for free vibration. Both the steps are solved by approximating the displacement fields according to Ritz method. The geometry of the pre-twisted double-tapered beam attached to a hub is already shown in Fig. 2.1 with appropriate axes and dimensions.

The results of this study are presented in four sections. First, some reduced problems are solved and the results are compared with those found in the relevant literatures, to validate the current model. Then the non-dimensional speed-frequency behavior of the beam is presented to show the effects of spin-softening and Coriolis force. Next, the effect of pre-twist angle has been shown for different aspect ratios (κ) of the beam. Finally, the non-dimensional speed-frequency behaviors of the beam are presented to exhibit the effects of different parameters such as size-dependent parameter (μ), axial gradation index (k_l), thickness gradation index (k_t), operating temperature (T_f), FGM composition, taperness parameters (C_b, C_h), slenderness parameter (ξ) and hub parameter (η).

As the present problem involves both chord-wise and flap-wise vibrations, there should be consistency in defining the size-dependent dimension and non-dimensional scheme of various parameters. So a parameter namely aspect ratio (κ) of the beam section at the hub end is introduced and is defined as $\kappa = b_{max} / h_{max}$. Accordingly, the size-dependent parameter (μ), slenderness parameter (ξ) and minimum area moment of inertia at the root end (I_{min}) are defined as follows:

For $\kappa > 1$: $\mu = h_{max} / l$; $\xi = L / h_{max}$; $I_{min} \left(= b_{max} \left(h_{max} \right)^3 / 12 \right)$. (4.1a)

For $\kappa \leq 1$: $\mu = b_{max} / l$; $\xi = L / b_{max}$; $I_{min} \left(= h_{max} \left(b_{max} \right)^3 / 12 \right)$. (4.1b)

The non-dimensional angular speed (Ω^*), non-dimensional frequency of vibration (λ) and hub parameter (η) are defined as follows:

$$\Omega^* = \Omega L^2 \left[\left(\rho_m A \right) / \left(E_m I_{min} \right) \right]^{1/2};\ \lambda = \omega L^2 \left[\left(\rho_m A \right) / \left(E_m I_{min} \right) \right]^{1/2};\ \eta = R_O / L .$$

Here $A(= b_{max} h_{max})$ is the cross sectional area at the hub end; E_m and ρ_m are Young's modulus and mass density of the metallic constituent evaluated at ambient temperature T_0 =300 K. Unless otherwise stated and except the validation study, the results are generated considering Stainless Steel (SUS304)/Silicon Nitride (Si_3N_4) composition and using the following values: l=17.6 μm, μ=1, ξ=25, η=0.25, $\bar{\beta} = 45^0$, $C_b = C_h$=0.5, k_l=1, k_t=1, T_f =700 K. For each parameter variation, the speed-frequency relation is shown for the first and second mode for each of chord-wise and flap-wise vibrations.

4.2. Validation Study

Due to lack of similar kind of analysis, several studies are done to validate the current model by comparing the results of various reduced problems with the available results in the literature. The variation of fundamental flap-wise frequencies with rotational speeds are compared with Zarrinzadeh et al. (2012) and the results are presented in Table 4.1. For this comparison, the non-dimensional frequency is defined as

$\lambda = \omega L^2 \left[(\rho_c A) / (E_c I_{min}) \right]^{1/2}$. This tabular data provides the speed-frequency variation for different hub parameters (η) for an axially functionally graded $(k_l = 2.0 \text{ and } k_t = 0.0)$ straight $(\bar{\beta} = 0)$ thickness-tapered $(C_h = 0.5, C_b = 0)$ rotating classical $(l = 0)$ beam of Alumina/Zirconia composition. Following values are considered for the above-mentioned comparison: ξ =50, E_m =70 GPa, E_c =200 GPa, ρ_m =2702 kg/m^3, ρ_c =5700 kg/m^3, $\upsilon_m = \upsilon_c$ =0.3. It is evident from Table 4.1, that the present model provides matching results with Zarrinzadeh et al. (2012).

Table 4.1: Comparison of fundamental flap-wise free vibration frequencies for different rotational speeds and hub parameters for an Alumina/Zirconia AFGM straight thickness-tapered rotating classical beam

Ω^*	η =0.0		η =0.1		η =1.0	
	Present	Zarrinzadeh et al. (2012)	Present	Zarrinzadeh et al. (2012)	Present	Zarrinzadeh et al. (2012)
1	4.7432	4.7452	4.7617	4.7638	4.9272	4.928
2	5.1331	5.1351	5.2015	5.2033	5.7781	5.7801
3	5.7189	5.721	5.8553	5.8573	6.9603	6.9619
4	6.4431	6.4441	6.6548	6.657	8.3238	8.3252
5	7.2564	7.258	7.5495	7.5504	9.7857	9.7875
6	8.1292	8.1307	8.5014	8.5035	11.3042	11.3059
7	9.0406	9.0416	9.4936	9.4948	12.8566	12.8579
8	9.977	9.9778	10.5097	10.5112	14.4306	14.4311
9	10.9303	10.9308	11.5438	11.5443	16.0185	16.0181
10	11.8954	11.8954	12.5887	12.5889	17.6166	17.6147
11	12.8689	12.8682	13.6436	13.6418	19.2213	19.2182
12	13.8491	13.8469	14.703	14.7005	20.8319	20.8267

A successful comparison with Salamat-talab et al. (2012) depicting the variation of normalized fundamental free vibration frequency with size-dependent parameter is presented in Fig. 4.1. For this comparison plot, an Aluminum/Alumina TFGM $\left(k_t = 1.0 \text{ and } k_l = 0.0\right)$ straight $\left(\bar{\beta} = 0\right)$ prismatic $\left(C_b = C_h = 0\right)$ non-rotating micro beam (l =15 μm) is considered with simply supported ends. The asymmetric TFGM is modeled by replacing $\left|\frac{z'}{h/2}\right|^{k_t}$ by $\left(\frac{z'}{h} + \frac{1}{2}\right)^{k_t}$ in Eq. 2.6. The result is produced with the following values: κ =2.0, ξ =10, E_m =70 GPa, E_c =380 GPa, ρ_m =2700 kg/m^3, ρ_c =3800 kg/m^3, $\upsilon_m = \upsilon_c$ =0.23, and the frequencies of vibration for the corresponding classical beam $\left(\omega_{cl}\right)$ are used to obtain the normalized frequencies. For a simply supported beam, the lowest order functions for approximating the displacement and rotation fields are found in Das (2018). It is to be mentioned that the results of Fig. 4.1 are generated with the three-dimensional stress-strain relationship, for which E_f is replaced by $E_f\left(1-\upsilon_f\right)/\left\{\left(1+\upsilon_f\right)\left(1-2\upsilon_f\right)\right\}$ in the first relation of (2.12) to calculate σ_x (Reddy, 2011). The comparison shows that the present result is in good agreement.

The first two flap-wise and chord-wise free vibration behavior of a homogeneous $\left(k_l = k_t = 0.0\right)$ pre-twisted $\left(\bar{\beta} = 45^0\right)$ prismatic $\left(C_b = C_h = 0\right)$ rotating classical $\left(l = 0\right)$ beam is compared with Yoo et al. (2001) and it is shown in Fig. 4.2 in non-dimensional speed-frequency plane. The results are generated with the following values: κ^2 =2.0, ξ =50, η =1. For Fig. 4.2, the non-dimensional speed $\left(\Omega^*\right)$ and frequency $\left(\lambda\right)$ are defined using $I_{max}\left(= h_{max}\left(b_{max}\right)^3/12\right)$ instead of I_{min} (referring to (4.1a)) as is considered in Yoo et al. (2001). Fig. 4.2, exhibiting mode-veering between the first flap-wise and chord-wise modes, shows excellent matching of the plots. The above comparisons thus validate the present model for BFGM pre-twisted double-tapered rotating micro beams.

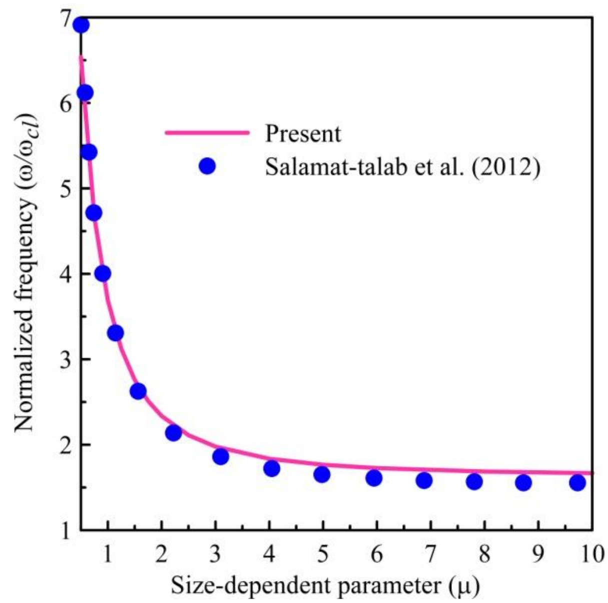

Fig. 4.1: Comparison plot for variation of normalized free vibration frequency with size-dependent parameter for a TFGM straight prismatic non-rotating micro beam with simply supported boundary condition.

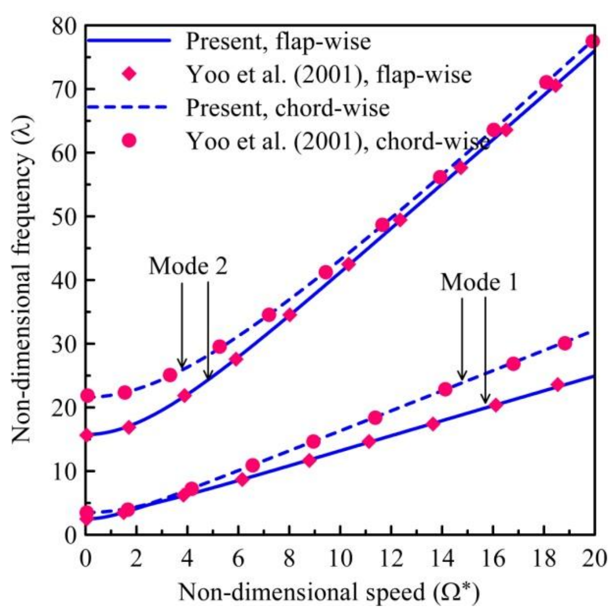

Fig. 4.2: Comparison of non-dimensional speed-frequency behavior for a homogeneous pre-twisted prismatic rotating classical beam.

4.3. Effect of Spin-softening and Coriolis Force

Unless otherwise mentioned, all figures for this and subsequent sections consist of four parts namely (a), (b), (c) and (d) representing non-dimensional speed-frequency behavior as follows: Each of (a) and (c) represents the first two modes for κ =0.5 and 2.0 respectively; Each of (b) and (d) represents the third and fourth modes for κ =0.5 and 2.0 respectively. For pre-twisted rotating beams, chord-wise and flap-wise motions are coupled and both contribute to all the bending vibratory modes, where one of them dominates over the other. For the above-mentioned category of figures, for κ =0.5, the first and third modes represent chord-wise-dominated vibration (called chord-wise vibration) and the second and fourth modes represent flap-wise-dominated vibration (called flap-wise vibration), and vice-versa for κ =2.0 (exception when mode-veering occurs). This means that even though the beam is thickness- and axially-graded, the order of occurrence of chord-wise and flap-wise motions are governed by the relative values of the principal area moments of inertia (contributed through A_2 and A_3 in (2.15)). A plot dominated by the chord-wise mode is designated by 'c' and that by the flap-wise mode is designated by 'f'. A plot exhibiting mode-switching phenomenon from flap-wise to chord-wise is designed by 'f-c', and vice-versa by 'c-f'.

Figs. 4.3(a)-(d) describe the effect of spin-softening on speed-frequency behavior. As discussed earlier, the spin-softening matrix (APPENDIX 2A) has no component corresponding to the out–plane-displacement w_0 and thus only affects the chord-wise modes. Here in Fig. 4.3, the speed-frequency behavior of different modes and aspect ratios are presented with and without considerations of spin-softening. It is due to spin-softening that the increase of frequency with speed in case of chord-wise modes is not as steep as in flap-wise modes. So, for κ =0.5 (Figs. 4.3(a) and (b)), the mode-veering (and subsequent mode-switching) phenomenon is unlikely to occur. But for κ =2.0, mode-veering can be observed between the first flap-wise and chord-wise modes (Fig. 4.3(c)). In case of second and third mode for κ =2.0 (Fig. 4.3(d)), mode-veering is not observed but it is likely to occur at higher speeds. These results point out the fact that the effect of spin-softening must not be neglected in dynamic analysis of rotating pre-twisted beams. It is also prominent that the spin-softening effect is of great importance for the first chord-wise mode than for its second mode. It is observed that the mode-veering and subsequent mode-switching is observed between the first flap-wise and chord-wise modes for all the other parametric variations presented for κ =2.0.

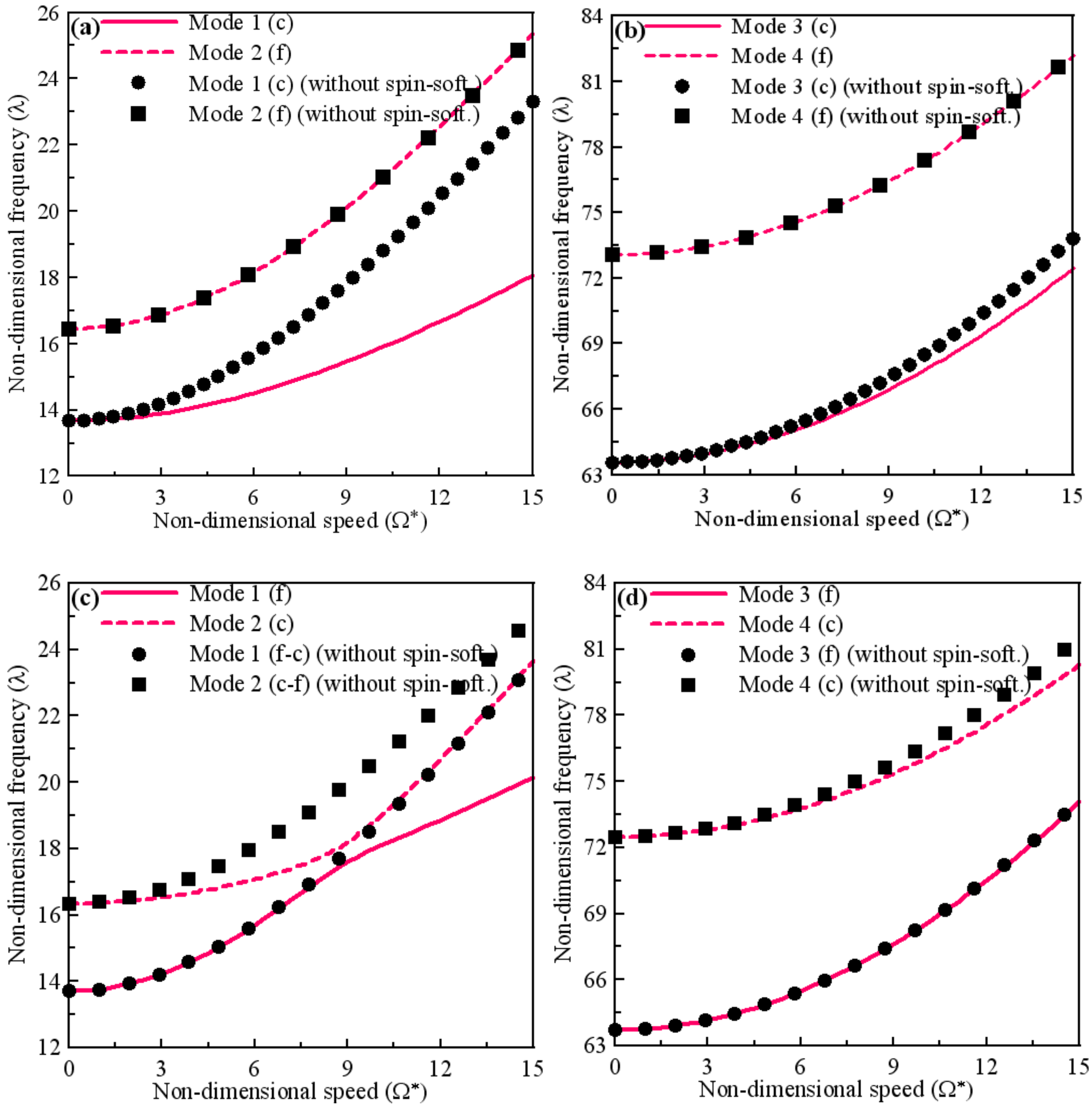

Fig. 4.3: Effect of spin-softening on speed-frequency behavior: **(a)** Modes 1 and 2 for κ =0.5, **(b)** Modes 3 and 4 for κ =0.5, **(c)** Modes 1 and 2 for κ =2.0, **(d)** Modes 3 and 4 for κ =2.0.

Figs. 4.4(a) and (b) show speed-frequency behavior with and without Coriolis effect for ξ=10 and 25 respectively. Both the figures show plots for the first and second chord-wise modes respectively for κ=1. A coupling between the stretching and chord-wise deformations occur due to the Coriolis effect. The second term in the last part (terms associated with Ω) of (2.24) affects the chord-wise vibration through dynamic axial deformation and is relevant for the plots of Fig. 4.4. The first term of the same part of (2.24) affects the axial vibration through dynamic chord-wise deformation and is not relevant here as the axial vibration is not studied in the present thesis work. The flap-wise modes, in spite of being coupled with the chord-wise modes, are not found to be influenced by Coriolis effect, and are not presented in Fig. 4.4. At higher angular speeds, the Coriolis effect is found to soften the chord-wise modes resulting in decrease in the vibration frequency. This effect is found to be significantly prominent at lower value of slenderness parameter (ξ), as because of this, the axial stiffness increases.

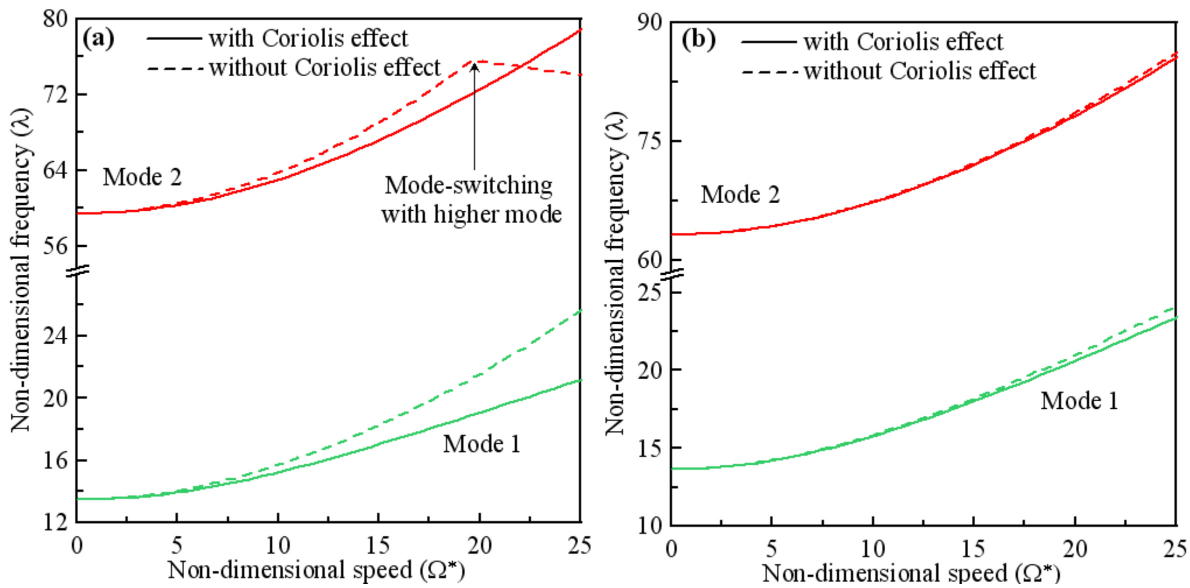

Fig. 4.4: Coriolis effect on speed-frequency behavior for the first two chord-wise modes for κ =1: **(a)** ξ =10, **(b)** ξ =25.

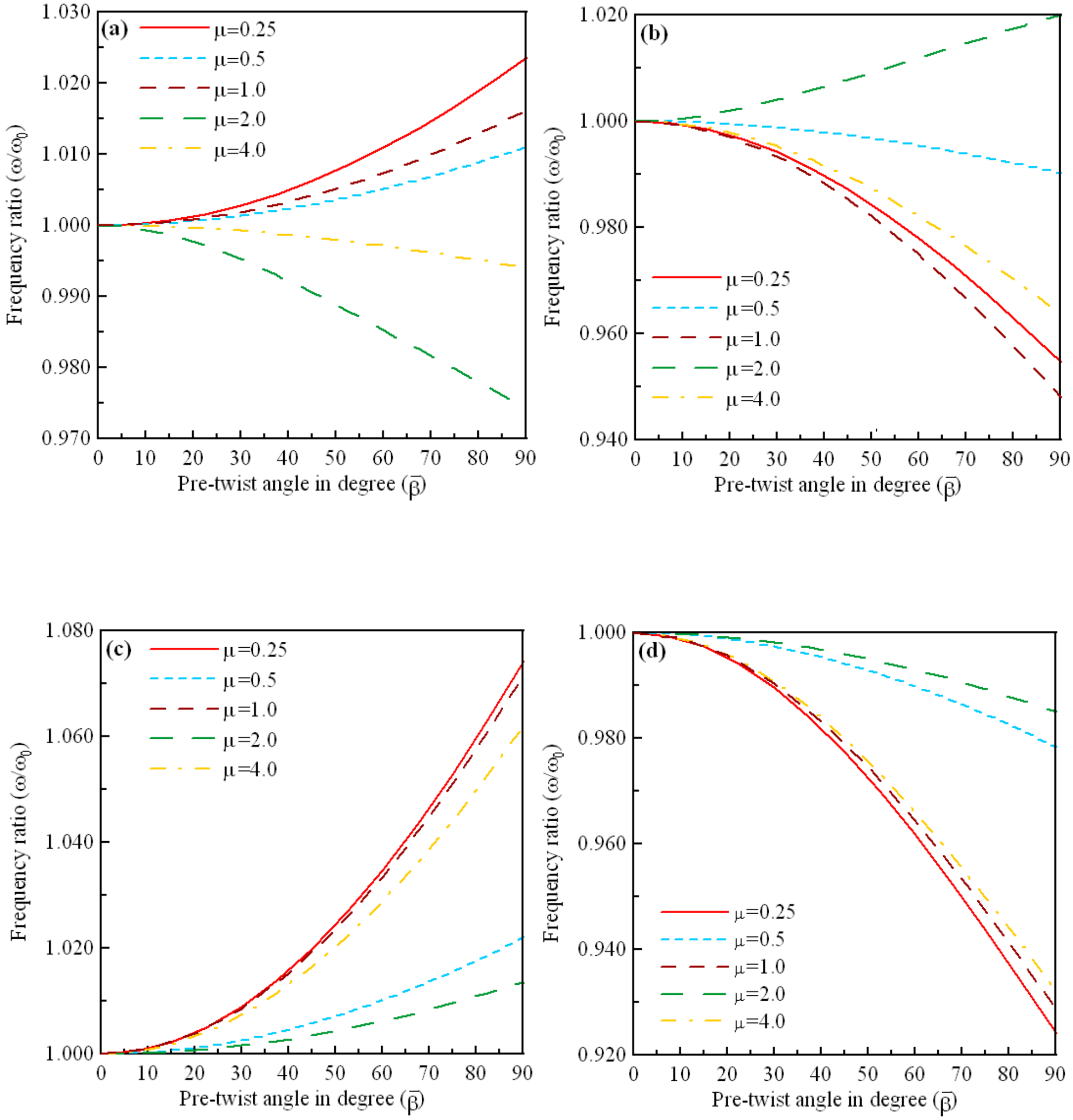

Fig. 4.5: Variation of frequency ratio with pre-twist angle for different aspect ratios at Ω^* =10: **(a)** Mode 1, **(b)** Mode 2, **(c)** Mode 3, **(d)** Mode 4.

4.4. Effect of Pre-twist Angle

Figs. 4.5(a)-(d) describe the variation of frequency ratio $\left(\omega / \omega_0\right)$ with pre-twist angle $\left(\bar{\beta}\right)$ for the first four modes respectively at Ω^*=10. It is clear from the results presented above that the aspect ratio κ has an important role in governing the vibration behavior of a pre-twisted rotating beam. Hence, the variations of frequency ratio with pre-twist angle are plotted for different values of κ. Here ω_0 is the mode-specific frequency of a non-rotating beam for respective values of κ. Fig. 4.5 depicts how the aspect ratio κ governs the change in frequency ratio with pre-twist angle variation. For any particular mode and κ value, with increase in the pre-twist angle, the frequency ratio monotonically changes. This is a significant deviation from the behavior of a square cross section $\left(\kappa = 1\right)$ homogeneous rotating beam where frequency ratio does not vary with pre-twist angle. It is evident that the relative values of the stiffness parameters $\left(A_2, A_3\right)$ and the inertia parameters $\left(\rho_2, \rho_3\right)$ have significant contribution in governing the effect of pre-twist angle.

4.5. Speed-Frequency Behavior for Different Parametric Variations

Figs. 4.6(a)-(d) show the speed-frequency behavior, for different size-dependent parameters $\left(\mu\right)$ including that of the classical theory (l=0). Fig. 4.6 shows that as the smallest cross sectional dimension approach to the order of the material length scale parameter, frequency increases due to enhanced beam stiffness. As the smallest cross sectional dimension increases so that $\mu \geq 10$, the size-effect becomes negligible and the micro beam starts behaving like a classical beam. The mode-veering phenomenon can be visualized in Fig. 4.6(c), for both classical and size-dependent beams. Also as μ increases, mode-veering region shifts to higher values of speeds.

For further understanding of mode-veering and mode-switching phenomena, it is important to visualize the mode shapes. Hence, Figs. 4.7(a)-(d) are presented referring Fig. 4.6(c) and (d) for μ=1, for the first four modes respectively, each showing mode shapes corresponding to the transverse displacements (v_0 and w_0) at two different non-dimensional speeds (5 and 15). With reference to Fig. 4.6(c), Figs. 4.7(a) and (b) show that before mode-switching (Ω^*=5), the first and the second modes are dominated by the flap-wise and chord-wise motions respectively, and vice-versa after the occurrence of mode-switching (Ω^*=15). The third and fourth modes (Figs. 4.7(c) and (d)) are dominated by the flap-wise and chord-wise motions respectively for the entire speed range as is evident from Fig. 4.6(d) which does not exhibit any mode-veering.

Figs. 4.8(a) and (b) present speed-frequency behavior for the first-second and third-fourth modes respectively for thickness gradation index (k_t)=0, each for different axial gradation indices (k_l). Similar plots for k_t=1 are shown in Figs. 4.8(c) and (d), and that for k_t=2 are shown in Figs. 4.8(e) and (f). Figs. 4.8(a)-(f) are presented for κ=0.5. Plots involving similar parametric variations with κ=2.0 are shown in Figs. 4.9(a)-(f). As can be seen from the relation (2.6), if either k_l or k_t or both are increased, proportion of metal in the beam increases. Stainless Steel/Silicon Nitride is considered as the beam constituent material for Figs. 4.8 and 4.9, where the Stainless Steel has a lesser value of elastic modulus and a greater value of density than its ceramic counterpart. Hence, increasing k_l or k_t or both, results in decrease of frequency, irrespective of the modes and aspect ratio considered. Further for κ=2.0, the first and second modes exhibit mode-veering and subsequent mode-switching (except for k_t=0 in Fig. 4.9(a) which seems to exhibit mode-veering at higher angular speeds). Also it can be seen that, with increase in either k_l or k_t or both, the mode-veering region shifts towards left implying it to occur at lower angular speeds.

Speed-frequency behaviors for different operating temperature (T_f) are presented in Figs. 4.10(a)-(d). At higher operating temperatures, the material properties, especially the elastic modulus, undergo thermo-elastic degradation. This leads to decrease in frequency with increasing temperature. The thermal effect is found to be more prominent on the second modes of vibration.

Figs. 4.11(a)-(d) present the speed-frequency behavior for different FGM compositions and show similar nature of the plots for all the compositions considered. All the compositions exhibit mode-veering between the first and second modes for κ=2.0. Further, Stainless Steel/Silicon Nitride and Titanium Alloy/Zirconia exhibit the highest and the lowest value of frequencies for any of the modes considered. The effect of changing FGM composition is found to have greater influence on the second modes compared to the first modes.

The speed-frequency behaviors, for varying taperness parameters (C_b, C_h), are depicted in Figs. 4.12(a)-(d), where, each case considers equal taperness parameter values in width and thickness directions $(C_b = C_h)$. Fig. 4.12 shows that the frequencies increase with increasing taperness parameters. Further, enhanced increase in frequency with the change in the taperness parameters is prominent at higher values of taperness parameters. Also, it is found that the mode-veering region shifts to the right i.e., towards the higher speed region as the taperness parameters increase. The shift in the frequencies for the respective first modes (between chord-wise and flap-wise) (Figs. 4.12(a) and (c)) increases with increasing taperness parameters and this trend is reverse for the respective second modes (Figs. 4.12(b) and (d)). For the present BFGM model, ceramic phase gradually increases compared to the metallic phase towards the free end and toward the extreme layers along z' direction. As for Stainless Steel/Silicon Nitride composition, the metallic constituent being less elastic and more heavier, and the flexural rigidity being higher order function of the cross sectional dimensions, increasing taperness parameters lead to the above-mentioned observations.

Figs. 4.13(a)-(d) present the speed-frequency behavior, each for different slenderness parameters. Decreasing slenderness parameter leads to lowering of the frequency values due to the pronounced effect of shear deformation. The decrease in frequency, which is found to be significant at lower values of slenderness parameters, is more pronounced for the flap-wise modes for κ=0.5 and for the chord-wise modes for κ=2.0. The reason is the obvious fact that the vibrations in these cases take place perpendicular to the thicker dimensions. Also, the effect of slenderness parameter is more significant for the second modes compared to the first modes. Further, the region of mode-veering is found almost unchanged with variation of the slenderness parameter.

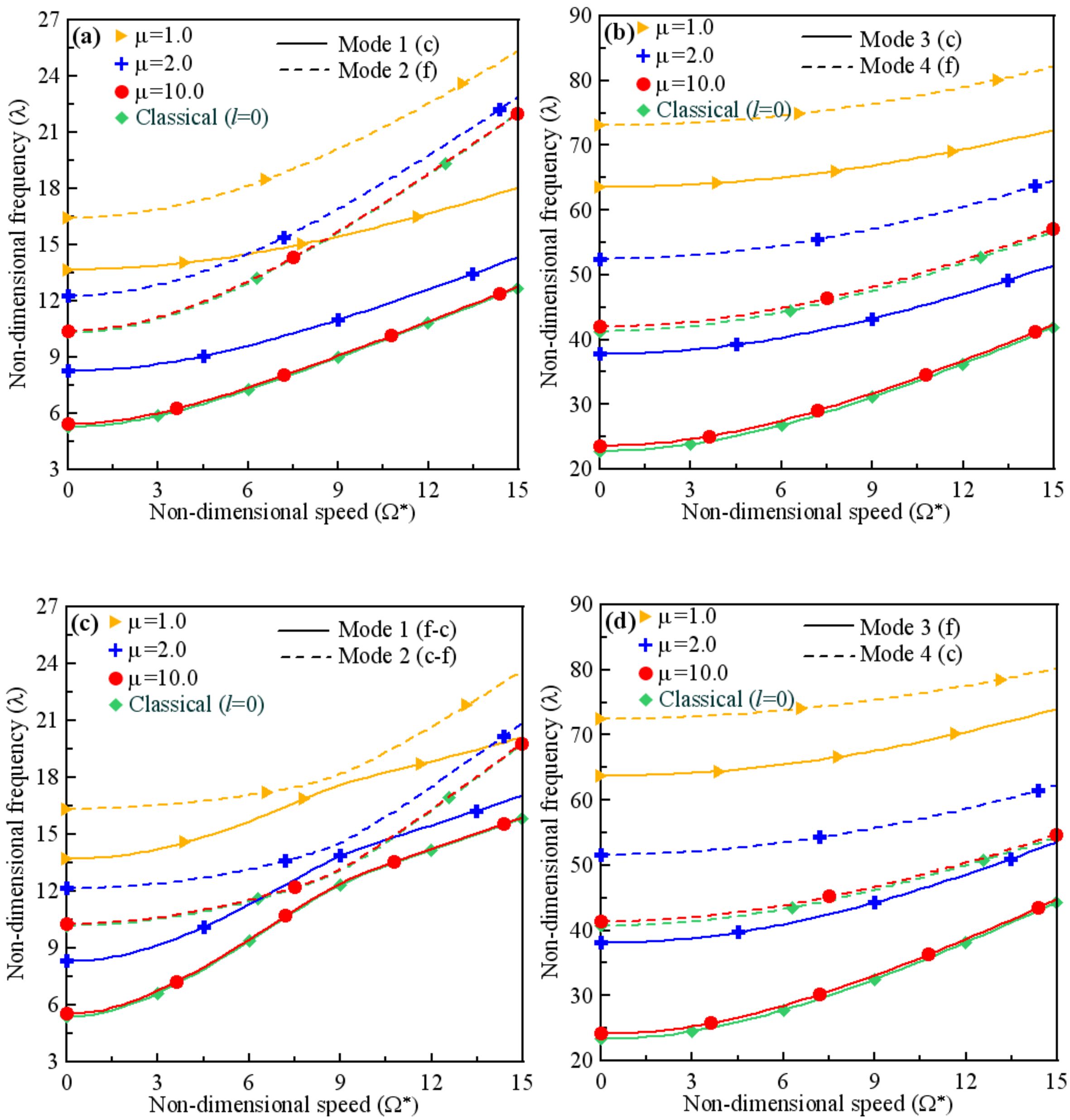

Fig. 4.6: Non-dimensional speed-frequency behavior for variation of size-dependent parameter: **(a)** Modes 1 and 2 for κ =0.5, **(b)** Modes 3 and 4 for κ =0.5, **(c)** Modes 1 and 2 for κ =2.0, **(d)** Modes 3 and 4 for κ =2.0.

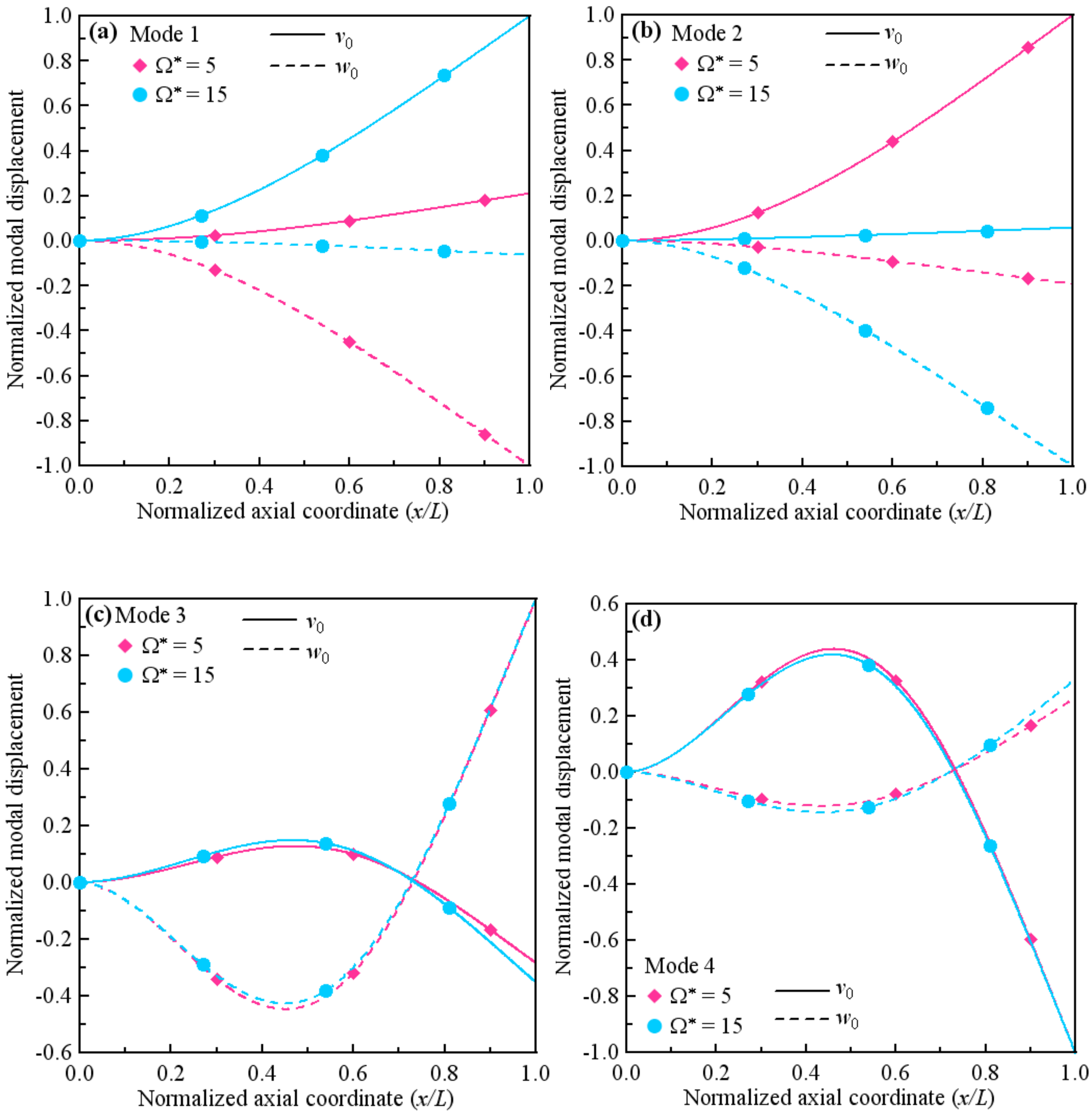

Fig. 4.7: Normalized mode shapes for the first four modes (with reference to Figs. 4.4**(c)** and **(d)** for μ=1) at two different speeds: **(a)** Mode 1, **(b)** Mode 2, **(c)** Mode 3, **(d)** Mode 4.

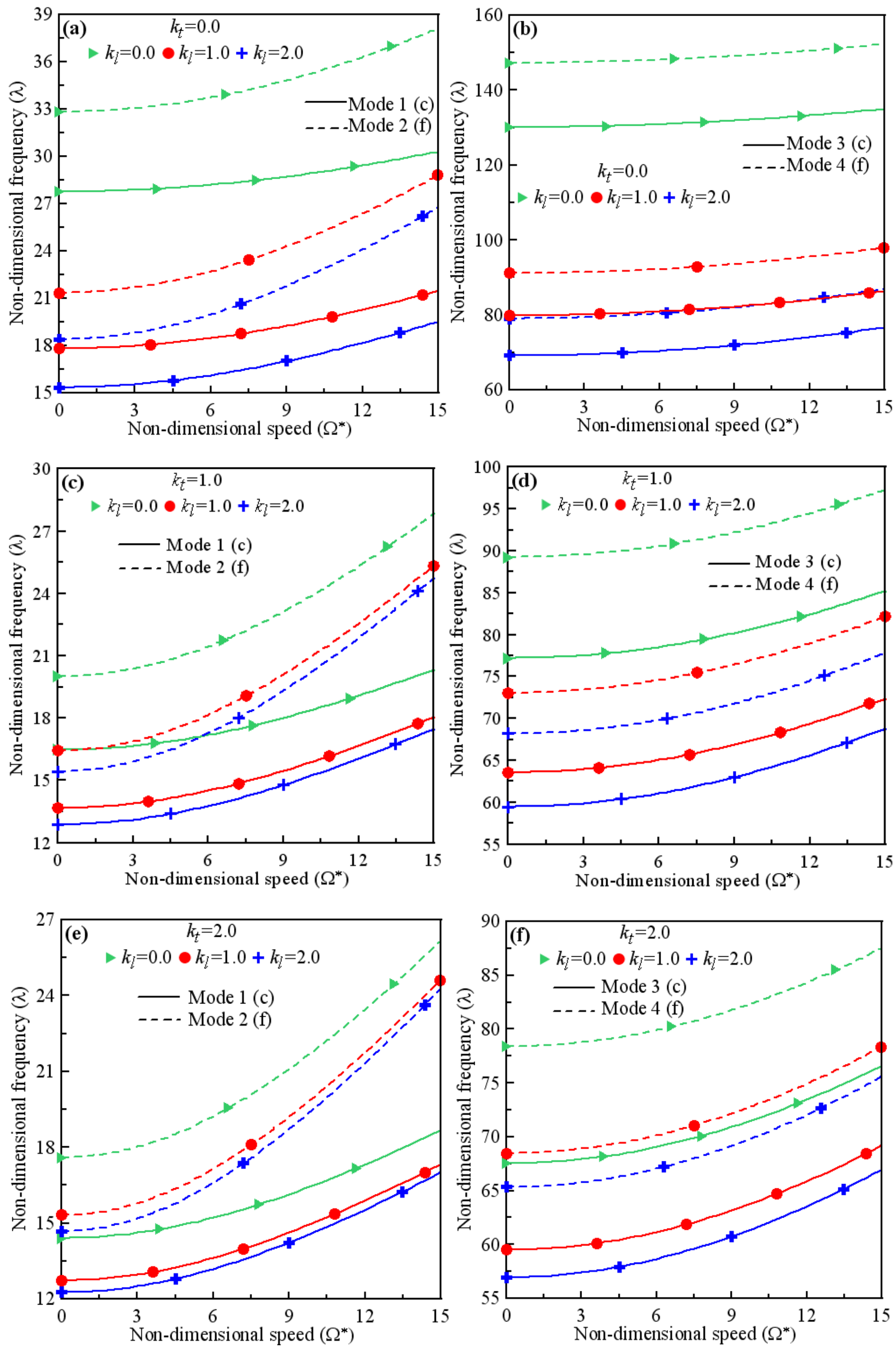

Fig. 4.8: Non-dimensional speed-frequency behavior for variation of axial gradation index for κ =0.5: **(a)** Modes 1 and 2 for k_t =0.0, **(b)** Modes 3 and 4 for k_t =0.0, **(c)** Modes 1 and 2 for k_t =1.0, **(d)** Modes 3 and 4 for k_t =1.0, **(e)** Modes 1 and 2 for k_t =2.0, **(f)** Modes 3 and 4 for k_t =2.0.

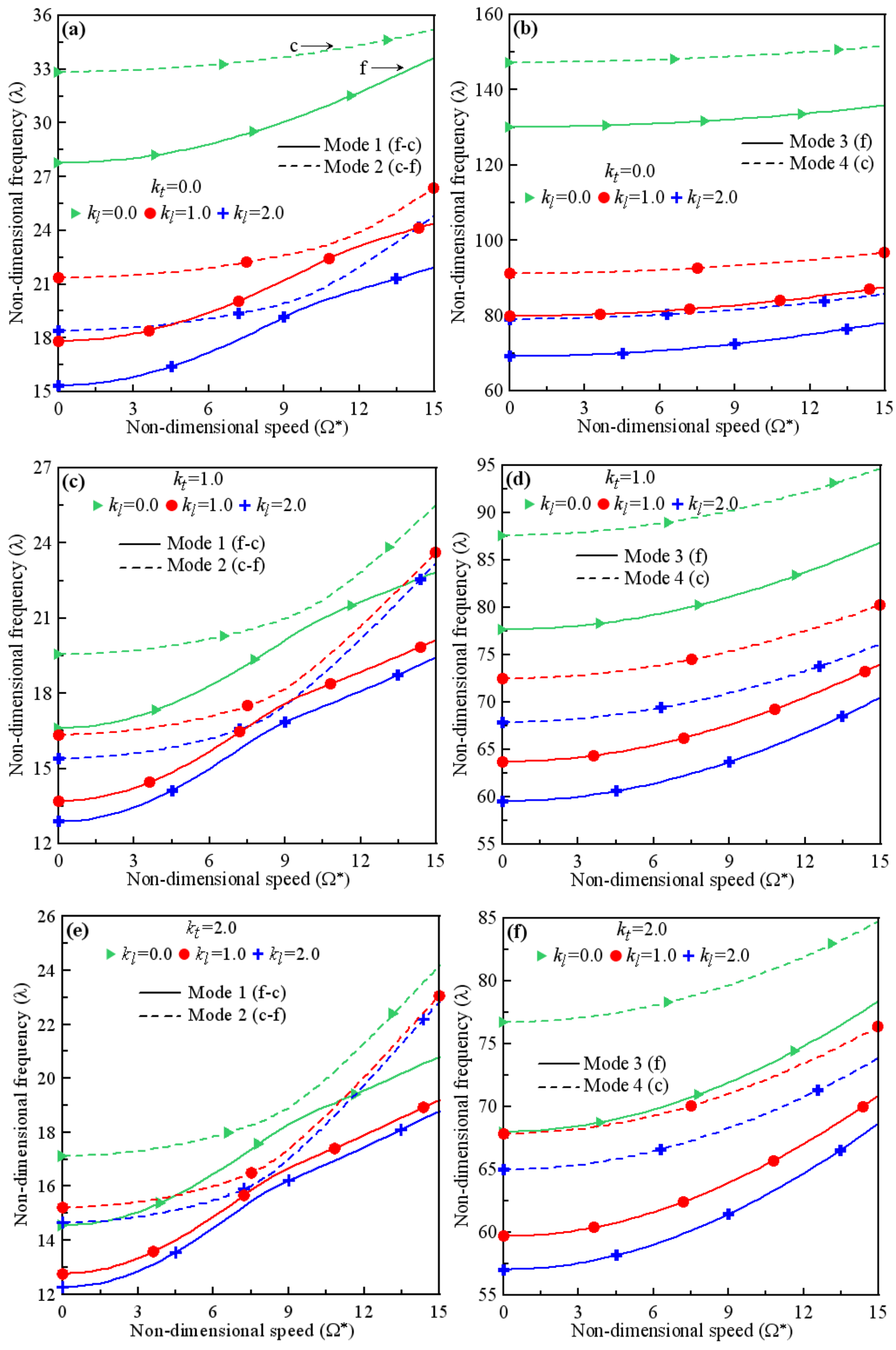

Fig. 4.9: Non-dimensional speed-frequency behavior for variation of axial gradation index for κ=2.0: **(a)** Modes 1 and 2 for k_t=0.0, **(b)** Modes 3 and 4 for k_t=0.0, **(c)** Modes 1 and 2 for k_t=1.0, **(d)** Modes 3 and 4 for k_t=1.0, **(e)** Modes 1 and 2 for k_t=2.0, **(f)** Modes 3 and 4 for k_t=2.0.

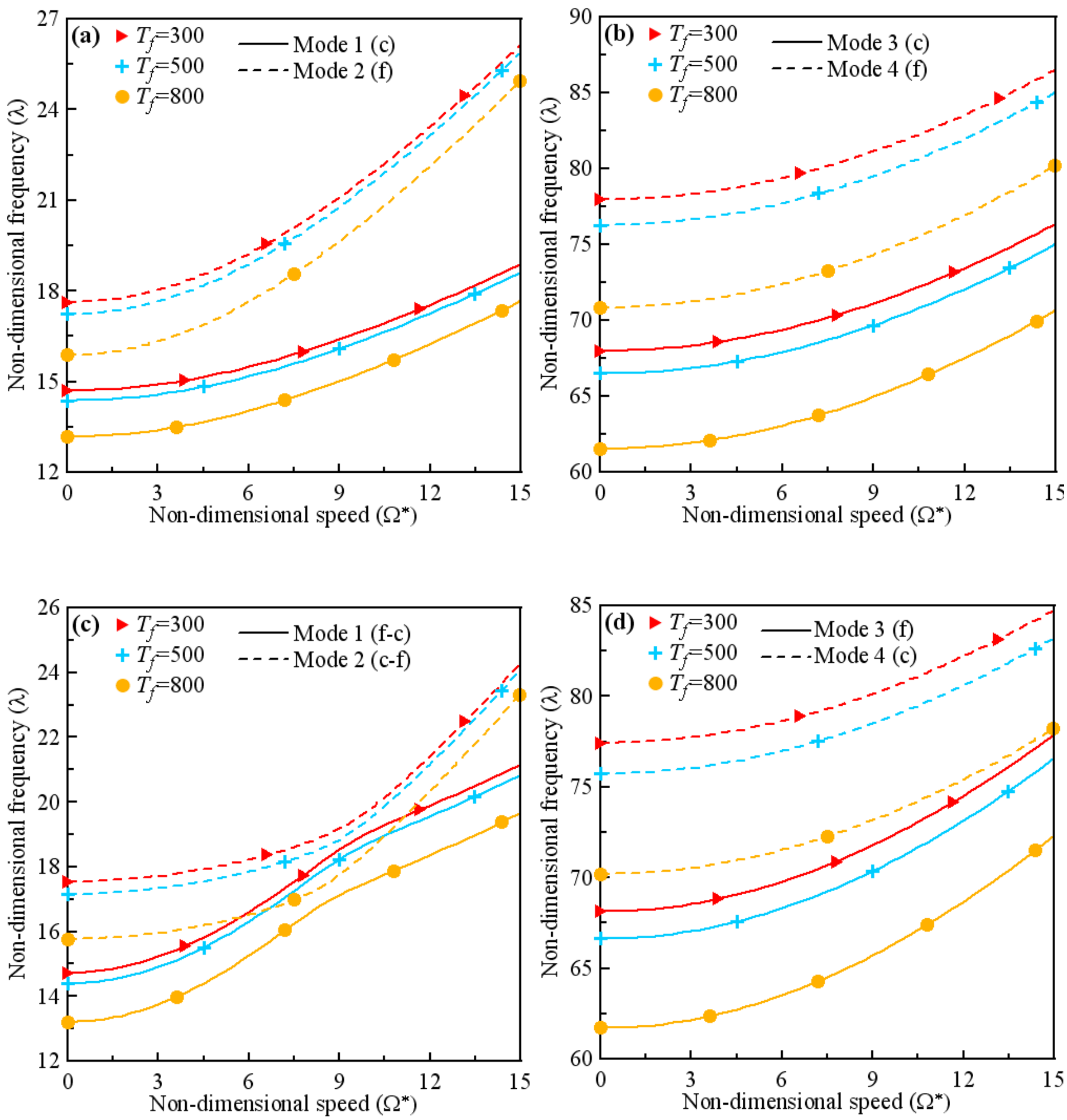

Fig. 4.10: Non-dimensional speed-frequency behavior for variation of operating temperature: **(a)** Modes 1 and 2 for κ =0.5, **(b)** Modes 3 and 4 for κ =0.5, **(c)** Modes 1 and 2 for κ =2.0, **(d)** Modes 3 and 4 for κ =2.0.

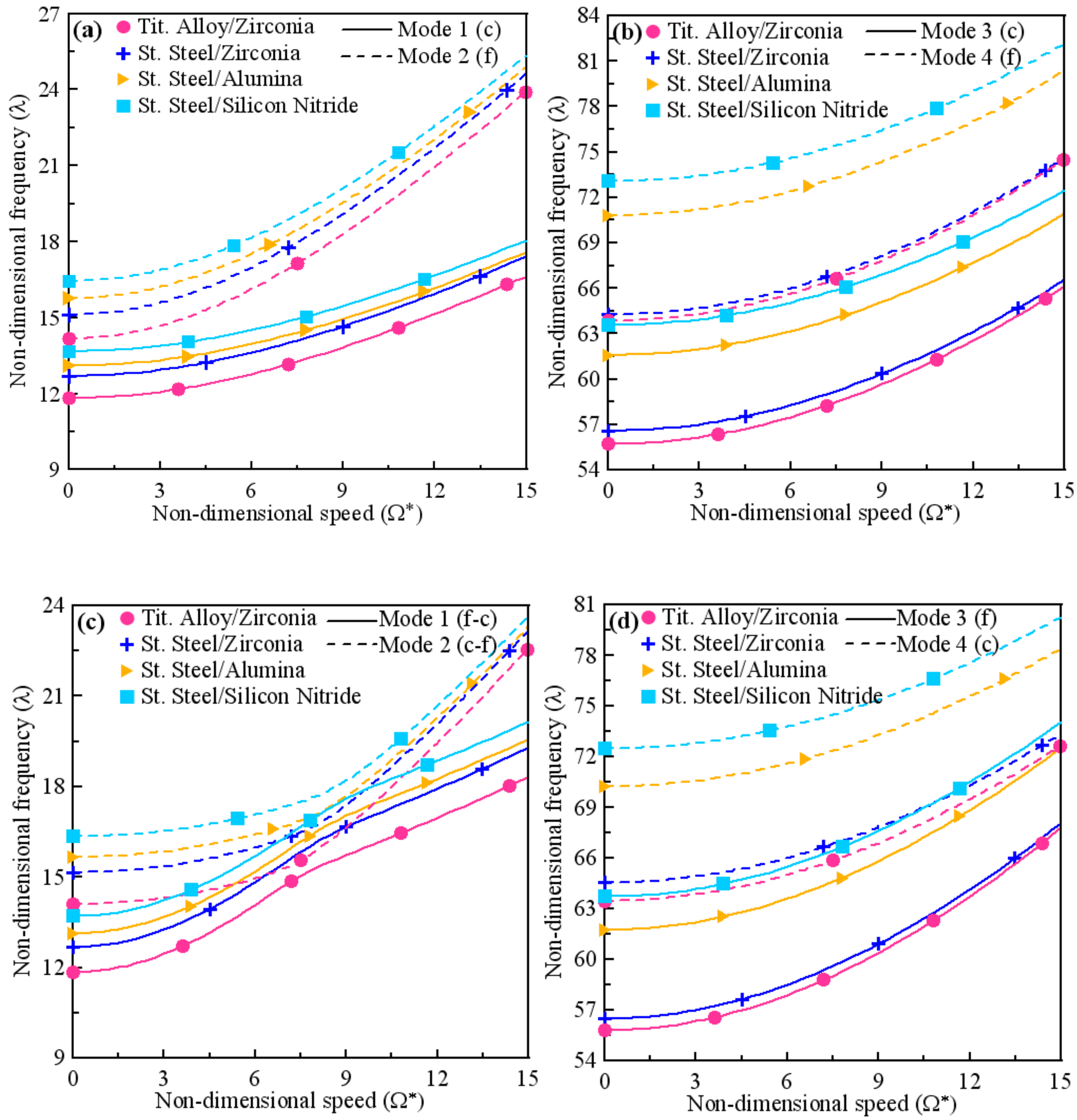

Fig. 4.11: Non-dimensional speed-frequency behavior for different FGM compositions: **(a)** Modes 1 and 2 for κ =0.5, **(b)** Modes 3 and 4 for κ =0.5, **(c)** Modes 1 and 2 for κ =2.0, **(d)** Modes 3 and 4 for κ =2.0.

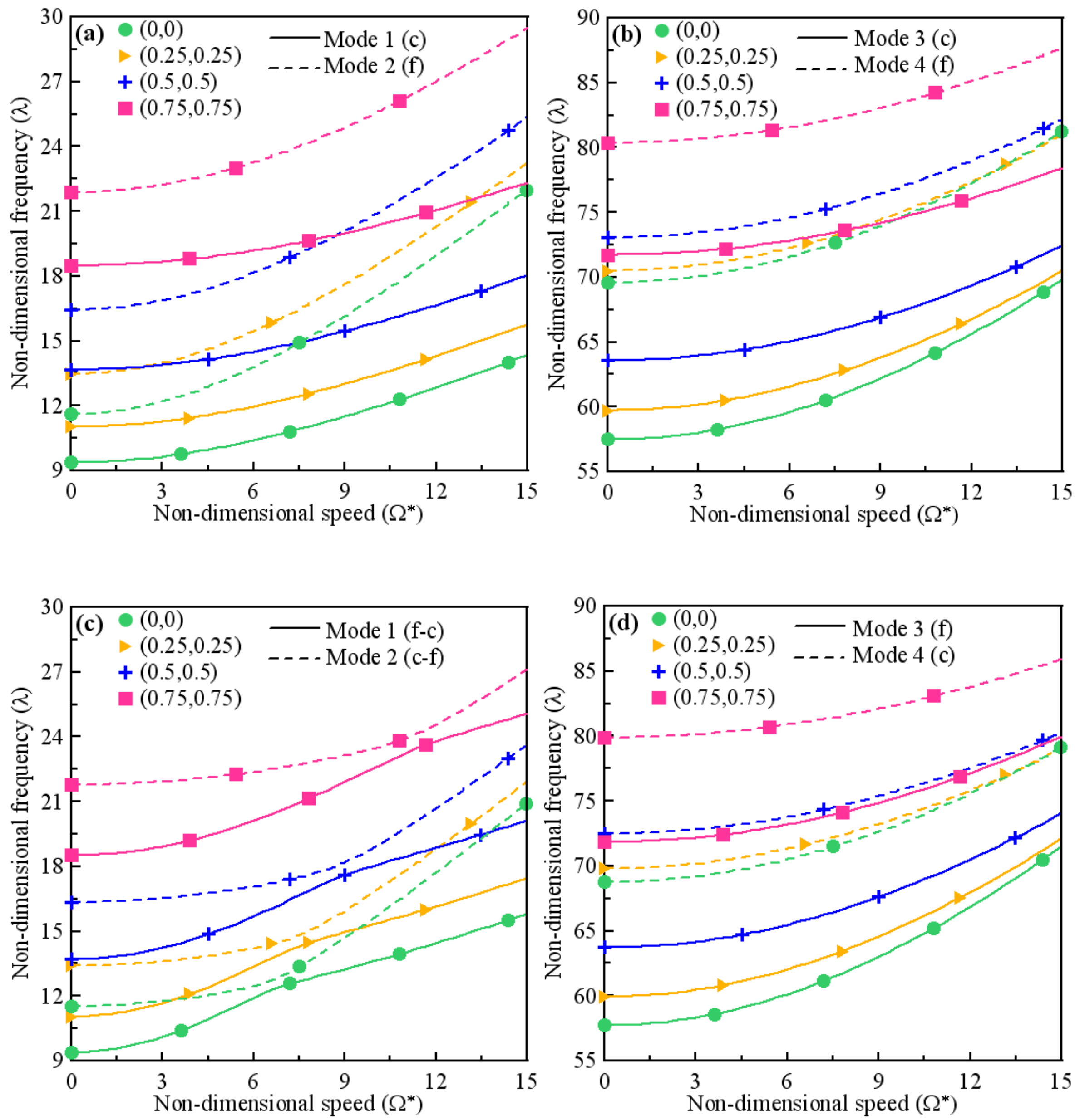

Fig. 4.12: Non-dimensional speed-frequency behavior for variation of taperness parameters: **(a)** Modes 1 and 2 for κ =0.5, **(b)** Modes 3 and 4 for κ =0.5, **(c)** Modes 1 and 2 for κ =2.0, **(d)** Modes 3 and 4 for κ =2.0.

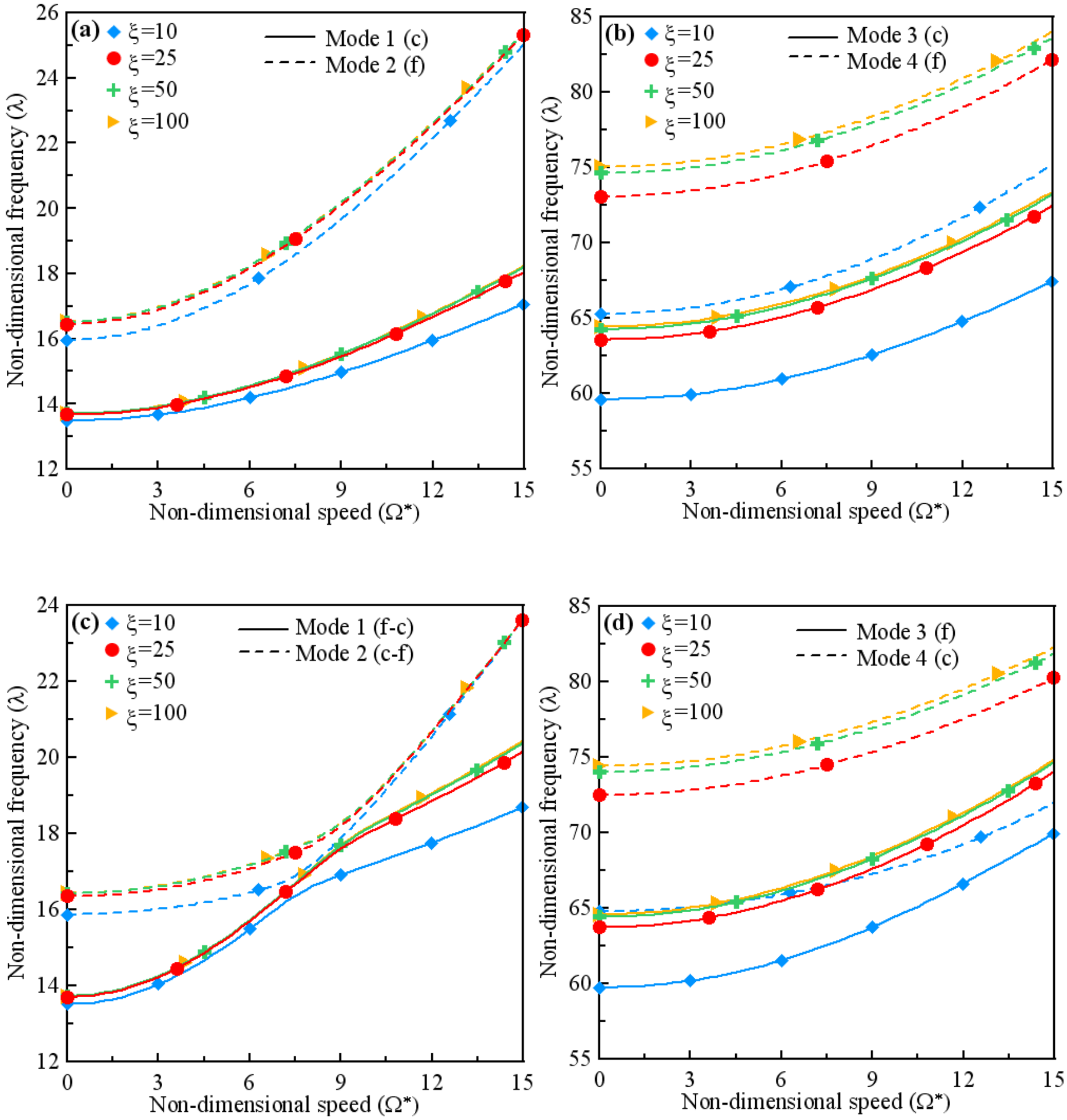

Fig. 4.13: Non-dimensional speed-frequency behavior for variation of slenderness parameter: **(a)** Modes 1 and 2 for κ=0.5, **(b)** Modes 3 and 4 for κ=0.5, **(c)** Modes 1 and 2 for κ=2.0, **(d)** Modes 3 and 4 for κ=2.0.

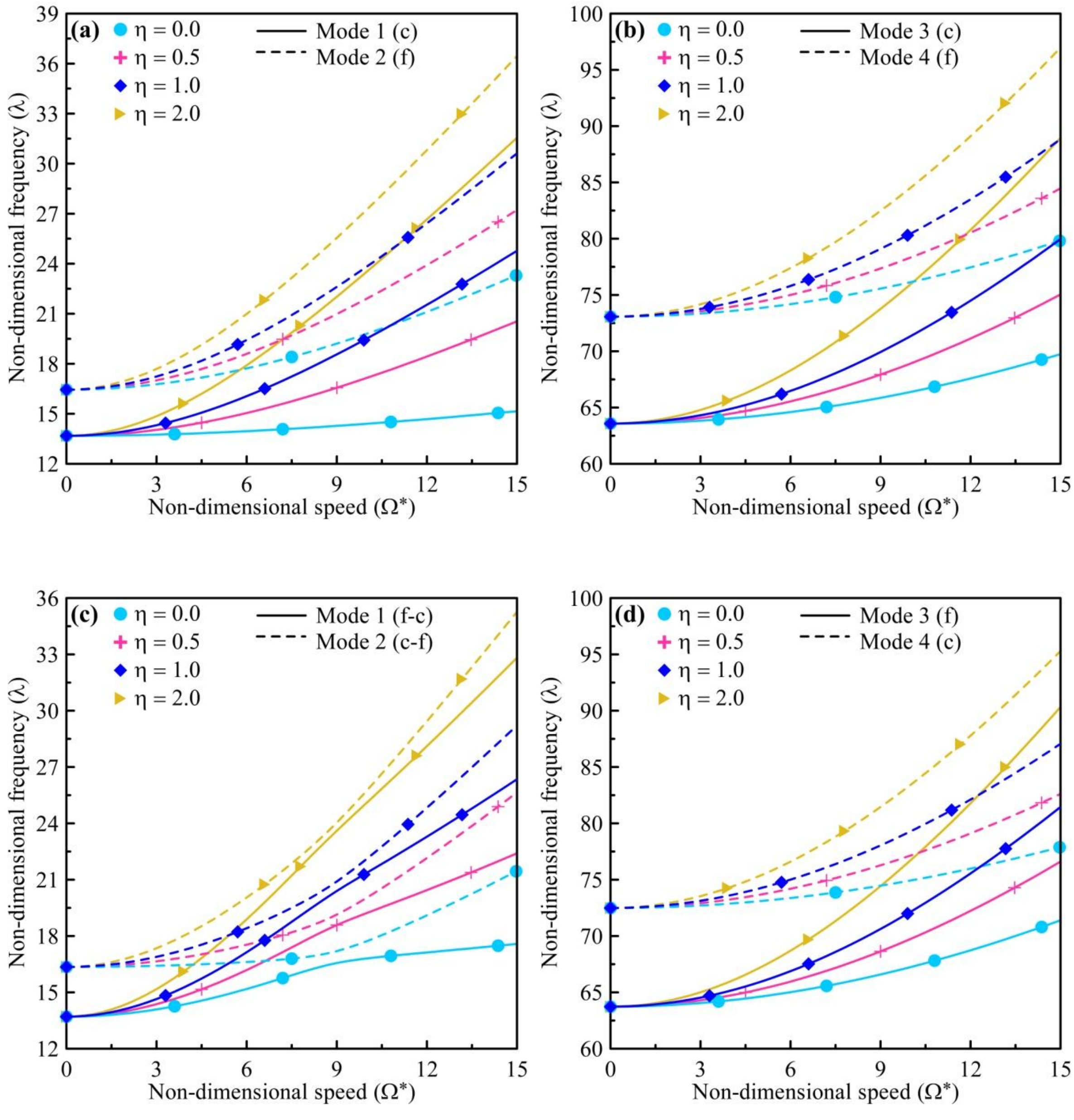

Fig. 4.14: Non-dimensional speed-frequency behavior for variation of hub parameter: **(a)** Modes 1 and 2 for κ =0.5, **(b)** Modes 3 and 4 for κ =0.5, **(c)** Modes 1 and 2 for κ =2.0, **(d)** Modes 3 and 4 for κ =2.0.

Figs. 4.14(a)-(d) present the speed-frequency behavior, each for different hub parameters. The figures reveal that for a particular aspect ratio and mode, speed-frequency curves for different hub parameters starts at the same point but diverges as speed increases. For higher speeds, the frequency increment is higher for higher value of the hub parameter. This behavior occurs due to enhancement of the centrifugal force as the hub parameter increases. Greater value of the hub parameter can be interpreted as that the beam is attached at a higher radius from the axis of rotation. This results in more centrifugal stiffening and subsequently higher frequency of vibration. Fig. 4.14(c) shows the mode veering and mode switching and this phenomenon occurs at higher speeds for higher hub parameter values.

4.6. Chapter Summary

The results of the study of free vibration behavior of BFGM pre-twisted double-tapered rotating micro beam are presented in this chapter. The present model is validated by comparing several results for the reduced problems available in the literature. The effects of spin-softening and Coriolis force are presented and discussed. The effect of pre-twist angle with regard to various aspect ratios are shown and discussed. An exhaustive sets of results involving non-dimensional speed-frequency behavior are presented for variations of different parameters such as size-dependent parameter, axial gradation index, thickness gradation index, operating temperature, FGM composition, taperness parameters, slenderness parameter and hub parameter. The results are of special importance for mode-veering and subsequent mode-switching phenomenon. The important findings are summarized as follows:

(i) Spin-softening and Coriolis effects significantly influence the chord-wise vibration frequencies but does not influence the flap-wise frequencies, though these two motions are coupled.

(ii) Free vibration frequencies increase monotonically with increase in the pre-twist angle.

(iii) The aspect ratio of beam section governs the influence of the pre-twist angle on frequency. It also influences the dominance of the chord-wise or the flap-wise motions and the mode-veering phenomenon.

(iv) As the beam cross sectional dimensions approach material length scale parameter, frequency increases due to increase in stiffness. The size effect seizes to exist when these dimensions become ten times the material length scale parameter.

(v) Increasing the thickness and axial gradation index reduces frequency of vibration.

(vi) High-temperature operating environment leads to decrease in the frequencies due to thermo-elastic degradation.

(vii) Different metal-ceramic FGM compositions show similar trend in free vibration behavior but the effect is greater on the second modes.

(viii) An increase in the values of both the taperness parameters leads to increase in the vibration frequencies.

(ix) At low values of the slender parameter, the effect of shear deformation exhibits strong influence, especially for the second modes.

(x) The hub parameter poses strong influence, leading to increase in frequency with its increase.

"This page is intentionally left blank"

Chapter 5

FREE VIBRATION BEHAVIOR OF TRANSVERESELY LOADED HOMOGENEOUS STRAIGHT PRISMATIC MICRO BEAM

5.1. Introduction

This chapter deals with the free vibration of a homogeneous straight prismatic micro beam under constant transverse loading. The free vibration behavior of a statically deflected micro beam under uniformly distributed static load is studied based on MCST and the mathematical formulation is based on TBT. In the first step of the problem, the beam configuration under large static deflection is obtained through a non-linear static analysis in which the governing equations are derived employing minimum potential energy principle and incorporating von Kármán geometric non-linearity. In the subsequent step, the free vibration behavior of the deflected micro beam is investigated employing Hamilton's principle and incorporating the tangent stiffness of the statically deflected beam configuration. The solutions of the governing equations for both the steps are obtained by approximating the displacement fields following Ritz method. The results for the first two vibration modes are presented in non-dimensional frequency-amplitude plane for clamped and simply supported boundary conditions.

5.2. Mathematical Formulation

For the present problem, displacement based mathematical formulation is employed. Fig. 5.1 shows a homogeneous straight prismatic beam of length L, thickness h and width b, under static uniformly distributed load p (in N/m).

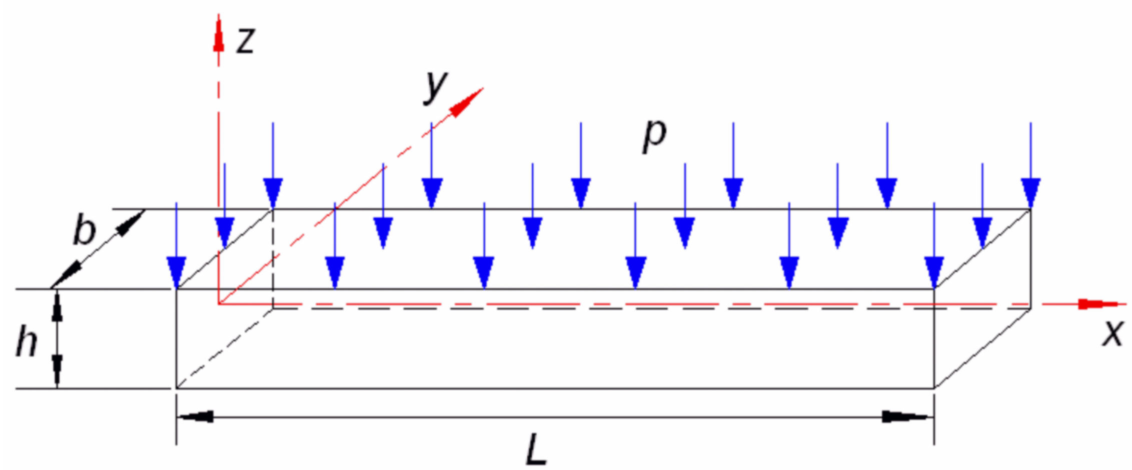

Fig. 5.1: Dimensions and axes of the homogeneous straight prismatic beam subjected to uniformly distributed load.

No displacement along y direction and no rotation with respect to z axis are considered. Following TBT, the displacement field along the x and z directions respectively are given by,

$$u(x,z) = u_0 - z\psi_y(x) \tag{5.1a}$$

$$w(x,z) = w_0 \tag{5.1b}$$

where u_0 and w_0 are the mid-plane displacements along the x and z directions respectively; ψ_y is the cross sectional rotation about the y direction. Hence, the displacement $(\vec{s}_Q)$ vector of any point $Q(x,z)$ are given by

$$\vec{s}_Q = \{u_0 - z\psi_y\}\hat{i} + (w_0)\hat{k} \tag{5.2}$$

Considering von Kármán non-linearity, the classical strain fields are derived to the following form:

$$\varepsilon_x = \frac{\partial u}{\partial x} + \frac{1}{2}\left(\frac{\partial w}{\partial x}\right)^2 = \left\{\frac{\partial u_0}{\partial x} - z\left(\frac{\partial \psi_y}{\partial x}\right)\right\} + \frac{1}{2}\left(\frac{\partial w_0}{\partial x}\right)^2 \tag{5.3a}$$

$$\gamma_{xz} = \frac{\partial u}{\partial z} + \frac{\partial w}{\partial x} = \frac{\partial w_0}{\partial x} - \psi_y \tag{5.3b}$$

Defining the rotation vector ($\vec{\theta}$) as $\vec{\theta} = \frac{1}{2}\left(\nabla \times \vec{s}_Q\right)$, its only nonzero component is derived as follows:

$$\theta_y = \frac{1}{2}\left(\frac{\partial u}{\partial z} - \frac{\partial w}{\partial x}\right) = \frac{1}{2}\left(-\psi_y - \frac{\partial w_0}{\partial x}\right) \tag{5.4}$$

Using (5.4), the only nonzero component of the curvature tensor, given by **χ** $= \frac{1}{2}\left[\nabla\vec{\theta} + \left(\nabla\vec{\theta}\right)^T\right]$, is derived to the following form:

$$\chi_{xy} = \chi_{yx} = \frac{1}{4}\left(-\frac{\partial \psi_y}{\partial x} - \frac{\partial^2 w_0}{\partial x^2}\right) \tag{5.5}$$

Table 5.1: Boundary conditions and the corresponding lowest order admissible functions for different beam configurations

Beam	Function	Boundary conditions
CC	$\phi_1^u = \left(x/L\right)\left\{1-\left(x/L\right)\right\}$	$u_0\big\|_{x=0} = 0, u_0\big\|_{x=L} = 0$
	$\phi_1^w = \left(x/L\right)\left\{1-\left(x/L\right)\right\}$	$w_0\big\|_{x=0} = 0, w_0\big\|_{x=L} = 0$
	$\phi_1^{ry} = \sin\left\{\left(\pi x\right)/L\right\}$	$\psi_y\big\|_{x=0} = 0, \psi_y\big\|_{x=L} = 0$
SS	$\phi_1^u = \left(x/L\right)\left\{1-\left(x/L\right)\right\}$	$u_0\big\|_{x=0} = 0, u_0\big\|_{x=L} = 0$
	$\phi_1^w = \left(x/L\right)\left\{1-\left(x/L\right)\right\}$	$w_0\big\|_{x=0} = 0, w_0\big\|_{x=L} = 0$
	$\phi_1^{ry} = \cos\left\{\left(\pi x\right)/L\right\}$	$\psi_y\big\|_{x=0} \neq 0, \psi_y\big\|_{x=L} \neq 0$
CS	$\phi_1^u = \left(x/L\right)\left\{1-\left(x/L\right)\right\}$	$u_0\big\|_{x=0} = 0, u_0\big\|_{x=L} = 0$
	$\phi_1^w = \left(x/L\right)\left\{1-\left(x/L\right)\right\}$	$w_0\big\|_{x=0} = 0, w_0\big\|_{x=L} = 0$
	$\phi_1^{ry} = \sin\left\{\left(\pi x\right)/2L\right\}$	$\psi_y\big\|_{x=0} = 0, \psi_y\big\|_{x=L} \neq 0$

Using one-dimensional form of linear elastic stress-strain relation (Reddy, 2011), the non-zero components of the classical stress tensor $\left(\sigma_{xx},\, \sigma_{xz}\right)$ are given by,

$$\sigma_{xx} = E\varepsilon_x,\; \sigma_{xz} = k_s G\gamma_{xz} \tag{5.6}$$

where k_s is the shear correction factor used to account for the non-uniformity of shear stress across the thickness of the section. In the present work, $k_s = \dfrac{5(1+\nu)}{6+5\nu}$ is considered (Reddy, 2011). Employing MCST, the only non-zero component of couple stress tensor $\left(m_{xy}\right)$ is given by,

$$m_{xy} = 2Gl^2\chi_{xy} \tag{5.7}$$

where l is the material length scale parameter that incorporates the size-effect. As for the present problem, the beam is considered as homogeneous and hence constant values of Young's modulus, Poisson ratio, shear modulus and density are considered by putting $E_f = E, \nu_f = \nu, G_f = G, \rho_f = \rho$. The value of the material length scale parameter l is taken to be constant.

The classical (U_{se}^{cl}) and non-classical (U_{se}^{ncl}) strain energies and work potential (U_{wp}) are derived to the form given below:

$$\begin{aligned}
U_{se}^{cl} &= \frac{1}{2}\int_V (\boldsymbol{\sigma} : \boldsymbol{\varepsilon})\, dV \\
&= \frac{EA}{2}\int_0^L \left[\left(\frac{du_0}{dx}\right)^2 + \frac{1}{4}\left(\frac{dw_0}{dx}\right)^4 + \left(\frac{dw_0}{dx}\right)^2\left(\frac{du_0}{dx}\right)\right] dx + \frac{EI}{2}\int_0^L \left(\frac{d\psi_y}{dx}\right)^2 dx \\
&\quad + \frac{k_s GA}{2}\int_0^L \left\{\left(\frac{dw_0}{dx}\right)^2 - 2\left(\frac{dw_0}{dx}\right)\psi_y + \left(\psi_y\right)^2\right\} dx,
\end{aligned} \tag{5.8a}$$

$$\begin{aligned}
U_{se}^{ncl} &= \frac{1}{2}\int_V (\mathbf{m} : \boldsymbol{\chi})\, dV \\
&= \frac{GAl^2}{8}\int_0^L \left\{\left(\frac{d^2 w_0}{dx^2}\right)^2 + \left(\frac{d\psi_y}{dx}\right)^2 + 2\left(\frac{d^2 w_0}{dx^2}\right)\left(\frac{d\psi_y}{dx}\right)\right\} dx,
\end{aligned} \tag{5.8b}$$

$$U_{wp} = -\int_0^L w_0 (p\, dx) \tag{5.9}$$

where $A(=bh)$ and $I\,(=bh^3/12)$ are the cross sectional area and area moment of inertia.

The displacement fields are approximated using Ritz method as follows:

$$u_0(x)=\sum_{j=1}^{n}c_j\,\phi_j^u(x),\quad w_0(x)=\sum_{j=1}^{n}c_{n+j}\,\phi_j^w(x),\quad \psi_y(x)=\sum_{j=1}^{n}c_{2n+j}\,\phi_j^{ry}(x) \tag{5.10}$$

where ϕ_j^u, ϕ_j^w and ϕ_j^{ry} are the set of orthogonal admissible functions with n number of functions in each set and c_j is the set of unknown parameters which are to be determined. The lowest order admissible functions for clamped-clamped (CC), simply supported-simply supported (SS) and clamped-simply supported (CS) beams are selected to satisfy the geometric boundary conditions and are given in Table 5.1. Putting the values of the assumed displacement fields given by (5.10) in (5.8a), (5.8b) and (5.9) and applying minimum potential energy principle given by Eq. (1.2), the governing equations are obtained as

$$\left[K^T\right]\left\{C\right\}=\left\{P\right\} \tag{5.11}$$

where $\left[K^T\right]$ and $\left\{P\right\}$ are the total stiffness matrix and load vector respectively, the components of which are as given below:

$$\left[k_{ij}^T\right]_{\substack{i=1,n\\ j=1,n}}=EA\int_0^L\frac{d\phi_i^u}{dx}\frac{d\phi_j^u}{dx}$$

$$\left[k_{ij}^T\right]_{\substack{i=1,n\\ j=n+1,2n}}=\frac{EA}{2}\int_0^L\left(\frac{dw_0}{dx}\right)\frac{d\phi_i^u}{dx}\frac{d\phi_{j-n}^w}{dx}\,dx$$

$$\left[k_{ij}^T\right]_{\substack{i=n+1,2n\\ j=n+1,2n}}=EA\int_0^L\left\{\left(\frac{du_0}{dx}\right)\frac{d\phi_{i-n}^w}{dx}\frac{d\phi_{j-n}^w}{dx}\,dx+\frac{1}{2}\int_0^L\left(\frac{dw_0}{dx}\right)^2\frac{d\phi_{i-n}^w}{dx}\frac{d\phi_{j-n}^w}{dx}\,dx\right\}$$

$$+kGA\int_0^L\frac{d\phi_{i-n}^w}{dx}\frac{d\phi_{j-n}^w}{dx}\,dx+\frac{GAl^2}{4}\int_0^L\frac{d^2\phi_{i-n}^w}{dx^2}\frac{d^2\phi_{j-n}^w}{dx^2}\,dx$$

$$\left[k_{ij}^T\right]_{\substack{i=n+1,2n\\ j=2n+1,3n}}=-kGA\int_0^L\frac{d\phi_{i-n}^w}{dx}\phi_{j-2n}^{ry}\,dx+\frac{GAl^2}{4}\int_0^L\frac{d^2\phi_{i-n}^w}{dx^2}\frac{d\phi_{j-2n}^{ry}}{dx}\,dx$$

$$\left[k_{ij}^{T}\right]_{\substack{i=2n+1,3n\\ j=n+1,2n}} = -kGA\int_0^L \phi_{i-2n}^{ry}\frac{d\phi_{j-n}^{w}}{dx}dx + \frac{GAl^2}{4}\int_0^L \frac{d\phi_{i-2n}^{ry}}{dx}\frac{d^2\phi_{j-n}^{w}}{dx^2}dx$$

$$\left[k_{ij}^{T}\right]_{\substack{i=2n+1,3n\\ j=2n+1,3n}} = EI\int_0^L \frac{d\phi_{i-2n}^{ry}}{dx}\frac{d\phi_{j-2n}^{ry}}{dx}dx + kGA\int_0^L \phi_{i-2n}^{ry}\phi_{j-2n}^{ry}dx + \frac{GAl^2}{4}\int_0^L \frac{d\phi_{i-2n}^{ry}}{dx}\frac{d\phi_{j-2n}^{ry}}{dx}dx$$

$$\{p_i\}_{i=1,n} = 0,\ \{p_i\}_{i=n+1,2n} = p\int_0^L \phi_{i-nu}^{w}dx,\ \{p_i\}_{i=2n+1,3n} = 0$$

Here A is the beam cross sectional area given by $A = b\times h$. Eq. (5.11) is nonlinear in nature involving unknown parameters c_j. It is solved by an iterative substitution method with successive relaxation (Das et al., 2009). The solution provides the deflected configuration of the beam.

The governing equation for free vibration of the statically deformed micro beam is derived using Hamilton's principle given by

$$\delta\left(\int_{t_1}^{t_2}\left(U_{ke} - U_{se}\right)dt\right) = 0 \tag{5.12}$$

where t is time and U_{ke} is the kinetic energy of the micro beam which is given as

$$U_{ke} = \frac{\rho A}{2}\int_0^L\left\{\left(\frac{dw_0}{dt}\right)^2 + \left(\frac{du_0}{dt}\right)^2\right\}dx + \frac{\rho I}{2}\int_0^L\left(\frac{d\psi_y}{dt}\right)^2 dx \tag{5.13}$$

where ρ is the density of the material of the beam. For investigating the small amplitude free vibration behavior, the tangent stiffness of the deflected beam configuration is to be considered. Using the relationship $\left[k_{ij}^{t}\right] = \frac{\partial}{\partial c_j}\left\{p_i^r\right\}$ (Das, 2018), the elements of the tangent stiffness matrix $\left[k_{ij}^{t}\right]$ are derived where $\left\{p_i^r\right\}$ is the restoring force vector defined as $\left\{p_i^r\right\} = \left[k_{ij}^{T}\right]\left\{c_j\right\}$.

The linear components of the total and tangent stiffness matrices are same. The nonlinear components of $\left[k_{ij}^{t}\right]$ are as follows:

$$\left[k_{ij}^{t}\right]_{\substack{i=1,n\\ j=n+1,2n}} = EA\int_0^L\left(\frac{dw_0}{dx}\right)\frac{d\phi_i^u}{dx}\frac{d\phi_{j-n}^{w}}{dx}dx$$

$$\left[k_{ij}^{t}\right]_{\substack{i=n+1,2n\\ j=1,n}} = EA\int_{0}^{L}\left(\frac{dw_0}{dx}\right)\frac{d\phi_{i-n}^{w}}{dx}\frac{d\phi_{j}^{u}}{dx}dx$$

$$\left[k_{ij}^{t}\right]_{\substack{i=n+1,2n\\ j=n+1,2n}} = EA\left[\int_{0}^{L}\left(\frac{du_0}{dx}\right)\frac{d\phi_{i-n}^{w}}{dx}\frac{d\phi_{j-n}^{w}}{dx}dx+\frac{3}{2}\int_{0}^{L}\left(\frac{dw_0}{dx}\right)^{2}\frac{d\phi_{i-n}^{w}}{dx}\frac{d\phi_{j-n}^{w}}{dx}dx\right]$$

Following Ritz method, the dynamic displacements and rotation fields are approximated as

$$u_0(x)=\sum_{j=1}^{n}d_j\,\phi_j^{u}(x)e^{\mathrm{i}\omega t},\quad w_0(x)=\sum_{j=1}^{n}d_{n+j}\,\phi_j^{w}(x)e^{\mathrm{i}\omega t},\quad \psi_y(x)=\sum_{j=1}^{n}d_{2n+j}\,\phi_j^{ry}(x)e^{\mathrm{i}\omega t} \qquad (5.14)$$

where d_j is the set of unknown coefficients determining vibration mode shapes, ω is the natural frequency of vibration and $\mathbf{i}=\sqrt{-1}$. Substituting (5.13) and the tangent stiffness matrix in Eq. (5.12) and using (5.14), the governing equation is derived as an eigenvalue problem as shown below:

$$\left[K\right]\left\{D\right\}-\omega^{2}\left[M\right]\left\{D\right\}=0 \qquad (5.15)$$

where $\left[M\right]$ is the mass matrix whose off-diagonal terms are zero. The elements of $\left[M\right]$ are given as follows:

$$\left[m_{ij}\right]_{\substack{i=1,n\\ j=1,n}}=\rho A\int_{0}^{L}\phi_i^{u}\phi_j^{u}dx,\left[m_{ij}\right]_{\substack{i=n+1,2n\\ j=n+1,2n}}=\rho A\int_{0}^{L}\phi_{i-n}^{w}\phi_{j-n}^{w}dx,\left[m_{ij}\right]_{\substack{i=2n+1,3n\\ j=2n+1,3n}}=\rho I\int_{0}^{L}\phi_{i-2n}^{ry}\phi_{j-2n}^{ry}dx$$

where I is the area moment of inertia of beam cross section given by $I=b\times h^{3}/12$. The solution of Eq. (5.15) gives the natural frequencies and the corresponding mode shapes.

5.3. Results and Discussion

The geometrically linear static deflection fields for different l/h values are compared with Reddy (2011) for a simply supported Timoshenko beam under sinusoidally varying distributed load (of amplitude *p*) and it is shown in Fig. 5.2(a). The natural frequencies of vibration for different h/l values for a simply supported Timoshenko beam are compared with Ma et al. (2008) and it is shown in Fig. 5.2(b). The comparison plot for Fig. 5.2(b) is generated by considering the three-dimensional form of constitutive relations as used in Ma et al. (2008). In that case, E is replaced by $E\left(1-\upsilon\right)/\left\{\left(1+\upsilon\right)\left(1-2\upsilon\right)\right\}$ in the first relation of (5.6). The comparison plots shown in Fig. 5.2 match very well with the available results and thus validate the present model.

The results of the present study are shown in normalized frequency (ω / ω_1) versus normalized static deflection amplitude (w_{max} / h) plane where w_{max} is the maximum static deflection and ω_1 is the natural frequency of vibration for the first mode. The results are generated with the following values: $l = 17.6 \times 10^{-6}\,\mathrm{m}$, $E = 200$ GPa, $\nu = 0.30$, $\rho = 7850$ kg/m^3, L/h=20 and b/h=2. Figs. 5.3(a) and (b) show the frequency-amplitude plots for the first two modes of vibration for a CC beam, each corresponding to different h/l values. Figs. 5.4(a) and (b) show the frequency-amplitude plots for the first two modes of vibration for a SS beam, each corresponding to different h/l values. Figs. 5.5(a) and (b) show the frequency-amplitude plots for the first two modes of vibration for a CS beam, each corresponding to different h/l values. In each of the plots of Figs. 5.3-5.5, the frequency-amplitude plots for a classical beam (l=0) are also shown. The results show that with increase in the static deflection for any specific h/l ratio, the beam becomes more stiffer due to geometric stiffening action, thus making the frequency to increase. With increasing h/l ratio, the frequency-amplitude plots get more and more curved from the initial point, and this is true irrespective of the vibration modes and boundary conditions. It indicates that the beam stiffness increases when the thickness becomes comparable with the material length scale parameter (decreasing h/l), and as a result the geometric stiffening effect due to large deflection becomes subdued. Further it is observed that the behavior of a micro beam becomes almost identical with that of a classical beam when h/l becomes ten or more.

5.4. Chapter Summary

The free vibration frequencies of a statically deflected Timoshenko micro beam under uniformly distributed static load are computed based on MCST. The results are presented in normalized frequency versus normalized static deflection amplitude plane for the first two vibration modes for CC, SS and CS micro beams. The results indicate that the beam stiffness increases when the thickness becomes comparable with the material length scale parameter, and as a result, the effect of geometric stiffening is lowered. The size effect is found to disappear when the thickness is ten times or more of the material length scale parameter.

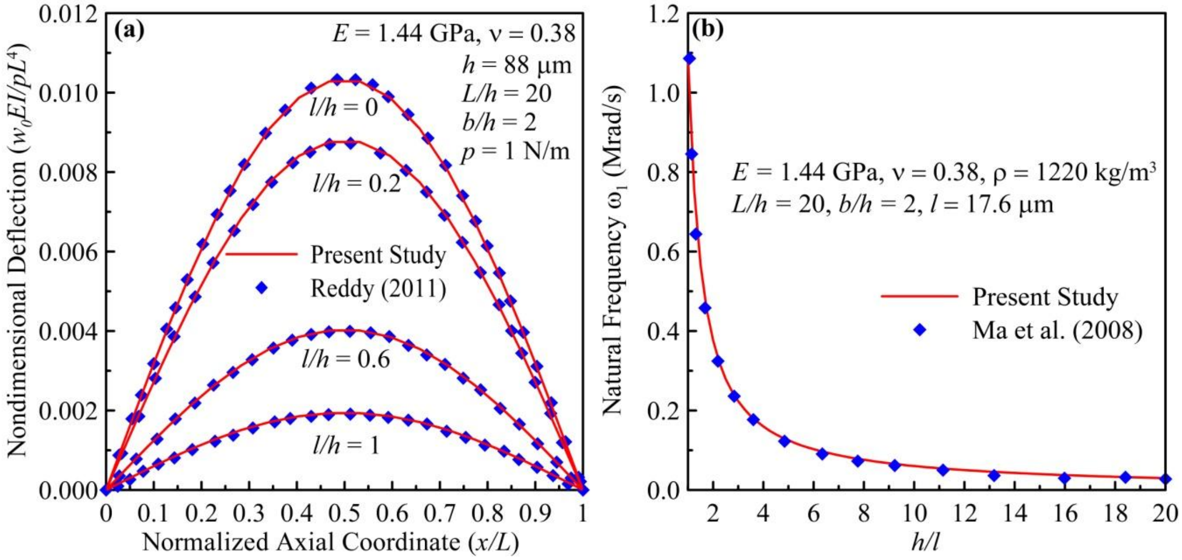

Fig. 5.2: Validation plots: **(a)** Static deflection fields, **(b)** Natural frequency of vibration.

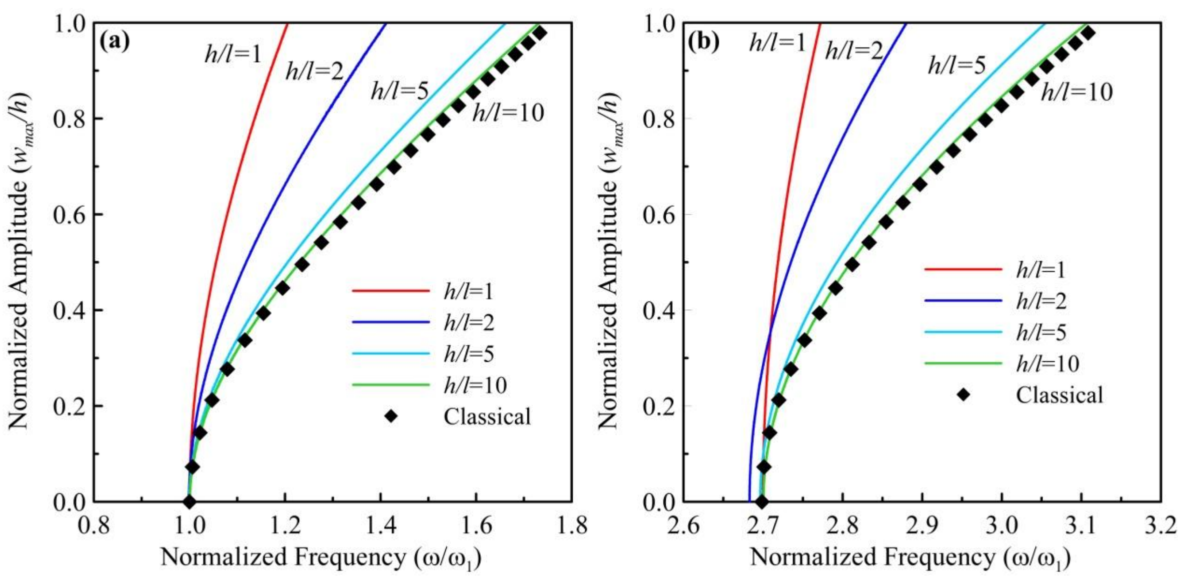

Fig. 5.3: Normalized frequency versus deflection amplitude plots for CC beam: **(a)** First mode, **(b)** Second mode.

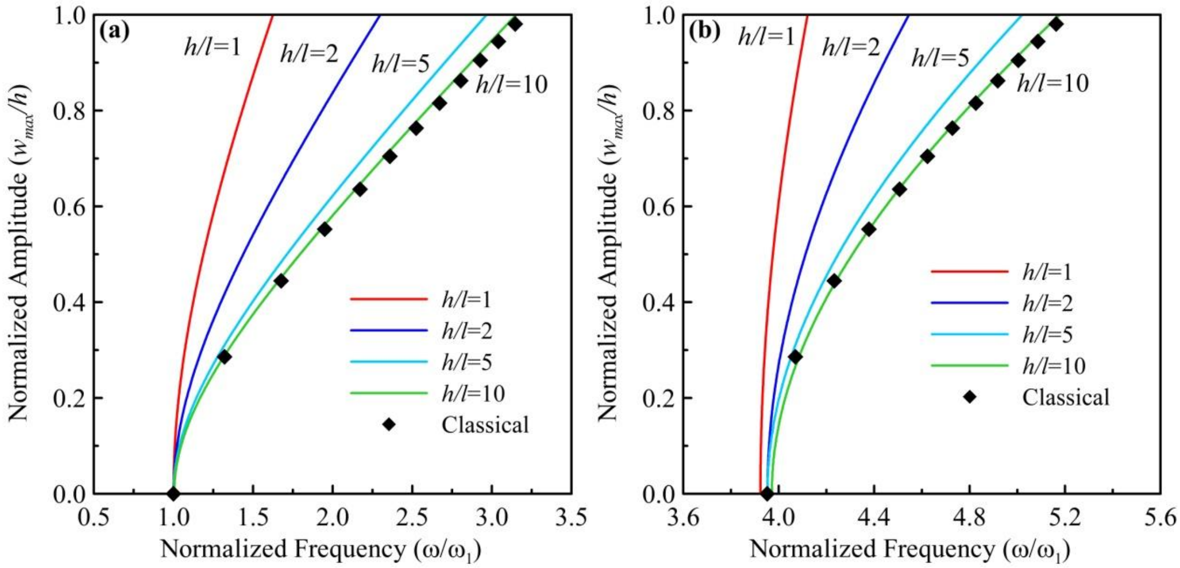

Fig. 5.4: Normalized frequency versus deflection amplitude plots for SS beam: **(a)** First mode, **(b)** Second mode.

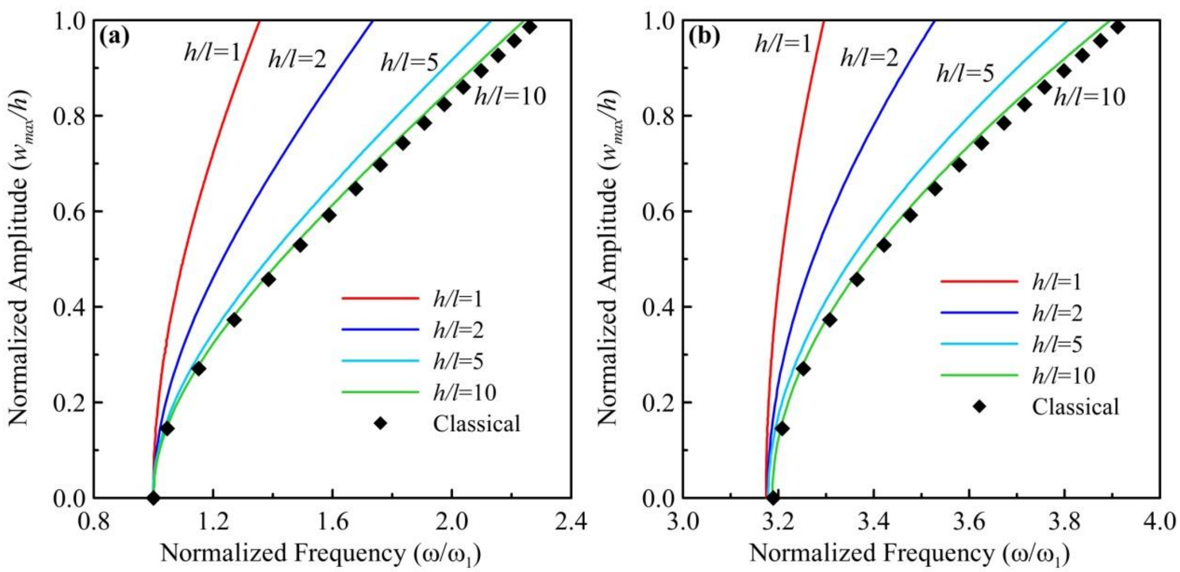

Fig. 5.5: Normalized frequency versus deflection amplitude plots for CS beam: **(a)** First mode, **(b)** Second mode.

Chapter 6

CONCLUSIONS

6.1. Conclusions

The present thesis work consists of three problems. The first two problems deal with the free vibration behavior of BFGM tapered rotating micro beams for straight and pre-twisted geometries. For these two problems, a cantilever beam attached with a hub, rotating at constant angular speed, is considered. This rotation results into a time-independent centrifugal force. The first step considers the determination of the centrifugally deformed configuration. The second step investigates the free vibration behavior in the neighborhood of this centrifugally deformed beam configuration. The third problem is about a homogeneous straight prismatic micro beam subjected to static uniformly distributed load in transverse direction. In this problem also, the large non-linear deformation of the micro beam due to transverse loading is calculated in the first step and, in the second step, the effect of large amplitude deformation on its free vibration behavior is studied.

For the problems involving BFGM beam, FGM modeling is done using Voigt's law and the temperature-dependence of the material properties are considered using Touloukian model. A displacement based approach is followed in formulating the steps of the problems and TBT along with von Kármán nonlinearity is used for strain displacement relationships. MCST is used to capture the size-dependent behavior for micro dimensions of the beam. The deformed shape of the beam due to time-independent centrifugal load or statically applied distributed transverse load is determined by forming the governing equation using minimum total potential energy theory. The set of equations is solved by approximating the displacement fields following Ritz method. Hamilton's principle in conjunction with tangent stiffness of the statically loaded beam is employed to formulate the governing equatios for free vibration. Then Ritz method is used to solve the system of governing equations in the form of eigenvalue problems. For the first two problems, a state-space approach is adapted to generate the eigenvalue problem.Some reduced problems have been solved and compared with well-established literatures to validate the present model. The results show very good matching.

For the first two problems, the non-dimensional speed-frequency behaviors for each of the first two chord-wise and flap-wise modes are presented to show the effects of various parameters like size-dependent thickness, axial and thickness gradation indices, taperness parameters, hub parameter, length-thickness ratio or slenderness parameter, operating temperature and FGM composition. For the straight rotating micro beam, the effect of size-dependent shear deformation is presented. For the pre-twisted rotating micro beam, the effects of spin-softening, Coriolis force and pre-twist angle are shown and discussed, and the mode-veering and subsequent mode-switching phenomena are presented. For the third problem, the results are presented in normalized frequency versus normalized static deflection amplitude plane for the first two vibration modes for CC, SS and CS micro beams.

The significant contributions and findings of the present thesis work are:

(i) This study developed an advanced mathematical model to describe the dynamic behavior of BFGM rotating micro-beam which is not available in the literature.

(ii) The proposed BFGM rotating micro beam model considers a symmetric through-thickness gradation in order to prevent bending of beam due to centrifugal loading and this is not considered in previous studies.

(iii) The BFGM rotating micro beam model incorporates geometric non-linearity, spin softening and Coriolis effect with great details of their effects which is unavailable in literature. It is clearly shown that the spin-softening and Coriolis acceleration affect only the chord-wise vibration modes of the beam.

(iv) In the present work of BFGM rotating micro beam, the beam is considered to be operating in an elevated temperature, often found in practical applications. This results into material degradation and thus shown to be significantly affecting its dynamic behavior.

(v) It is clear from the results that as the cross-sectional dimensions approach the material length scale parameter, the stiffness and frequency increase, which is the character of micro beams. This size-dependent behavior diminishes when the dimensions are ten times or more of the material length scale parameter.

(vi) Various parameters like the size-dependent thickness, axial and thickness gradation indices, taperness parameters, hub parameter, length-thickness ratio or slenderness parameter, operating temperature and FGM composition are found to have significant effect on the speed-frequency behavior of the BFGM rotating micro beam.

(vii) In case of BFGM pre-twisted rotating micro beam, aspect ratio of beam cross-section is shown to be a very important parameter and its' effects are presented in great detail which is unavailable in previous studies. Also, a significant contribution of this study is how the aspect ratio influences the mode-veering and mode-switching phenomena.

(viii) For the statically loaded homogeneous micro beam, the effect of large deflection amplitude on its free vibration behavior has been shown for the first time through this thesis work.

6.2. Future Scope of Work

The present study is on the free vibration characteristics of centrifugally loaded and statically loaded BFGM and homogeneous micro beams. Following are some of the considerations that can be taken up for further research in the field of FGM micro structural elements:

(i) This study can be extended to forced vibration behavior of the beams, considering damping into the mathematical formulation.

(ii) In case of the rotating beam, the beam is considered as a cantilever which is rigidly clamped to a rotating hub. In practical cases, this boundary is not fixed and allows some deformation. Thus, elastically-deformable boundary condition can be considered and its effect on the free vibration behavior can be studied.

(iii) Here, the size-dependent behavior is incorporated using MCST. The other available size-dependent theories like strain gradient theory, non-local theory, surface elasticity theory etc. can be considered to model the micro beams.

"This page is intentionally left blank"

Bibliography

Adair D and Jaeger M (2017) Vibration analysis of a uniform pre-twisted rotating Euler–Bernoulli beam using the modified Adomian decomposition method. *Mathematics and Mechanics of Solids* DOI: 10.1177/1081286517720843.

Amirouche F, Zhou Y and Johnson T (2009) *Current micropump technologies and their biomedical applications. Microsystem Technologies 15: 647-666.*

Anderson GL (1975) On the extensional and flexural vibrations of rotating bars. *International Journal of Non-linear Mechanics* 10: 223-236.

Anthoine A (2000) Effect of couple-stresses on the elastic bending of beams. *International Journal of Solids and Structures* 37: 1003-1018.

Arvin H (2017) Free vibration analysis of micro rotating beams based on the strain gradient theory using the differential transform method: Timoshenko versus Euler-Bernoulli beam models. *European Journal of Mechanics A/Solids* 65: 336-348.

Arvin H (2018) The flapwise bending free vibration analysis of micro-rotating Timoshenko beams using the differential transform method. *Journal of Vibration and Control* 24: 4868–4884.

Arvin H and Bakhtiari-Nejad F (2011) Non-linear modal analysis of a rotating beam. *International Journal of Non-linear Mechanics* 46: 877-897.

Asghari M, Kahrobaiyan MH and Ahmadian MT (2010) A nonlinear Timoshenko beam formulation based on the modified couple stress theory. *International Journal of Engineering Science* 48: 1749–1761.

Asghari M, Rahaeifard M, Kahrobaiyan MH and Ahmadian MT (2011) The modified couple stress functionally graded Timoshenko beam formulation. *Materials and Design* 32: 1435–1443.

Attia MA and Mahmoud FF (2016) Modeling and analysis of nanobeams based on nonlocal-couple stress elasticity and surface energy theories. *International Journal of Mechanical Sciences* 105: 126–134.

Avramov KV, Pierre C and Shyriaieva N (2007) Flexural-flexural-torsional nonlinear vibrations of pre-twisted rotating beams with asymmetric cross-sections. *Journal of Vibration and Control* 13: 329–364.

Azimi M, Mirjavadi SS, Shafiei N and Hamouda AMS (2017) Thermo-mechanical vibration of rotating axially functionally graded nonlocal Timoshenko beam. *Applied Physics A* 123: 104.

Bambill DV, Guerrero GI and Felix DH (2017) Natural vibrations of micro beams with nonrigid supports. *Journal of Vibration and Control* 23: 3233–3246.

Bambill DV, Rossit CA, Rossi RE, Felix DH and Ratazzi AR (2013) Transverse free vibration of non uniform rotating Timoshenko beams with elastically clamped boundary conditions. *Meccanica* 48:1289–1311.

Banerjee JR (2001) Free vibration analysis of a twisted beam using the dynamic stiffness method. *International Journal of Solids and Structures* 38: 6703-6722.

Banerjee JR and Kennedy D (2014) Dynamic stiffness method for inplane free vibration of rotating beams including Coriolis effects. *Journal of Sound and Vibration* 333: 7299–7312.

Banerjee JR, Su H and Jackson DR (2006) Free vibration of rotating tapered beams using the dynamic stiffness method. *Journal of Sound and Vibration* 298: 1034–1054.

Bazoune A and Khulief YA (1992) A finite beam element for vibration analysis of rotating tapered Timoshenko beams. *Journal of Sound and Vibration* 156: 141-164.

Beskou SP, Tsepoura KG, Polyzos D and Beskos DE (2003) Bending and stability analysis of gradient elastic beams. *International Journal of Solids and Structures* 40: 385–400.

Das D (2017) Free vibration and buckling analyses of geometrically non-linear and shear-deformable FGM beam fixed to the inside of a rotating rim. *Composite Structures* 179: 628–645.

Das D (2018) A new tangent stiffness based formulation to study the free vibration behavior of transversely loaded Timoshenko beam with geometric non-linearity. *Journal of Vibration and Control* 24: 1716-1727.

Das D, Sahoo P and Saha K (2009a) Out-of-plane free vibration analysis of rotating tapered beams in post-elastic regime. *Materials and Design* 30: 2875–2894.

Das D, Sahoo P and Saha K (2009b) Nonlinear vibration analysis of clamped skew plates by a variational method. *Journal of Vibration and Control* 15: 985-1017.

Dehrouyeh-Semnani AM (2015) The influence of size effect on flapwise vibration of rotating microbeams. *International Journal of Engineering Science* 94: 150–163.

Dehrouyeh-Semnani AM and Nikkhah-Bahrami M (2015) The influence of size-dependent shear deformation on mechanical behavior of microstructures-dependent beam based on modified couple stress theory. *Composite Structures* 123: 325–336.

Dehrouyeh-Semnani AM, BehboodiJouybari M and Dehrouyeh M (2016) On size-dependent lead-lag vibration of rotating microcantilevers. *International Journal of Engineering Science* 101: 50–63.

Ebrahimi F and Hashemi M (2016) On vibration behavior of rotating functionally graded double-tapered beam with the effect of porosities. *Proceedings of IMechE Part G Journal of Aerospace engineering* 230: 1903-1916.

Ebrahimi F and Mokhtari M (2015) Transverse vibration analysis of rotating porous beam with functionally graded microstructure using the differential transform method. *Journal of the Brazilian Society of Mechanical Sciences and Engineering* 37:1435–1444.

Efraim E and Eisenberger M (2007) Exact vibration analysis of variable thickness thick annular isotropic and FGM plates. *Journal of Sound and Vibration* 299: 720–738.

Epstein AH and Senturia SD (1997) Macro power from micro machinery. *Science* 276:1211.

Eringen AC (1983) On differential equations of nonlocal elasticity and solutions of screw dislocation and surface waves. *Journal of Applied Physics* 54: 4703-4710.

Esfahani SE, Kiani Y and Eslami MR (2013) Non-linear thermal stability analysis of temperature dependent FGM beams supported on non-linear hardening elastic foundations. *International Journal of Mechanical Sciences* 69: 10–20.

Fang J, Zhou D and Dong Y (2018a) Three-dimensional vibration of rotating functionally graded beams. *Journal of Vibration and Control* 24: 3292-3306.

Fang J, Gu J and Wang H (2018b) Size-dependent three-dimensional free vibration of rotating functionally graded microbeams based on a modified couple stress theory. *International Journal of Mechanical Sciences* 136: 188–199.

Fazelzadeh SA, Malekzadeh P, Zahedinejad P and Hosseini M (2006) Vibration analysis of functionally graded thin-walled rotating blades under high temperature supersonic flow using the differential quadrature method. *Journal of Sound and Vibration* 306: 333–348.

Filiz S, Bediz B, Romero LA and Ozdoganlar OB (2014) Three dimensional dynamics of pretwisted beams: A spectral-Tchebychev solution. *Journal of Sound and Vibration* 333: 2823–2839.

Fleck NA and Hutchinson JW (1997) Strain gradient plasticity. *Advances in Applied Mechanics* 33: 295-361.

Fleck NA, Muller GM, Ashby MF and Hutchinson JW (1994) Strain gradient plasticity: Theory and experiment. *Acta Metallurgica et Materialia* 42: 475-487.

Fox CHJ (1985) The free vibration of compact rotating radial cantilevers. *Journal of Sound and Vibration* 98: 325-336.

Fuchiyama T, Noda N, Tsuji T and Obata Y (1993) Analysis of thermal stress and stress intensity factor of functionally gradient materials. *Ceramic Transactions, Functionally Gradient Materials* 34: 425–432.

Fukui Y (1990) Fundamental investigation of functionally gradient material manufacturing system using centrifugal force. *JSME International Journal* 34: 144-148.

Fukui Y, Yamanaka N and Wakashima K (1993) The stresses and strains in a thick-walled tube of functionally graded material under uniform thermal loading. *JSME International Journal* 36: 156-162.

Ghadiri M and Shafiei N (2016) Vibration analysis of rotating functionally graded Timoshenko microbeam based on modified couple stress theory under different temperature distributions. *Acta Astronautica* 121: 221–240.

Ghayesh MH, Farokhi H and Amabili M (2013) Nonlinear dynamics of a microscale beam based on the modified couple stress theory. *Composites: Part B* 50: 318–324.

Goupee AJ and Vel SS (2006) Optimization of natural frequencies of bidirectional functionally graded beams. *Structural and Multidisciplinary Optimization* 32: 473-484.

Bibliography

Gunda JB and Ganguli R (2008) New rational interpolation functions for finite element analysis of rotating beams. *International Journal of Mechanical Sciences* 50: 578-588.

Guo S, He Y, Liu D, Lei J and Li Z (2018) Dynamic transverse vibration characteristics and vibro-buckling analyses of axially moving and rotating nanobeams based on nonlocal strain gradient theory. *Microsystem Technologies* 24: 963–977.

Gurtin ME and Murdoch AI (1978) Surface stress in solids. *International Journal of Solids and Structures* 14: 431-440.

Hao D and Wei C (2016) Dynamic characteristics analysis of bi-directional functionally graded Timoshenko beams. *Composite Structures* 141: 253-263.

Huang CL, Lin WY and Hsiao KM (2010) Free vibration analysis of rotating Euler beams at high angular velocity. *Computers and Structures* 88: 991–1001.

Ilkhani MR and Hosseini-Hashemi SH (2016) Size dependent vibro-buckling of rotating beam based on modified couple stress theory. *Composite Structures* 143: 75–83.

Iverson BD and Garimella SV (2008) Recent advances in microscale pumping technologies: a review and evaluation. *Microfluidics and Nanofluidics* 5: 145-174.

Jin ZH and Noda N (1993) Minimization of thermal stress intensity factor for a crack in a metal-ceramic mixture. *Ceramic Transactions, Functionally Gradient Materials* 34: 47-54.

Kahrobaiyan MH, Asghari M and Ahmadian MT (2014) A Timoshenko beam element based on the modified couple stress theory. *International Journal of Mechanical Sciences* 79: 75–83.

Kapuria S, Bhattacharyya M and Kumar AN (2008) Bending and free vibration response of layered functionally graded beams: A theoretical model and its experimental validation. *Composite Structures* 82: 390–402.

Kim H and Chung J (2016) Nonlinear modeling for dynamic analysis of a rotating cantilever beam. *Nonlinear Dynamics* 86:1981–2002.

Koiter WT (1964) Couple-stresses in the theory of elasticity: I and II. *Philosophical Transactions of the Royal Society of London B* 67: 17-44.

Koizumi M (1993) The concept of FGM. *Ceramic Transactions*, *Functionally Gradient Materials* 34: 3–10.

Kong S, Zhou S, Nie Z and Wang K (2008) The size-dependent natural frequency of Bernoulli–Euler micro-beams. *International Journal of Engineering Science* 46: 427–437.

Kong S, Zhou S, Nie Z and Wang K (2009) Static and dynamic analysis of micro beams based on strain gradient elasticity theory. *International Journal of Engineering Science* 47: 487–498.

Kosasih B and Jafari SA (2014) High-efficiency shrouded micro wind turbine for urban-built environment. *Applied Mechanics and Materials* 493: 294-299.

Lam DCC and Chong ACM (1999) Indentation model and strain gradient plasticity law for glassy polymers. *Journal of Materials Research* 14: 3784-3788.

Lam DCC, Yang F, Chong ACM, Wang J and Tong P (2003) Experiments and theory in strain gradient elasticity. *Journal of the Mechanics and Physics of Solids* 51: 1477–1508.

Lee SY, Lin SM and Lin YS (2009) Instability and vibration of a rotating Timoshenko beam with precone. *International Journal of Mechanical Sciences* 51: 114–121.

Lei J, He Y, Guo S, Li Z and Liu D (2016) Size-dependent vibration of nickel cantilever microbeams: Experiment and gradient elasticity. *AIP Advances* 6: 1052021.

Li L and Zhang D (2015) Dynamic analysis of rotating axially FG tapered beams based on a new rigid–flexible coupled dynamic model using the B-spline method. *Composite Structures* 124: 357–367.

Li L, Zhang DG and Zhu WD (2014) Free vibration analysis of a rotating hub-functionally graded material beam system with the dynamic stiffening effect. *Journal of Sound and Vibration* 333: 1526–1541.

Li X, Bhushan B, Takashima K, Baek CW and Kim YK (2003) Mechanical characterization of micro/nanoscale structures for MEMS/NEMS applications using nanoindentation techniques. *Ultramicroscopy* 97: 481–494.

Li X, Li L, Hu Y, Ding Z and Deng W (2017) Bending, buckling and vibration of axially functionally graded beams based on nonlocal strain gradient theory. *Composite Structures* 165: 250–265.

Li Z , He Y, Lei J, Han S, Guo S and Liu D (2018) Experimental investigation on size-dependent higher-mode vibration of cantilever microbeams. *Microsystem Technologies* DOI: https://doi.org/10.1007/s00542-018-4244-0.

Librescu L, Oh SY and Song O (2005) Thin-walled beams made of functionally graded materials and operating in a high temperature environment: vibration and stability. *Journal of Thermal Stresses* 28: 649–712.

Liebold C and Müller WH (2016) Comparison of gradient elasticity models for the bending of micromaterials. *Computational Materials Science* 116: 52–61.

Lin SC and Hsiao KM (2001) Vibration analysis of a rotating Timoshenko beam. *Journal of Sound and* v*ibration* 240: 303-322.

Lin SM and Lee SY (2002) The forced vibration and boundary control of pretwisted Timoshenko beams with general time dependent elastic boundary conditions. *Journal of Sound and* v*ibration* 254: 69-90.

Lin SM, Wu CT and Lee SY (2003) Analysis of rotating nonuniform pretwisted beams with an elastically restrained root and a tip mass. *International Journal of Mechanical Sciences* 45: 741–755.

Liu HK, Pan CH and Liu PP (2008) Dimension effect on mechanical behavior of silicon micro-cantilever beams. *Measurement* 41: 885–895.

London AP, Epstein AH and Kerrebrock JL (2001) High-pressure bipropellant microrocket engine. *Journal of Propulsion and Power* 17:780-787.

Lü CF, Chen WQ and Lim CW (2009) Elastic mechanical behavior of nano-scaled FGM films incorporating surface energies. *Compoites Science and Technology* 69: 1124-30.

Lü CF, Lim CW and Chen WQ (2009) Size-dependent elastic behavior of FGM ultra-thin films based on generalized refined theory. *International Journal of Solids and Structures* 46: 1176-1185.

Ma HM, Gao XL and Reddy JN (2008) A microstructure-dependent Timoshenko beam model based on a modified couple stress theory. *Journal of the Mechanics and Physics of Solids* 56: 3379–3391.

Ma LS and Lee DW (2011) A further discussion of nonlinear mechanical behavior for FGM beams under in-plane thermal loading. *Composite Structures* 93: 831–842.

Ma Q and Clarke DR (1995) Size dependent hardness of silver single crystal. *Journal of Materials Research* 10: 853-863.

Maganti NVR and Nalluri MR (2015) Flapwise bending vibration analysis of functionally graded rotating double-tapered beams. *International Journal of Mechanical and Materials Engineering* 10:21.

Mahi A, Bedia EAA, Tounsi A and Mechab I (2010) An analytical method for temperature-dependent free vibration analysis of functionally graded beams with general boundary conditions. *Composite Structures* 92: 1877–1887.

Malekzadeh P, Atashi MM and Karami G (2009) In-plane free vibration of functionally graded circular arches with temperature-dependent properties under thermal environment. *Journal of Sound and Vibration* 326: 837–851.

Mazanoglu K and Guler S (2017) Flap-wise and chord-wise vibrations of axially functionally graded tapered beams rotating around a hub. *Mechanical Systems and Signal Processing* 89: 97–107.

McFarland AW and Colton JS (2005) Role of material microstructure in plate stiffness with relevance to microcantilever sensors. *Journal of Micromechanics and Microengineering* 15: 1060–1067.

Mehra A, Zhang X, Ayón AA, Waitz IA, Schmidt MA and Spadaccini CM (2000) A six-wafer combustion system for a silicon micro gas turbine engine. *Journal of Microelectromechanical Systems* 9: 517-527.

Meriam JL and Kraige LG (2013) *Engineering Mechanics Dynamics*. Wiley India Pvt. Ltd, Delhi.

Mindlin RD (1964) Micro-structure in linear elasticity. *Archive for Rational Mechanics and Analysis* 16: 51-78.

Mindlin RD and Tiersen HF (1962) Effects of couple-stresses in linear elasticity. *Archive for Rational Mechanics and Analysis* 11: 415-448.

Mirjavadi SS, Afshari BM, Shafiei N, Rabby S and Kazemi M (2017) Effect of temperature and porosity on the vibration behavior of two-dimensional functionally graded micro-scale Timoshenko beam. *Journal of Vibration and Control* DOI: 10.1177/1077546317721871.

Mori T and Tanaka K (1973) Average stress in matrix and average elastic energy of materials with misfitting inclusions**.** *Acta Metallurgica* 21**:** 571-574.

Naguleswaran S (1994) Lateral vibration of a centrifugally tensioned uniform Euler-Bernoulli beam. *Journal of Sound and Vibration* 176: 613-624.

Nguyen TT and Lee J (2018) Interactive geometric interpretation and static analysis of thin-walled bidirectional functionally graded beams. *Composite Structures* 191: 1-11.

Nix WD (1989) Mechanical properties of thin films. *Metallurgical Transactions A* 20A: 2217-2245.

Noda N and Jin ZH (1993) Thermal stress intensity factors for a crack in a strip of a functionally gradient material. *International Journal of Solids and Structures* 30: 1039–1056.

Noori J, Fariborz SJ and Vafa JP (2016) A higher-order micro-beam model with application to free vibration. *Mechanics of Advanced Materials and Structures* 23: 443:450.

Oh SY, Librescu L and Song O (2003) Vibration of turbomachinery rotating blades made-up of functionally graded materials and operating in a high temperature field. *Acta Mechanica* 166: 69–87.

Oh Y and Yoo HH (2016) Vibration analysis of rotating pretwisted tapered blades made of functionally graded materials. *International Journal of Mechanical Sciences* 119: 68-79.

Ozgumus OO and Kaya MO (2007) Energy expressions and free vibration analysis of a rotating double tapered Timoshenko beam featuring bending-torsion coupling. *International Journal of Engineering Science* 45: 562-586.

Pal S and Das D (2017) A tangent stiffness–based approach to study free vibration of shear- deformable functionally graded material rotating beam through a geometrically non-linear analysis. *Journal of Strain Analysis for Engineering Design* 52: 310–332.

Pal S and Das D (2018) Free vibration analysis of functionally graded double-tapered beam rotating in thermal environment considering geometric nonlinearity, shear deformability, and Coriolis effect. *Proceedings of IMechE Part G Journal of Aerospace engineering* 232: 2244–2262.

Park SK and Gao XL (2006) Bernoulli–Euler beam model based on a modified couple stress theory. *Journal of Micromechanics and Microengineering* 16: 2355–2359.

Park SK and Gao XL (2008) Variational formulation of a modified couple stress theory and its application to a simple shear problem. *Zeitschrift für angewandte Mathematik und Physik* 59: 904–917.

Peddieson J, Buchanan GR and McNitt RP (2003) Application of nonlocal continuum models to nanotechnology. *International Journal of Engineering Science* 41: 305–312.

Pei J, Tian F and Thundat T (2004) Glucose biosensor based on the microcantilever. *Analytical Chemistry* 76: 292-297.

Piovan MT and Sampaio R (2009) A study on the dynamics of rotating beams with functionally graded properties. *Journal of Sound and Vibration* 327: 134–143.

Pydah A and Sabale A (2017) Static analysis of bi-directional functionally graded curved beams. *Composite Structures* 160: 867–876.

Rabin BH and Heaps RJ (1993) Powder processing of Ni-Al_20_3 FGM. *Ceramic Transactions, Functionally Gradient Materials* 34: 173–180.

Rajasekaran S (2013) Free vibration of centrifugally stiffened axially functionally graded tapered Timoshenko beams using differential transformation and quadrature methods. *Applied Mathematical Modelling* 37: 4440–4463.

Rajasekaran S and Khaniki HB (2017) Bending, buckling and vibration of small-scale tapered beams. *International Journal of Engineering Science* 120: 172–188.

Ramesh MNV and Rao NM (2013) Free vibration analysis of pre-twisted rotating FGM beams. *International Journal of Mechanics and Materials in Design* 9:367–383.

Reddy JN (2002) *Energy Principles and Variational Methods in Applied Mechanics*. John Wiley & Sons, USA.

Reddy JN (2007) Nonlocal theories for bending, buckling and vibration of beams. *International Journal of Engineering Science* 45: 288–307.

Reddy JN (2011) Microstructure-dependent couple stress theories of functionally graded beams. *Journal of the Mechanics and Physics of Solids* 59: 2382–2399.

Reddy JN and Chin CD (1998) Thermomechanical analysis of functionally graded cylinders and plates. *Journal of Thermal Stresses* 21: 593-626.

Reddy JN, Wang CM and Kitipornchai S (1999) Axisymmetric bending of functionally graded circular and annular plates. *European Journal of Mechanics- A/Solids* 18: 185-199.

Sata N (1993) Characteristic of SiC-TiB_2 Composites as the surface layer of SiC-TiB2-Cu functionally gradient katerial produced by self-propagating high-temperature synthesis. *Ceramic Transactions, Functionally Gradient Materials* 34: 109–116.

Shafiei N, Kazemi M and Fatahi L (2017) Transverse vibration of rotary tapered microbeam based on modified couple stress theory and generalized differential quadrature element method. *Mechanics of Advanced Materials and Structures* 24: 240-252.

Shafiei N, Kazemi M and Ghadiri M (2016a) On size-dependent vibration of rotary axially functionally graded micro beam. *International Journal of Engineering Science* 101: 29–44.

Shafiei N, Mousavi A and Ghadiri M (2016b) Vibration behavior of a rotating non-uniform FG microbeam based on the modified couple stress theory and GDQEM. *Composite Structures* 149: 157–169.

Shahba A, Attarnejad R and Zarrinzadeh H (2013) Free vibration analysis of centrifugally stiffened tapered functionally graded beams. *Mechanics of Advanced Materials and Structures* 20: 331–338.

Shahba A, Attarnejad R, Marvi MT and Hajilar S (2011a) Free vibration and stability analysis of axially functionally graded tapered Timoshenko beams with classical and non-classical boundary conditions. *Composites: Part B* 42: 801–808.

Shahba A, Attarnejad R, Semnani SJ, Shahriari V and Dormohammadi AA (2011b) Derivation of an efficient element for free vibration analysis of rotating tapered Timoshenko beams using basic displacement functions. *Proceedings of IMechE Part G Journal of Aerospace engineering* 226: 1455-1469.

Shames IH and Dym CL (2009) *Energy and Finite Element Methods in Structural Mechanics*. New Age International Publishers, Delhi.

Shavezipur M and Hashemi SM (2009) Free vibration of triply coupled centrifugally stiffened nonuniform beams, using a refined dynamic finite element method. *Aerospace Science and Technology* 13: 59–70.

Shen HS (2009) *Functionally Graded Materials: Nonlinear Analysis of Plates and Shells*. CRC Press, Boca Raton FL.

Shen HS and Wang ZX (2014) Nonlinear analysis of shear deformable FGM beams resting on elastic foundations in thermal environments. *International Journal of Mechanical Sciences* 81: 195–206.

Shenas AG, Ziaee S and Malekzadeh P (2016) Vibrational behavior of rotating pre-twisted functionally graded microbeams in thermal environment. *Composite Structures* 157: 222–235.

Shooshtari A, Kalhori H and Masoodian A (2011) Investigation for dimension effect on mechanical behavior of a metallic curved micro-cantilever beam. *Measurement* 44: 454–465.

Şimşek M (2015) Bi-directional functionally graded materials (BDFGMs) for free and forced vibration of Timoshenko beams with various boundary conditions. *Composite Structures* 133: 968–978.

Şimşek M and Kocatürk T (2009) Free and forced vibration of a functionally graded beam subjected to a concentrated moving harmonic load. *Composite Structures* 90: 465–473.

Song O, Librescu L and Oh SY (2001) Dynamics of pretwisted rotating thin-walled beams operating in a temperature environment. *Journal of Thermal Stresses* 24: 255-279.

Stelmashenko NA, Walls MG, Brown LM and Milman YV (1993) Microindentations on W and Mo oriented single crystal: An STM study. *Acta Metallurgica et Materialia* 41: 2855-2865.

Swaminathan M and Rao JS (1977) Vibrations of rotating, pretwisted and tapered blades. *Mechanism and Machine Theory* 12: 331-337.

Tang C and Alici G (2011) Evaluation of length-scale effects for mechanical behavior of micro- and nanocantilevers: I. Experimental determination of length-scale factors. *Journal of Physics D: Applied Physics* 44: 335501.

Thai HT, Vo TP, Nguyen TK and Kim SE (2017) A review of continuum mechanics models for size-dependent analysis of beams and plates. *Composite Structures* 177: 196-219.

Touloukian YS (1967) *Thermophysical Properties of High Temperature Solid Materials*. McMillan, New York.

Toupin RA (1962) Elastic materials with couple-stresses. *Archive for Rational Mechanics and Analysis* 11: 385-414.

Trinh LC, Vo TP, Thai HT and Nguyen TK (2018) Size-dependent vibration of bi-directional functionally graded microbeams with arbitrary boundary conditions. *Composites Part B* 134:225-245.

Wang GF and Feng XQ (2007) Effects of surface elasticity and residual surface tension on the natural frequency of microbeams. *Applied Physics Letters* 90: 231904.

Wang Q (2005) Wave propagation in carbon nanotubes via nonlocal continuum mechanics. *Journal of Applied Physics* 98: 124301.

Wang YG, Lin WH and Liu N (2015) Nonlinear bending and post-buckling of extensible microscale beams based on modified couple stress theory. *Applied Mathematical Modelling* 39: 117–127.

Watson B, Friend J and Yeo L (2009) Micromotor of less than 1 mm^3 volume for in vivo medical procedures. *Proceedings of the Third International Conference on Quantum, Nano and Micro Technologies (ICQNM 2009)* 81-85 DOI: 10.1109/ICQNM.2009.14.

Williamson RL, Rabin BH and Drake JT (1993) Finite element analysis of thermal residual stresses at graded ceramic metal interfaces. Part I. Model description and geometrical effects. *Journal of Applied Physics* 74:1310-1320.

Wright AD, Smith CE, Thresher RW and Wang JLC (1982) Vibration modes of centrifugally stiffened beams. *Journal of Applied Mechanics* 49: 197-202.

Yamanouchi M, Koizumi M, Hirai T and Shiota I (eds.) (1990) *Proceedings of the First International Symposium on Functionally Gradient Materials*, Japan.

Yamaoka H, Yuki M, Tahara K, Irisawa T, Watanabe R and Kawasak A (1993) Fabrication of functionally gradient material by slurry stacking and sintering process. *Ceramic Transactions, Functionally Gradient Materials* 34: 165–172.

Yang F, Chong ACM, Lam DCC and Tong P (2002) Couple stress based strain gradient theory for elasticity. *International Journal of Solids and Structures* 39: 2731–2743.

Yang JP, Lau GK, Tan CP, Chong NB, Thubthimthong B and He ZM (2012) An electro-thermal micro-actuator based on polymer composite for application to dual-stage positioning systems of hard disk drives. *Sensors and Actuators A: Physical* 187: 98-104.

Yang T, Tanga Y, Lid Q and Yang XD (2018) Nonlinear bending, buckling and vibration of bi-directional functionally graded nanobeams. *Composite Structures* 204: 313–319.

Yokoyama T (1988) Free vibration characteristics of rotating Timoshenko beams. *International Journal of Mechanical Sciences* 30: 743 755.

Yoo HH, Park JH and Park J (2001) Vibration analysis of rotating pre-twisted blades. *Computers and Structures* 79: 1811-1819.

Zarrinzadeh H, Attarnejad R and Shahba A (2012) Free vibration of rotating axially functionally graded tapered beams. *Proceedings of IMechE Part G Journal of Aerospace engineering* 226: 363-379.

Zhang DG (2013) Nonlinear bending analysis of FGM beams based on physical neutral surface and high order shear deformation theory. *Composite Structures* 100: 121–126.

Zhao G, Du J and Wu Z (2017) A geometric softening phenomenon of a rotating cantilever beam. *Archive of Applied Mechanics* 87:1049–1059.

Zhao J, Zhou S, Wang B and Wang X (2012) Nonlinear microbeam model based on strain gradient theory. *Applied Mathematical Modelling* 36: 2674–2686.

Zhu TL (2012) Free flapewise vibration analysis of rotating double-tapered Timoshenko beams. *Archive of Applied Mechanics* 82:479–494.

List of Publications

JOURNAL:

1. Bhattacharya S and Das D (2019) Free vibration analysis of bidirectional-functionally graded and double-tapered rotating micro-beam in thermal environment using modified couple stress theory. *Composite Structures* 215: 471-492.

CONFERENCE:

1. Bhattacharya S and Das D. A study on free vibration behavior of micro beam under large static deflection using modified couple stress theory. *63rd Congress of Indian Society of Theoretical and Applied Mechanics* Bangalore, 20-23 December 2018.

BOOK CHAPTER:

1. Bhattacharya S and Das D. A study on free vibration behavior of micro beam under large static deflection using modified couple stress theory. *Lecture Notes in Mechanical Engineering: Advances in Fluid Mechanics and Solid Mechanics, Proceedings of the 63rd Congress of Indian Society of Theoretical and Applied Mechanics 2018* Springer, Editors: Maity D, Siddheshwar PG and Saha S. (Accepted)